Biocatalytic CO_2 hydrogenation to formate and structural analysis of C-phycocyanin

ニュエン, キャカ フン

2024

Doctor thesis

Biocatalytic CO_2 hydrogenation to formate and structural analysis of C-phycocyanin

「生体触媒による CO_2 の水素化反応からのギ酸生成と C-phycocyanin の構造解析」

Hung Khac Nguyen

Department of Chemistry and Biochemistry
Graduate School of Engineering
Kyushu University

Content

Chapter 1

Introduction

1.1 General introduction

The net increase in greenhouse gas concentrations is mainly caused by the excessive emissions of CO_2, which have exceeded the capacity of the Earth's natural absorption and regulation systems. Therefore, resolving this issue requires an expedited reduction in CO_2 emissions; however, most research today has focused on limiting the global temperature rise to 2°C to achieve carbon neutrality by 2050 [1,2]. To address this issue, developing efficient systems to capture and convert inorganic CO_2 into useful fuels has received extensive attention among scientific communities and is considered one of the most important catalytic reactions. Among them, converting CO_2 into formate ($HCOO^-$) has received increased attention because of the growing importance of carbon abatement technologies and carbon-neutral chemical feedstocks [3]. More significantly, formate/ formic acid is considered one of the best liquid organic hydrogen carriers thanks to its high volumetric hydrogen density (53 $g \cdot L^{-1}$), non-flammability, and low toxicity [4]. Therefore, formic acid plays an important role in the carbon-neutral energy cycle system.

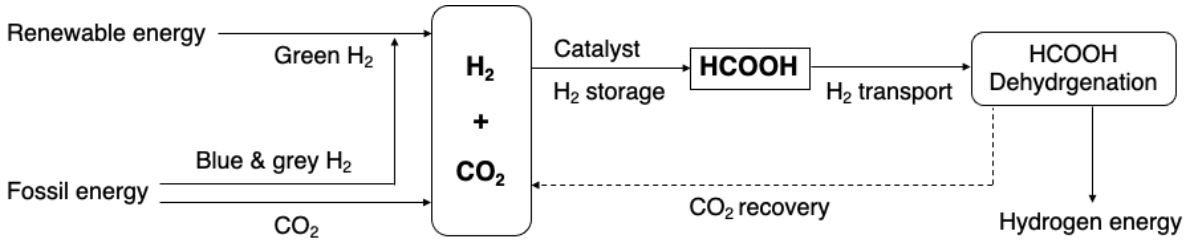

Fig. 1. Schematic model of formate-based hydrogen energy cycle system

To realize the formate-based energy cycle system as shown in **Fig. 1**, a highly effective catalytic system for CO_2 hydrogenation to formate is essential. Many synthetic catalyst-based technologies that achieve high reaction efficiency through electrochemistry or photochemistry rely on precious metals and volatile organic solvents, meaning that high costs, environmental vulnerability, and low product selectivity are challenges for these technologies [5–7]. On the other hand, biocatalysts are becoming an attractive option for CO_2 reduction because they overcome these issues due to their exceptional catalytic efficiency, substrate or product

selectivity, and environmental viability. Numerous investigations on the biocatalytic hydrogenation of CO_2 into formate utilizing living bacteria are underway [8–13]. For example, biocatalytic formate production using biocatalytic cells of *Thermoanaerobacter kivui* and *Acetobacterium woodii* efficiently proceeds via catalytic reactions of unique hydrogen-dependent CO_2 reductases (HDCR) under strict anaerobic conditions [13,14]. Sargent et al. utilized *Escherichia coli* as the biocatalyst, which requires a high-pressurized bioreactor for supplying a high-pressurized gas to enhance the reaction rate of formate production [12]. However, these systems possess bottlenecks in stabilizing enzymes in living cells and achieving highly reusable methods due to the production of undesired byproducts and requirements of strict anaerobic and/or highly pressurized reaction conditions. Furthermore, the separation of reaction products from cultural cells should be leveraged to harvest pure chemicals, which is a critical issue for practical and cost-effective applications. Therefore, the next challenge for the biocatalytic conversion of CO_2 into chemical feedstock in general and formate in particular is to develop a robust system that can capture and selectively reduce CO_2 effectively under very mild conditions for wider application.

1.2 *Citrobacter* sp. S-77

We used our isolated bacterium, *Citrobacter* sp. S-77 (S-77) for H_2-driven CO_2 reduction into formate under very mild reaction conditions. Strain S-77 was isolated from a tepid spring (21°C) in Aso-Kuju National Park, Oita, Japan by our laboratory and contains a membrane-bound [NiFe] hydrogenase (Hyd) [15] and membrane-bound [Mo] formate dehydrogenase (FDH) [16]. These two enzymes have potential to construct an effective biocatalytic system for CO_2 conversion.

1.2.1 Hydrogenase from *Citrobacter* sp. S-77

Hydrogenases (Hyd) are enzyme that can catalyze the reversible oxidation of H_2 with high efficiency. The enzyme can be found in periplasm or cytoplasm and exist in either soluble or membrane-bound structure. In nature, there are three distinct types of hydrogenases which are called [NiFe] hydrogenase, [FeFe]hydrogenase and [Fe]hydrogenase based on the metals in their active sites [17,18].

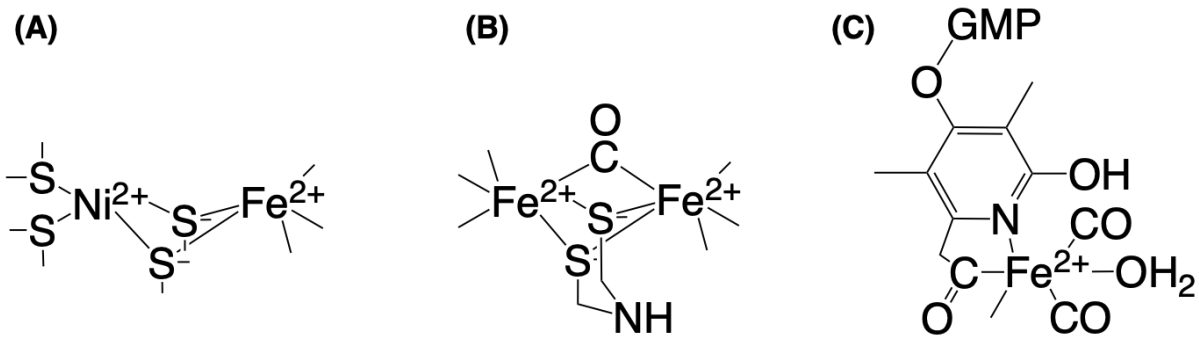

Fig 2. Active sites structure of (A) [NiFe] hydrogenase, (B) [FeFe] hydrogenase and (C) [Fe] hydrogenase (C).

Among these three types, S-77 contains membrane-bound [NiFe] hydrogenase. [NiFe] hydrogenase consists of a large and a small subunit. The Ni-Fe active site is located in the large subunit. The general structure of the active site contains Ni and Fe ions bridged with two Cys thiolates. There are two more Cys bounded to Ni ion while Fe ion is bounded by one CO and two CN^- [18]. [NiFe] hydrogenase is more useful for the oxidation of H_2 than H_2 evolution [17]. Therefore, [NiFe] hydrogenase is of great interest for its application in H_2 oxidation electrodes and biocatalytic systems [19]. The oxidation mechanism of [NiFe] hydrogenase is described in **Fig. 3**:

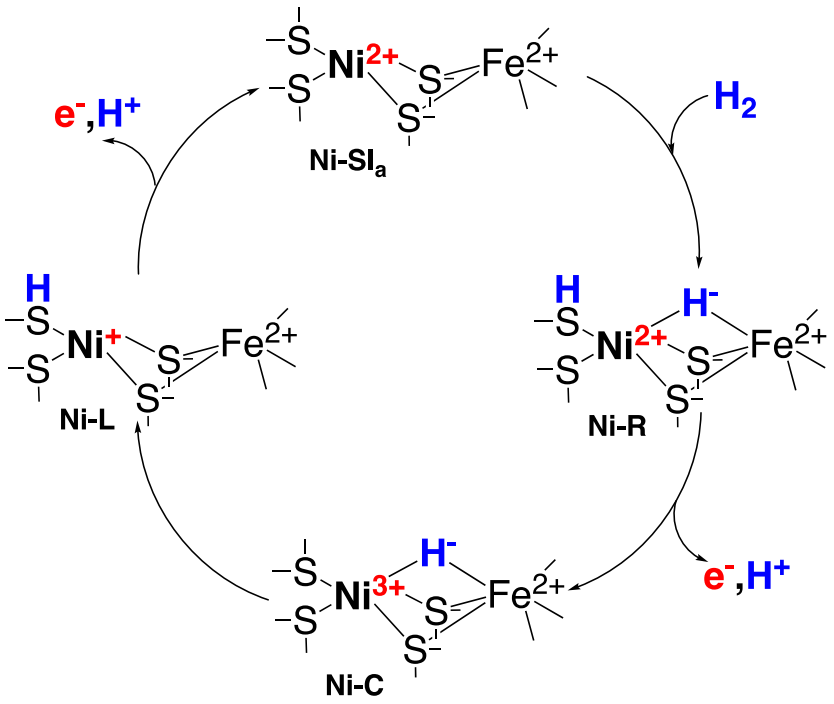

Fig. 3. Mechanism of H_2 oxidation by [NiFe] hydrogenase

H_2 was heterolytically cleaved, and a hydride bridge was formed between Ni-Fe. After that a one-electron oxidation took place and change the state of Ni ions from Ni-R to Ni-C. The Ni^{3+} and H^- then converted into Ni^+ and H^+. Finally, Ni+ was oxidized to back to the starting complex ($Ni\text{-}SI_a$), released H^+ and 1 electron [20,21]. In total, two electrons were released after oxidation, which were transferred by the electron transfer (ET) chain in the small subunit of [NiFe] hydrogenase to use for other reduction process. This mechanism allows [NiFe] hydrogenase to oxidize H_2 with high rate and efficiency that are equivalent to those of Pt [19]. More importantly, the previous report showed that the [NiFe] hydrogenase of S-77 has a unique proximal [4Fe–4S] cluster in the small subunit, which protects the Ni-Fe active site even in the presence of O_2 [22]. This suggests that [NiFe] hydrogenase from S-77 can be activated and oxidize H_2 under mild conditions with the presence of O_2.

1.2.2 Formate dehydrogenase from *Citrobacter* sp. S-77

Formate dehydrogenase (FDH) are enzyme that catalyzes the 2-electron oxidation of formic acid (HCOOH) to CO_2 and the reverse reduction of CO_2 to HCOOH [23–25]. Based on the active sites, FDH can be divided into non-metal and metal-containing types [23]. The metal-containing types are highly conserved and often contain molybdenum (Mo) or tungsten (W) bounded by two molybdopterin guanine dinucleotide molecules, a selenocysteine ligand and a sulfide [23–25].

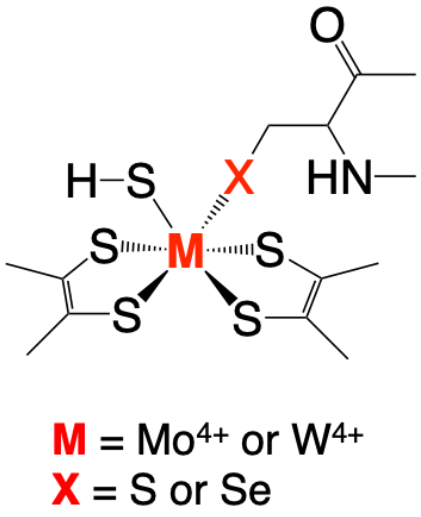

Fig. 4. Active site structure of metal-dependent formate dehydrogenase.

The S-77 was reported to contain the molybdenum-dependent FDH. The catalytic mechanism of reversible oxidation of formate/ reduction of CO_2 has not been elucidated to date. A proposed catalytic reduction mechanism of FDH suggested that the reaction occurs via hydride transfer (**Fig. 5**)

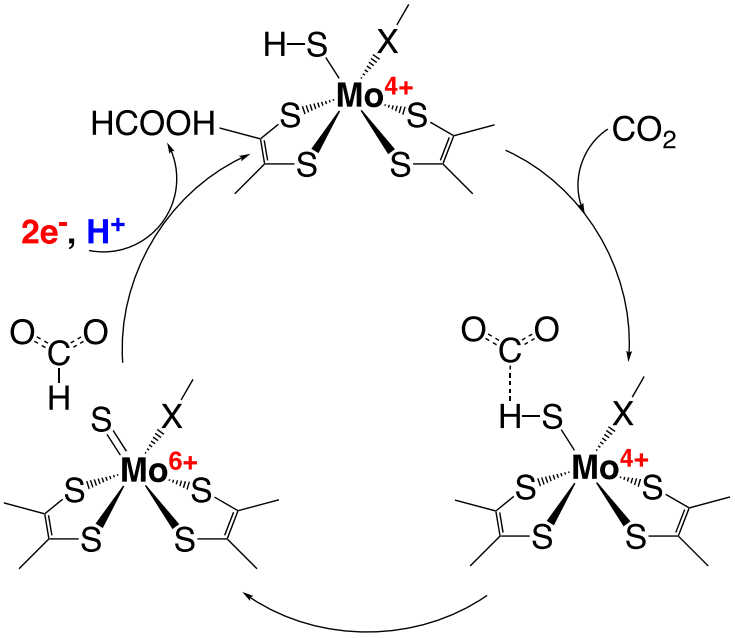

Fig. 5. Proposed mechanism for CO_2 reduction by formate dehydrogenase

According to the proposed mechanism, CO_2 first binds to the protonated sulfo ligand. The direct hydride transfer then took place and conversed Mo^{4+} to Mo^{6+}. Finally, Mo^{6+} was reduced by accepting 2 electrons and releasing formate, thus completing the catalytic cycle. Despite the fact the catalytic mechanism is unclear, formate dehydrogenase receives attention across various fields for its high catalytic efficiency and potential solvency to global warming. More importantly, the previous reports showed that the FDH from S-77 exhibited not only high activity but also O_2 stability and thermostability [16]. Therefore, it can be a strong candidate to construct a biocatalytic system for CO_2 conversion.

1.2.3 Application of *Citrobacter* sp. S-77 for biocatalytic system

In summary, the S-77 contains a membrane-bound [NiFe] hydrogenase which exhibited a high level of H_2 oxidation [15], surpassing the catalytic activity of the platinum catalyst in hydrogen fuel cells. The structural analysis revealed that the Hyd of S-77 has a unique proximal [4Fe–4S] cluster, which protects the NiFe active site even in the presence of O_2 [22]. A

membrane-bound [Mo]formate dehydrogenase (FDH) was also purified from S-77, which exhibited high activity, O_2 stability, and thermostability [16]. Furthermore, S-77 possesses a formate transport protein of FocA, which is a member of the formate-nitrite transporter (FNT) family. The FocA enables the possible route to transport formate from the cytoplasmic side to the periplasmic side via the formate channel [26,27]. One of the bottlenecks in biocatalytic systems that hinder their wider application is their instability, especially in aerobics conditions [13,14,28]. S-77 can overcome this issue thanks to its highly stable enzyme of [NiFe] hydrogenase and [Mo] formate hydrogenase that can be activated in aerobics condition. These advantages make S-77 a promising candidate for constructing a robust biocatalytic system that can convert CO_2 to formate selectively, and efficiently in mild conditions. In this thesis, I demonstrate the biocatalytic systems from S-77 that have high efficiency, stability, and reusability that can be applied to a larger scale.

1.3 The light-harvesting C-phycocyanin from *Thermoleptolyngbya* sp. O-77

Phycobilisome (PBS), which attaches to the thylakoid membrane of cyanobacteria and algae, is a water-soluble light-harvesting protein complex that is unlike the light-harvesting protein complex that binds to the thylakoid membrane of higher plants [29,30]. PBS plays an important role in the photosynthetic system through light energy absorption and facilitating the high-efficiency transfer to photosystem I and II in water [31–34]. PBS, which has a molecular weight from 7 to 15 MDa, is composed of a core and peripheral rod protein complex with acidic chromophore polypeptides (phycobiliproteins, PBPs) and hydrophobic polypeptides called linker proteins [35]. The giant protein complex of PBS typically consists of three pigment proteins: phycoerythrin, phycocyanin, and allophycocyanin [36,37]. Among these three proteins, C-phycocyanin (CPC) is the most abundant component. It consists of two different polypeptides (the α and β subunits) that form αβ structures of monomers, trimers, or hexamers

[38]. Owing to its abundance, water-solubility, and non-toxicity, CPC has garnered interest from researchers in various fields, including biotechnological and pharmaceutical applications [39,40]. The open-chain tetrapyrroles of phycocyanobilin (PCB) are the major light receptors in CPC [34]. PCB is covalently bound to the conserved cysteine residues via thioether linkages by attaching one PCB to the α subunit of CPC and two PCBs to the β subunit [41,42]. *In vitro* studies demonstrated that conventional CPC can exist as three forms of monomer, trimer, and hexamer, suggesting that the biosynthesis pathway of CPC is based on the assembly of monomer (αβ) into trimers $(\alpha\beta)_3$ and hexamers $(\alpha\beta)_6$, followed by the insertion of linker proteins *in vivo* [43,44].

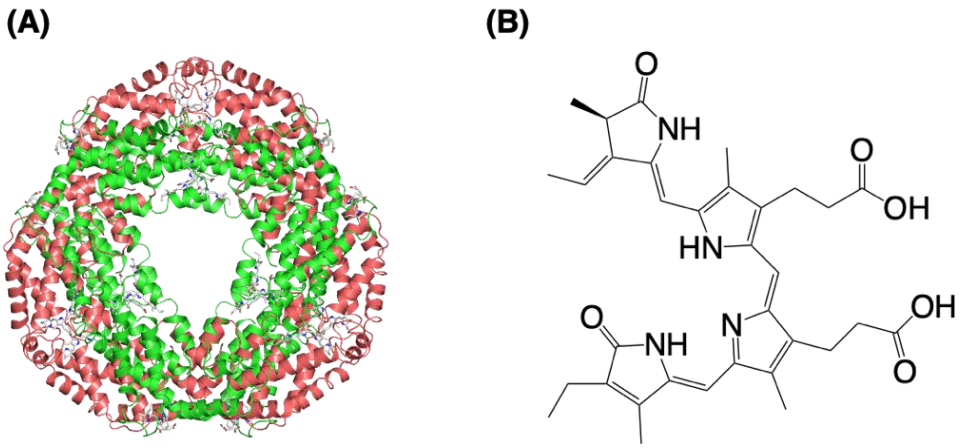

Fig. 6. General structure of (A) hexamer C-phycocyanin and (B) phycocyanobilin.

During the studies of oxygenic photosynthesis, we isolated a thermophilic and non-heterocystous cyanobacterium *Leptolyngbya* sp. O-77 from a hot spring [45]. The O-77 strain grows well at high temperatures of 50°C–60°C, with an optimal growth temperature of 55°C. Owing to its thermophilic characteristics, the O-77 strain was re-classified into the new genus of *Leptolyngbya*-like thermophilic cyanobacterium, named *Thermoleptolyngbya* sp. O-77 [46]. Following studies of photosystem II and water-soluble light-harvesting complexes [45,47], we presented the first report of the non-conventional octameric CPC from the O-77 strain (CPC_{O77}) [48] (**Fig. 8**). In the study, CPC_{O77} can be assembled spontaneously *in vitro* from an equilibrium between the two structures, hexamer, and octamer. This raises the question of the self-assembly

mechanisms of CPC; however, the assembly mechanism has not been elucidated. Therefore, in this thesis, I demonstrated an *in vitro* reassembly experiment by using the isolated α and β subunits dissociated from native CPC_{O77}. These subunits are the fundamental building blocks that constitute the monomers and other oligomers of CPC and any change in the subunit structure and sequence might affect the overall structure and the overall assembly process. Therefore, the study of CPC subunits should be considered essential for understanding the assembly mechanism [49,50].

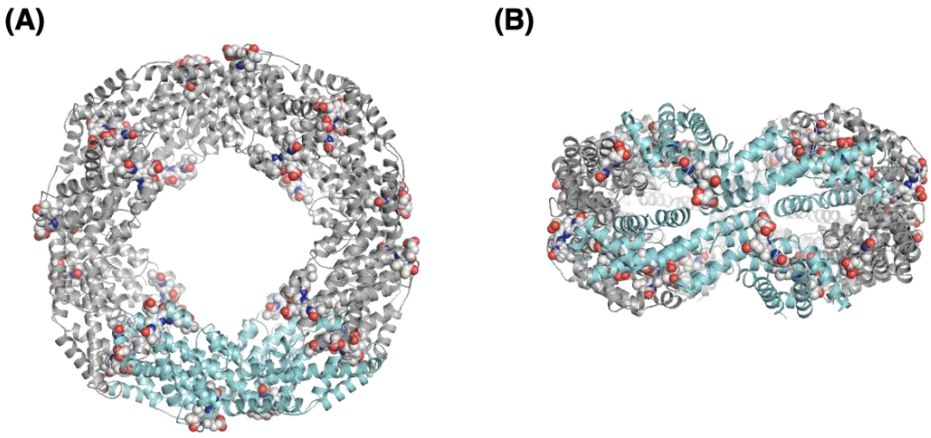

Fig. 8. (A) Top view and (B) side view of crystal structure of the non-conventional octamer CPC_{O77}

1.4 Arrangement of Dissertation

In this dissertation, I described the strategies to construct a robust biocatalytic system for selective CO_2 conversion to formate using *Citrobacter* sp. S-77, i.e. encapsulated whole-cell biocatalytic system (Chapter 2) and encapsulated plasma membrane biocatalytic system (Chapter 3). I also demonstrated the disassembly and reassembly of C-phycocyanin from *Thermoleptolyngbya* sp. O-77 to study the assembly mechanism of the non-conventional octamer C-phycocyanin.

In Chapter 2, a novel encapsulated whole-cell biocatalytic system was designed to selectively convert CO_2 to formate. This robust system obtains high stability, reusability, and efficiency in mild reaction conditions.

In Chapter 3, a novel strategy using the S-77 plasma membrane was presented for the first time. This system significantly enhances the efficiency of the CO_2 hydrogenation to formate.

In Chapter 4, I demonstrated the disassembly and reassembly of CPC_{O77}. The subunits of $CPC_{O77\ were}$ isolated and structurally analyzed by X-ray crystallography for the first time. Furthermore, the results suggest that the assembly of non-conventional octamer CPC_{O77} is a natural and reversible process.

In Chapter 5, I provided some conclusions and remarks on the work that has been accomplished in this description.

1.5 References

[1] C. Hepburn, E. Adlen, J. Beddington, E. A. Carter, S. Fuss, N. Mac Dowell, J. C. Minx, P. Smith, C. K. Williams, *Nature* **2019**, *575*, DOI 10.1038/s41586-019-1681-6.

[2] N. Mac Dowell, P. S. Fennell, N. Shah, G. C. Maitland, *Nat Clim Chang* **2017**, *7*, DOI 10.1038/nclimate3231.

[3] A. M. Appel, J. E. Bercaw, A. B. Bocarsly, H. Dobbek, D. L. Dubois, M. Dupuis, J. G. Ferry, E. Fujita, R. Hille, P. J. A. Kenis, C. A. Kerfeld, R. H. Morris, C. H. F. Peden, A. R. Portis, S. W. Ragsdale, T. B. Rauchfuss, J. N. H. Reek, L. C. Seefeldt, R. K. Thauer, G. L. Waldrop, *Chem Rev* **2013**, *113*, DOI 10.1021/cr300463y.

[4] Z. Wang, J. Qian, Z. Sun, Z. Zhang, M. He, Q. Chen, *Catalysts* **2023**, *13*, DOI 10.3390/catal13081168.

[5] A. Alok, R. Shrestha, S. Ban, S. Devkota, B. Uprety, R. Joshi, *J Environ Chem Eng* **2022**, *10*, DOI 10.1016/j.jece.2021.106922.

[6] W. H. Wang, Y. Himeda, J. T. Muckerman, G. F. Manbeck, E. Fujita, *Chem Rev* **2015**, *115*, DOI 10.1021/acs.chemrev.5b00197.

[7] J. Wu, Y. Huang, W. Ye, Y. Li, *Advanced Science* **2017**, *4*, DOI 10.1002/advs.201700194.

[8] A. Alissandratos, H. K. Kim, C. J. Easton, *Bioresour Technol* **2014**, *164*, DOI 10.1016/j.biortech.2014.04.064.

[9] F. Leo, F. M. Schwarz, K. Schuchmann, V. Müller, *Appl Microbiol Biotechnol* **2021**, *105*, DOI 10.1007/s00253-021-11463-z.

[10] T. B. Madavi, S. Chauhan, A. Keshri, H. Alavilli, K. Y. Choi, S. D. V. N. Pamidimarri, *Biofuels, Bioproducts and Biorefining* **2022**, *16*, DOI 10.1002/bbb.2331.

[11] C. Mourato, M. Martins, S. M. da Silva, I. A. C. Pereira, *Bioresour Technol* **2017**, *235*, DOI 10.1016/j.biortech.2017.03.091.

[12] M. Roger, F. Brown, W. Gabrielli, F. Sargent, *Current Biology* **2018**, *28*, DOI 10.1016/j.cub.2017.11.050.

[13] F. M. Schwarz, V. Müller, *Biotechnol Biofuels* **2020**, *13*, DOI 10.1186/s13068-020-1670-x.

[14] K. Schuchmann, V. Müller, *Science (1979)* **2013**, *342*, DOI 10.1126/science.1244758.

[15] S. Eguchi, K. S. Yoon, S. Ogo, *J Biosci Bioeng* **2012**, *114*, DOI 10.1016/j.jbiosc.2012.05.018.

[16] N. T. Nguyen, T. Yatabe, K. S. Yoon, S. Ogo, *J Biosci Bioeng* **2014**, *118*, DOI 10.1016/j.jbiosc.2014.03.011.

[17] W. Lubitz, H. Ogata, O. Rüdiger, E. Reijerse, *Chem Rev* **2014**, *114*, DOI 10.1021/cr4005814.

[18] C. Tard, C. J. Pickett, *Chem Rev* **2009**, *109*, DOI 10.1021/cr800542q.

[19] R. M. Evans, E. J. Brooke, S. A. M. Wehlin, E. Nomerotskaia, F. Sargent, S. B. Carr, S. E. V. Phillips, F. A. Armstrong, *Nat Chem Biol* **2016**, *12*, DOI 10.1038/nchembio.1976.

[20] H. Tai, S. Hirota, *ChemBioChem* **2020**, *21*, DOI 10.1002/cbic.202000058.

[21] H. Ogata, W. Lubitz, Y. Higuchi, *Dalton Transactions* **2009**, DOI 10.1039/b903840j.

[22] N. D. M. Noor, H. Matsuura, K. Nishikawa, H. Tai, S. Hirota, J. Kim, J. Kang, M. Tateno, K. S. Yoon, S. Ogo, S. Kubota, Y. Shomura, Y. Higuchi, *Chemical Communications* **2018**, *54*, DOI 10.1039/c8cc06261g.

[23] Y. Amao, *Journal of CO_2 Utilization* **2018**, *26*, DOI 10.1016/j.jcou.2018.06.022.

[24] D. Niks, R. Hille, *Protein Science* **2019**, *28*, DOI 10.1002/pro.3498.

[25] L. B. Maia, J. J. G. Moura, I. Moura, *Journal of Biological Inorganic Chemistry* **2015**, *20*, DOI 10.1007/s00775-014-1218-2.

[26] A. B. Waight, J. Love, D. N. Wang, *Nat Struct Mol Biol* **2010**, *17*, DOI 10.1038/nsmb.1740.

[27] M. Kammel, R. Gary Sawers, *Microbiology (United Kingdom)* **2022**, *168*, DOI 10.1099/mic.0.001168.

[28] M. Roger, T. C. P. Reed, F. Sargent, *Appl Environ Microbiol* **2021**, *87*, DOI 10.1128/AEM.00299-21.

[29] R. Croce, H. Van Amerongen, *Nat Chem Biol* **2014**, *10*, DOI 10.1038/nchembio.1555.

[30] M. Watanabe, M. Ikeuchi, *Photosynth Res* **2013**, *116*, DOI 10.1007/s11120-013-9905-3.

[31] N. Adir, S. Bar-Zvi, D. Harris, *Biochim Biophys Acta Bioenerg* **2020**, *1861*, DOI 10.1016/j.bbabio.2019.07.002.

[32] G. Ferraro, P. Imbimbo, A. Marseglia, R. Lucignano, D. M. Monti, A. Merlino, *Biochim Biophys Acta Bioenerg* **2020**, *1861*, DOI 10.1016/j.bbabio.2020.148236.

[33] B. R. Green, W. W. Parson, *Advances in photosynthesis and respiration ;* **2003**, *13*.

[34] R. MacColl, *J Struct Biol* **1998**, *124*, DOI 10.1006/jsbi.1998.4062.

[35] R. R. Sonani, S. Patel, B. Bhastana, K. Jakharia, M. G. Chaubey, N. K. Singh, D. Madamwar, *Bioresour Technol* **2017**, *245*, DOI 10.1016/j.biortech.2017.08.129.

[36] A. R. Grossman, M. R. Schaefer, G. G. Chiang, J. L. Collier, *Microbiol Rev* **1993**, *57*, DOI 10.1128/mr.57.3.725-749.1993.

[37] L. N. Liu, X. L. Chen, Y. Z. Zhang, B. C. Zhou, *Biochim Biophys Acta Bioenerg* **2005**, *1708*, DOI 10.1016/j.bbabio.2005.04.001.

[38] P. M. Gault, H. J. Marler, *Handbook on Cyanobacteria: Biochemistry, Biotechnology and Applications*, **2009**.

[39] N. T. Eriksen, *Appl Microbiol Biotechnol* **2008**, *80*, DOI 10.1007/s00253-008-1542-y.

[40] Y. C. Seo, W. S. Choi, J. H. Park, J. O. Park, K. H. Jung, H. Y. Lee, *Int J Mol Sci* **2013**, *14*, DOI 10.3390/ijms14011778.

[41] M. Kupka, H. Scheer, *Biochim Biophys Acta Bioenerg* **2008**, *1777*, DOI 10.1016/j.bbabio.2007.10.009.

[42] T. J. Ashaolu, K. Samborska, C. C. Lee, M. Tomas, E. Capanoglu, Ö. Tarhan, B. Taze, S. M. Jafari, *Int J Biol Macromol* **2021**, *193*, DOI 10.1016/j.ijbiomac.2021.11.064.

[43] W. M. Schluchter, G. Shen, R. M. Alvey, A. Biswas, N. A. Saunée, S. R. Williams, C. A. Mille, D. A. Bryant, *Adv Exp Med Biol* **2010**, *675*, DOI 10.1007/978-1-4419-1528-3_12.

[44] L. David, A. Marx, N. Adir, *J Mol Biol* **2011**, *405*, DOI 10.1016/j.jmb.2010.10.036.

[45] H. Nakamori, T. Yatabe, K. S. Yoon, S. Ogo, *J Biosci Bioeng* **2014**, *118*, DOI 10.1016/j.jbiosc.2014.01.009.

[46] K. Sciuto, I. Moro, *Mol Phylogenet Evol* **2016**, *105*, DOI 10.1016/j.ympev.2016.08.010.

[47] K. Yamada, T. Yatabe, K. S. Yoon, S. Ogo, *J Organomet Chem* **2022**, *964*, DOI 10.1016/j.jorganchem.2022.122302.

[48] T. Minato, T. Teramoto, N. Adachi, N. K. Hung, K. Yamada, M. Kawasaki, M. Akutsu, T. Moriya, T. Senda, S. Ogo, Y. Kakuta, K. S. Yoon, *Commun Biol* **2021**, *4*, DOI 10.1038/s42003-021-02767-x.

[49] R. Inoue, Y. Sakamaki, T. Takata, K. Wood, K. Morishima, N. Sato, A. Okuda, M. Shimizu, R. Urade, N. Fujii, M. Sugiyama, *Sci Rep* **2021**, *11*, DOI 10.1038/s41598-021-82250-z.

[50] V. Eckey, H. Landmesser, E. Schneider, *Biochim Biophys Acta Biomembr* **2010**, *1798*, DOI 10.1016/j.bbamem.2010.03.001.

Chapter 2

Selective formate production from H_2 and CO_2 using encapsulated whole-cells under mild reaction conditions.

(*J. Biosci. Bioeng.*, **2023**, 136, 182–189)

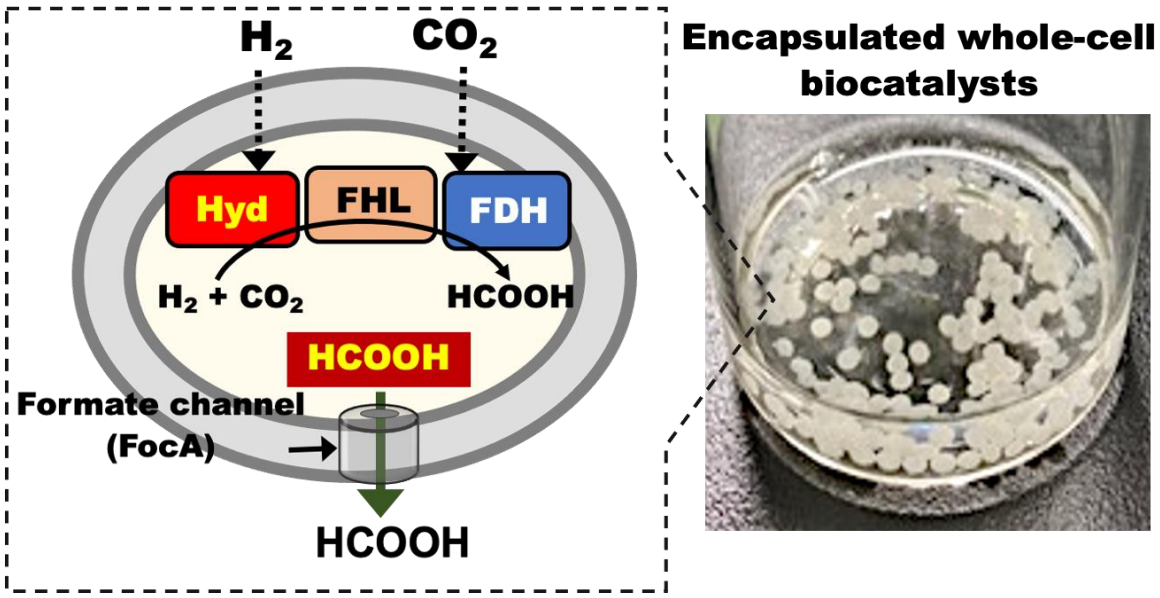

ABSTRACT

Biocatalytic CO_2 reduction into formate is a crucial strategy for realizing the carbon-neutral energy cycle system. In this chapter, I designed an efficient biocatalytic system to produce formate selectively by coupling two enzymatic activities of H_2 oxidation by [NiFe] hydrogenase and CO_2 reduction by [Mo] formate dehydrogenase using encapsulated bacterial cells of *Citrobacter sp*. S-77. The encapsulated whole-cell catalyst was made by living cells depositing into polyvinyl alcohol and gellan gum cross-linked by calcium ions to form hydrogel beads. Formate production using encapsulated cells was carried out under the resting state conditions in the gas mixture of H_2/CO_2 (70:30, v/v%). The whole-cell biocatalyst showed highly efficient and selective catalytic production of formate, reaching the specific rate of formate production of 110 $mmol \cdot L^{-1} \cdot g_{protein}^{-1} \cdot h^{-1}$ at 30°C, pH 7.0, and 0.1 MPa. The encapsulated cells can be reused at least 8 times while keeping their high catalytic activities for formate production under mild reaction conditions.

2.1. Introduction

The CO_2 conversion into formate has received increasing attention because formate is a desirable liquid organic hydrogen carrier and chemical feedstock [1]. Various types of homogeneous and heterogeneous catalysts have been synthesized to develop efficient systems for the catalytic production of formate from CO_2 and H_2 [2–4]. However, these systems still require expensive noble metals as active sites [5] and high overpotentials with high pressures and temperatures. Recently, biocatalytic CO_2 reduction into useful fuels has gained broad attention, however, industrial utilization of traditional enzyme catalysts is limited by issues such as enzyme stability and laborious downstream processing for enzyme purification and characterization. Whole-cell biocatalysis overcomes these problems by 1) avoiding multistep enzyme extraction and purification, 2) preserving inherent optimal conditions for enzyme cascades in cellular metabolic pathways, allowing for achieving robust catalysis for maximum productivity, and 3) lowering the overall cost of the system [6]. Formate production in culturing liquid medium using whole-cell catalysis has been reported in several microorganisms. For example, biocatalytic formate production using whole-cells of *Thermoanaerobacter kivui* and *Acetobacterium woodii* efficiently proceeds via catalytic reactions of unique hydrogen-dependent CO_2 reductases under strict anaerobic conditions [7,8]. Other report utilized *Escherichia coli* as the biocatalyst, which requires a high-pressurized bioreactor for supplying a high-pressurized gas to enhance the reaction rate of formate production [9]. However, these systems' drawback is in stabilizing enzymes in living cells and achieving highly reusable methods due to the production of undesired byproducts and requirements of strict anaerobic and/or highly pressurized reaction conditions. More importantly, the separation of reaction products from cultural cells is equivalent to harvesting pure chemicals, which becomes a critical issue for practical and cost-effective applications.

Inspired by the above-mentioned reports, I used in this study our laboratory's isolated bacterium, *Citrobacter* sp. S-77 (S-77) for H_2-driven CO_2 reduction into formate under very mild reaction conditions. The S-77 contains highly active and O_2-stable membrane-bound [NiFe] hydrogenase and [Mo] formate dehydrogenase, including FHL composed of two catalytic sites of [NiFe] hydrogenase and [Mo] formate dehydrogenase [10,11], which resulted in the heterogenous catalytic and highly selective formate production under very mild conditions, even in the presence of O_2. Furthermore, S-77 possesses a formate transport protein of FocA, which is a member of the formate-nitrite transporter (FNT) family. The FocA enables the possible route to transport formate from the cytoplasmic side to the periplasmic side via the formate channel [12,13]. Considering these advantages, I developed a system using the resting cells for the selective production of formate from H_2-driven CO_2 reduction by coupling enzyme activities of Hyds and FDHs under mild reaction conditions. Another issue that needs to be addressed is physical damage to the cell by collecting and washing, which decreases the reusability of the systems. Therefore, to overcome this difficulty of whole-cell culture conditions, including instability, strict reaction conditions, and limited reusability, I come up with an interesting solution through the immobilization of the whole-cell S-77 in a hydrogel matrix by cross-linking with water-soluble polymers of gellan gum (GG) and polyvinyl alcohol (PVA). The encapsulated whole-cell system in hydrogel beads successfully acts as a heterogeneous catalyst for selective formate production and leads to enhanced stability and reusability without losing catalytic activity. This robust biocatalytic system has great potential to develop an efficient formate production from H_2-driven CO_2 reduction under mild reaction conditions.

2.2. Materials and Methods

2.2.1. Chemicals

Yeast extract powder and hipolypepton were purchased from Funakoshi Co., Ltd. (Japan). Magnesium sulfate heptahydrate ($MgSO_4 \cdot 7H_2O$) and nickel(II) chloride hexahydrate ($NiCl_2 \cdot 6H_2O$) were purchased from Sigma-Aldrich (Japan). Dipotassium hydrogen phosphate (K_2HPO_4), potassium hydrogen phosphate (KH_2PO_4), sodium chloride (NaCl), ammonium sulfate $(NH_4)_2SO_4$), sodium formate (HCOONa), D(+)-glucose, ammonium iron(III) citrate, brown, calcium chloride ($CaCl_2$), sodium hydroxide (NaOH), sodium tungstate(VI) dihydrate ($Na_2WO_4 \cdot 2H_2O$), disodium molybdate(VI) dihydrate ($Na_2MoO_4 \cdot 2H_2O$), sodium selenite ($Na_2S_2O_3$), gellan gum (GG), polyvinyl alcohol (PVA), (±)-dithiothreitol (DTT), 2-amino-2-hydroxymethyl-1,3-propanediol hydrochloride (Tris·HCl), methyl viologen (MV), and sodium bicarbonate ($NaHCO_3$) were purchased from FUJIFILM Wako Pure Chemical Corporation (Japan). Deuterium oxide (D_2O) and ^{13}C-sodium bicarbonate ($NaH^{13}CO_3$) were purchased from Cambridge Isotope Laboratories (USA). All chemical reagents were used as received unless otherwise specified.

2.2.2. Cell culture

Citrobacter sp. S-77 cells were grown in 20-L plastic bottles at 30°C for 5 days with the supplements of the following reagents ($g \cdot L^{-1}$): 3.0 g yeast extract, 3.0 g hipolypeptone, 0.5 g $MgSO_4 \cdot 7H_2O$, 2.0 g K_2HPO_4, 1.0 g KH_2PO_4, 3.0 g $(NH_4)_2SO_4$, 1.0 g (±)-D-glucose, 2.0 g HCOONa, 0.2 g ammonium iron(III) citrate, and 0.1 g of $CaCl_2$ and the minor mineral components of 0.1 μM $NiCl_2$, 0.1 μM Na_2WO_4, 0.1 μM Na_2MoO_4, and 0.2 μM $Na_2Se_2O_3$ (as of the final concentration of the medium at pH 7.0). Collected cells were suspended in 20 mM potassium phosphate (KP) buffer (pH 7.0) containing 1.0 mM DTT and 0.1 mM NaCl, used as a standard buffer in this study.

2.2.3. Preparation of plasma membrane and soluble cell extracts

The collected S-77 cells were disrupted by sonication three times for 3 min in an ice bath at 60 W with an Ultrasonic Disruptor UD-200 (Tomy Seiko Inc., Japan). The broken cells were centrifuged at 5000g for 20 min to remove cell debris and unbroken cells. The resulting supernatant was further subjected to ultracentrifugation (Optima L-90K, Beckman Coulter Inc., USA) at 100,000g for 1 h at 4°C to give the membrane and soluble cell extracts. The harvested membrane was washed and suspended with the same buffer solutions. The protein concentrations of the membrane suspension and soluble cell extracts were determined by the Lowry method using the DC protein assay (Bio-Rad, USA). Bovine serum albumin was used as a standard protein for the calibration curve. The weight of dried cells cannot be measured accurately because collected cells contained various debris such as culture medium and many chemical byproducts. Therefore, in this experiment, the rate of formate production was determined by the more reliable cellular protein concentration, rather than by the weight of dried cells.

2.2.4. Encapsulation of whole-cells in hydrogel beads

Encapsulation of bacterial cells was carried out by adding PVA solution into the living S-77 cell suspension. The PVA/S-77 mixture was then added to the GG solution (2%) to be the final concentrations of PVA (1%) and GG (0.5%). The resulting solution was added dropwise into the 2% calcium chloride solution. The encapsulated whole-cell S-77 in PVA and GG (GG/PVA/S-77) were used as biocatalysts for formate production as the resting cell reaction under mild reaction conditions at 30°C, pH 7.0, and 0.1 MPa after washing with the standard buffer three times.

2.2.5. Enzyme assay

Hyd and FDH activities were determined spectrophotometrically by using a V-670 spectrophotometer (JASCO, Japan) following the reduction of MV at 30°C in glass cuvettes sealed with a rubber stopper and an aluminum cap under N_2. The reaction solutions containing the membrane suspension or the cell extracts in 50 mM KP buffer (pH 7.0) were prepared in a Coy anaerobic chamber (Coy Laboratory Products, USA) under an atmosphere of 98% N_2 and 2% H_2. To perform H_2 oxidation, H_2 was flashed for 5 min in the Hyd assay mixture, whereas formate oxidation was performed by the addition of sodium formate to be the final concentration of 10 mM, followed by flushing with Ar for 5 min in the FDH assay mixture. The reactions using Hyd and FDH were carried out under anaerobic conditions at 30°C by the initiation of adding MV solution at the final 10 mM concentrations. Enzymatic activities were calculated by the increase in absorbance of MV (ε = 9.8 $mM^{-1} \cdot cm^{-1}$) at 578 nm. Note that the specific activities of H_2 and formate oxidations were calculated by 2-electron reactions of MV. At least three independent experiments were performed to plot the data analysis. Steady-state kinetic parameters and K_m values of H_2 and CO_2 were determined by fitting the data to the Michaelis-Menten equation using nonlinear regression. The data were analyzed by using the Enzyme kinetics Module1.1 of Sigmaplot 8.0 software (Jandel Scientific, CA, USA).

2.2.6. Procedure for biocatalytic formate production

Biocatalytic CO_2 conversion into formate was performed by using glass bottles (ca. 177 mL) sealed with a rubber stopper and an aluminum cap. The harvested S-77 cells were washed with a standard KP buffer three times before use. The procedure for the reaction using whole-cell S-77 was as follows: 10 mL of washed cells suspended in 200 mM phosphate buffer (pH 7.0) were added to bottles (approximately 167 mL headspace) and the reaction solution was bubbled with Ar gas for 5 min (>200 $mL \cdot min^{-1}$). The reaction solution was subsequently bubbled with the gas mixture of H_2 (140 $mL \cdot min^{-1}$) and CO_2 (60 $mL \cdot min^{-1}$) for 5 min and

incubated at 30°C for a period of time. The analysis for the reaction using GG/PVA/S-77 was as follows: After the reaction of encapsulated cells for 24 h, the reaction solution was collected and centrifuged at 3500g, and the resulting supernatant solution was filtered for determination of formate by HPLC analysis. The procedure for the reuse experiment using hydrogel beads GG/PVA/S-77 was as follows: The hydrogel beads were added to the reaction solution of 200 mM KP buffer and then flushed by Ar gas for 5 min (>200 $mL \cdot min^{-1}$). The reaction solution was subsequently flowed by the gas mixture of H_2 (140 $mL \cdot min^{-1}$) and CO_2 (60 $mL \cdot min^{-1}$) for 5 min. After the reaction for 3 h, the hydrogel beads GG/PVA/S-77 were washed with 200 mM KP buffer and used for the next reuse experiment. All of the reactions were performed at 30°C. At least three independent experiments were performed to plot the data analysis.

2.2.7. SEM images of encapsulated cells

The images of the encapsulated living cells in hydrogel beads were observed by the analysis of a scanning electron microscope (SEM. SU8000, Hitachi Co., Japan). Three hydrogel beads of GG, GG/PVA, and GG/PVA/S-77 were prepared and washed with the standard KP buffer. The washed beads were dehydrated with a graded series of ethanol solutions (30, 50, 75, 90, 95%) for 10 min and dried at room temperature overnight. The dried samples were mounted onto sample holders using carbon double-sided tape, and then sputter coated with a palladium layer by a JFC-1600 auto fine coated for enhancing the conductivity. The SEM images of all samples were recorded at an accelerating voltage of 5.0 kV.

2.2.8. Analysis of formate

Qualitative analysis of formate was performed by using an AVANCE III HD 600 nuclear magnetic resonance (NMR) spectrometer (Bruker, USA) with 5-mm tubes (^1H, 600.13 MHz; ^{13}C, 150.92 MHz). Chemical shifts (δ) were reported in parts per million (ppm)

downfield from $Si(CH_3)_4$ (solvent, D_2O) for ^1H and ^{13}C NMR spectra. Formate was quantitatively analyzed by using a high-performance liquid chromatography (HPLC) system (Agilent) with an ion-exclusion chromatography column (Shodex RSpak KC-811) and HPLC-UV Detection (Agilent) at 210 nm. A 0.1% H_3PO_4 aqueous solution was used as the eluent (flow rate, 1.0 $mL \cdot min^{-1}$). The column oven temperature was maintained at 40°C. The identity of the formate was confirmed by HPLC and ^1H NMR profiles with those of the standard formate. To confirm the H_2-driven CO_2 reduction to ^{13}C-formate production, 200 mM $NaH^{13}CO_3$ was used as a sole carbon source.

2.3. Results and Discussion

2.3.1. Gene clusters involving H_2 and formate metabolism.

The whole genomic sequence of a heterotrophic and facultative anaerobic bacterium *Citrobacter* sp. S-77 was obtained and available at the NCBI homepage (www.ncbi.nlm.nih.gov)[10,11,14]. From the genome sequence, eight gene clusters involving the H_2 and formate metabolisms were identified: three Hyds (Hyd-1–3) and five FDHs (two FDH-H, two FDH-N, and one FDH-O), where Hyd-3 and FDH-H form the FHL complex (**Fig. 1, Table 1**), which are highly homologous to those of *E. coli*. Although one of two FDH-N was expressed within the S-77 cultured in the presence of sodium formate [14], the expressions of the remaining seven proteins are unknown. According to the genome, S-77 contains at least three distinct genes encoding hydrogenases, which correspond to Hyd-1, Hyd-2, and Hyd-3. Hyd-1, known as O_2-tolerant [NiFe]hydrogenase [14–16], consists of three components of HydABC corresponding to large- and small-subunit and a membrane-anchored protein of two heme b containing cytochrome, respectively. The large- and small-subunit of hydrogenase complex are translocated across the cytoplasmic membrane by the twin-arginine transport (Tat) pathway and harbor a membrane-anchored cytochrome b. The Hyd-1 eventually faces the

surface of the periplasmic side of the membrane, whereas Hyd-2 has an unusual structure consisting of a heterotetramer of HybOABC. The genes of *hybO* and *hybC* correspond to small- and large-subunit, respectively, however, the additional structural genes of *hybA* and *hybB* are still poorly understood. Based on the analysis of amino acid sequence arrangement, the *hybA* contains a Tat signal sequence of initial 32 amino acids with four predicted 4Fe-4S cluster binding sites with the 16 conserved cysteine residues [14–16]. Additionally, the *hybB* is predicted to act as the membrane anchor subunit of the Hyd-2 complex and to function as a membrane-anchored cytochrome b, however, the *hybB* lacks the cofactor heme b binding motif [14,16]. The membrane-integrated parts and the assembly process of the Hyd-2 complex are still unknown. Another unique hydrogenase Hyd-3, called formate hydrogenlyase (FHL), is fused with two functionally different parts of formate dehydrogenase H (FDH-H) and [NiFe] hydrogenase [17,18]. In FHL complexes, formate, generated in the cytoplasm, is oxidized into CO_2, two electrons, and two protons by FDH-H, and electrons and protons are used for the production of H_2 by the hydrogenase portion. Hyd-1, Hyd-2, two FDH-N, and FDH-O are located in the periplasm, whereas the FHL complex is located in the cytoplasm (**Fig. 1B**). Therefore, by separating disrupted S-77 into the soluble cell extracts containing the FHL complex and membrane containing Hyd-1,2, FDH-N, and FDH-O, protein mixtures that catalyze CO_2 hydrogenation reaction into formate can be obtained.

In the mechanism of formate excretion of living cells under H_2 and CO_2, it has been thought that there are at least two pathways to produce formate: by the FHL complex in the cytoplasm (path A) and by the combination of Hyd and FDH in the plasma membrane (path B). Path A's possible route to transport formate is via the transport protein FocA, a member of the formate-nitrite transporter (FNT) family [19,20]. Based on the genomic sequence analysis, S-77 possesses three distinct FNT-encoding genes: FocA (WP_003831909), NirC (WP_045449812), and YfdC (WP_045445741). FocA can transport formate through the channel across the

membrane from the inside of the cytoplasm to the outside of the periplasm, whereas NirC is thought to be a nitrite transporter [21]. Although the function of YfdC remains unclear, a computational study indicated that the YfdC channel is not an anion transporter [22]. These considerations suggested that the formate produced by using the cytoplasmic FHL complex was transported to the periplasmic space by FocA. The structural study of FocA in *E. coli* revealed a symmetric pentamer structure, in which the protomer is similar to the aquaporin [21]. This structure combined with the residues analysis suggested that FocA is a selective, passive channel that only allows formate to pass [21,23]. After passing through the FocA channel, the formate in the periplasmic space, including the formate produced by path B, is diffused outside of the cell *via* porins (**Fig. 1B**) [24]

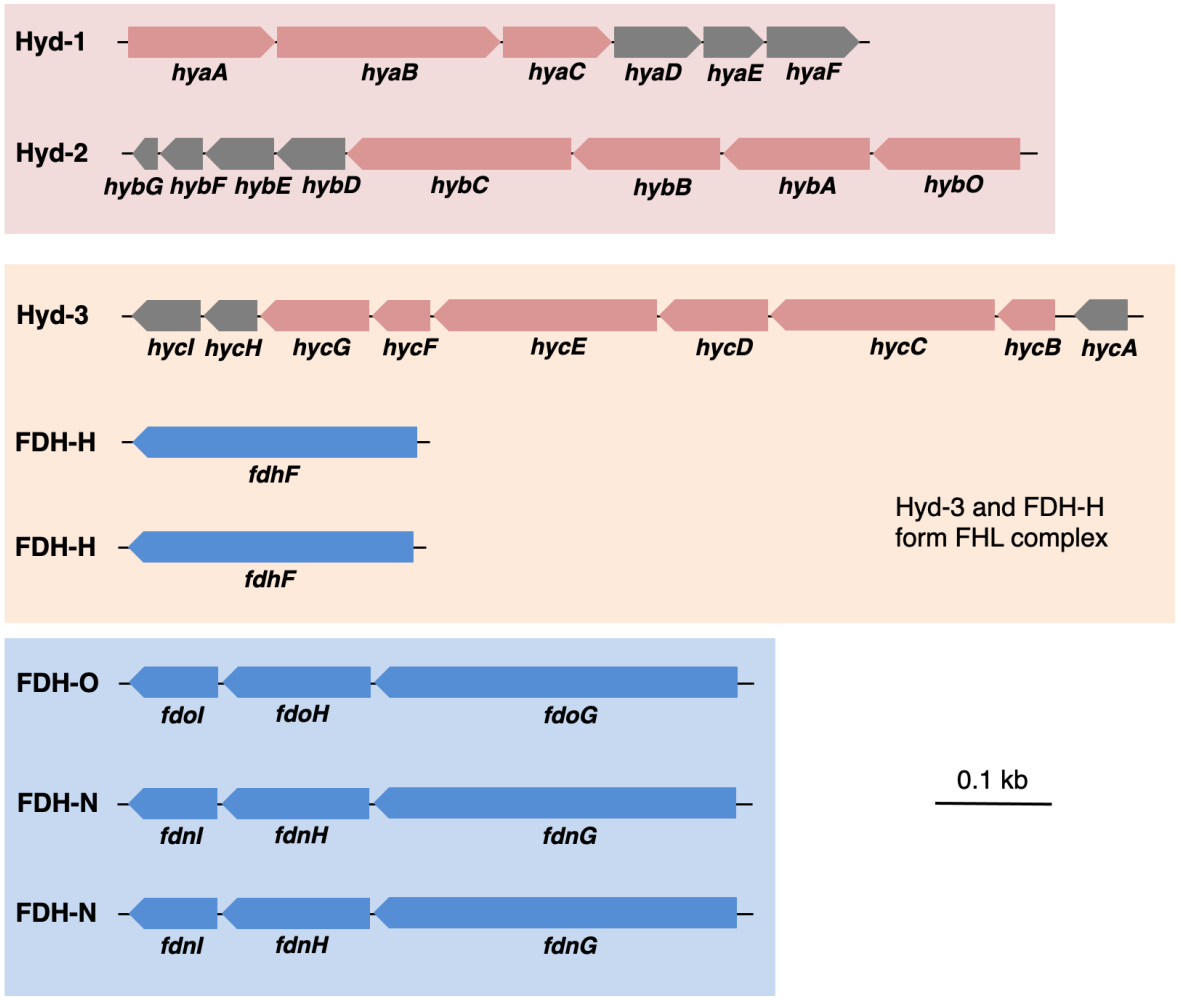

Fig. 1. 8 gene clusters of *Citrobacter* sp. S-77 involving the H_2 and formate metabolisms.

Table 1. Gene clusters of *Citrobacter* sp. S-77 involving the H_2 and formate metabolisms.

enzyme	gene	code
Hyd-1	hyaA	WP_045449661
	hyaB	WP_045443778
	hyaC	WP_045443781
	hyaD	WP_045443784
	hyaE	WP_045443787
	hyaF	WP_045443790
Hyd-2	hybG	WP_003024459
	hybF	WP_045447504
	hybE	WP_045447507
	hybD	WP_045447510
	hybC	WP_045447513
	hybB	WP_045447516
	hybA	WP_045447519
	hybO	WP_045447522
Hyd-3	hycI	WP_045446662
	hycH	WP_003037385
	hycG	WP_045446665
	hycF	WP_045446668
	hycE	WP_045446672
	hycD	WP_045446675
	hycC	WP_045446678
	hycB	WP_045446680
	hycA	WP_045446683

enzyme	gene	code
FDH-O	fdoI	WP_045449236
	fdoH	WP_045449238
	fdoG	WP_144243092
FDH-N	fdnI	WP_045445814
	fdnH	WP_045445817
	fdnG	WP_071829001
FDH-N	fdnI	WP_045442973
	fdnH	WP_045442976
	fdnG	WP_136345514
FDH-H	fdhF	WP_081918179
FDH-H	fdhF	WP_045441935

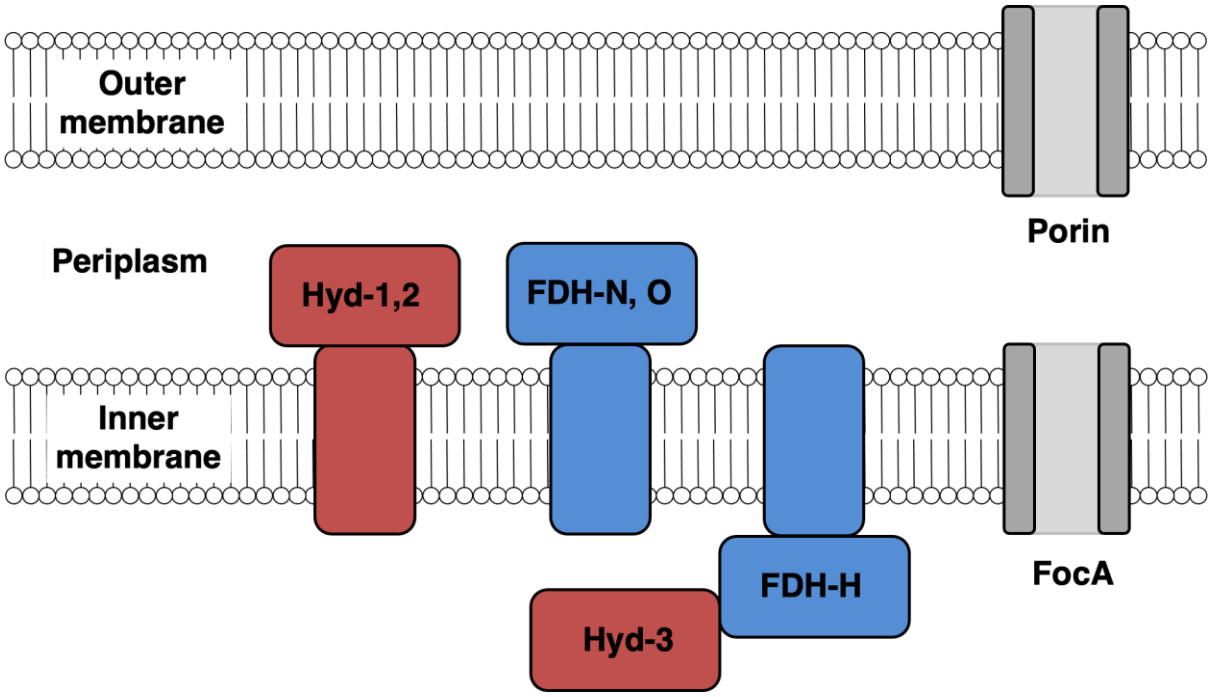

Fig. 2. Schematic representation of the cross-section of the membrane in *Citrobacter* sp. S-77

2.3.2. Enzymes involving H_2 and formate metabolism.

S-77 contains three different membrane-bound [Mo]formate dehydrogenase of FDH-N and FDH-O including FHL fused with two different functional parts of [Mo]formate dehydrogenase and [NiFe]hydrogenase (**Fig. 1**). Initially, to determine the potential activities of H_2 and formate oxidation, the activities of hydrogenase and formate dehydrogenase were determined. The harvested cells were disrupted to separate the soluble cell extracts and insoluble membranes. Then, a spectrophotometric enzyme assay was performed by reducing MV. Consequently, the H_2 oxidation activity of the soluble cell extracts (4.98 $\mu mol \cdot min^{-1} \cdot mg^{-1}$) was higher than that of the membrane (0.36 $\mu mol \cdot min^{-1} \cdot mg^{-1}$), and the formate-oxidation activity of the soluble cell extracts (0.51 $\mu mol \cdot min^{-1} \cdot mg^{-1}$) was also higher than that of the plasma membrane fraction (0.03 $\mu mol \cdot min^{-1} \cdot mg^{-1}$). The enzyme activities of the soluble cell extracts were higher than those of the membrane, indicating that FHL complexes mainly contributed to the formate production in the soluble cell extracts. This result

is in good agreement with previous reports showing that FHL reacts reversibly from CO_2 to formic acid [25,26].

2.3.3. Catalytic CO_2 hydrogenation to formate production

Next, the catalytic reaction using S-77 as the whole-cell biocatalyst was performed in the presence of H_2 and CO_2. The reaction rate of formate production using whole-cells without encapsulation depended on the gas phase condition of CO_2 and H_2 (**Fig. 3**). The optimum CO_2 conversion into formate was observed under a mixed gas condition of H_2:CO_2 (70:30, v/v, %). Notably, there were no detectable peaks of formate production by HPLC analysis in the presence of 100% CO_2 or 100% H_2 alone (**Fig. 3**), indicating that the formate produced was dependent on the substrate level of H_2/CO_2. conditions.

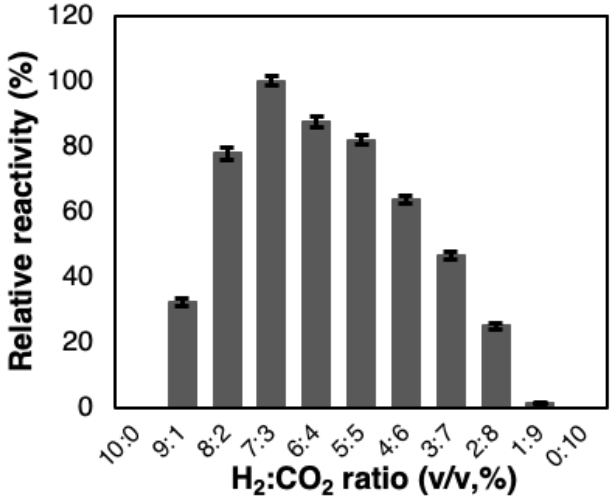

Fig. 3. Formate production dependence on H_2/CO_2 gas ratio

The catalytic reaction was then performed by changing pH values in a range between pH 7.0– pH 9.0. As a result, the maximum yield of formate was observed at pH 8.0, indicating that the reaction is favorable in the weak basic media of pH 8.0 (**Fig. 4**). It may be due to the solvation effect which reduces the entropy gap between CO_2 (g)/H_2 (g) and formic acid in aqueous conditions [5,27]. This effect makes the equilibrium in favor of formic acid formation with negative Gibbs energy ($\Delta_rG° = -4$ kJ·mol^{-1}). When increasing the pH value above 8.0, the

yield of formate decreased presumably because enzymes involving H_2 and formate metabolism are not stable in this pH region [11].

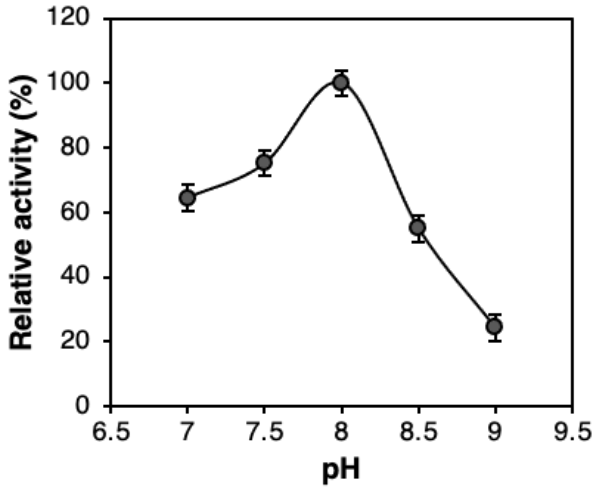

Fig. 4. Formate production dependence on pH conditions.

To elaborate on the effect of pH change caused formate production, catalytic reactions were performed using different concentrations of KP buffers. As a result, the yield of formate production increased with increasing the concentration of KP buffers (**Fig. 5A**).

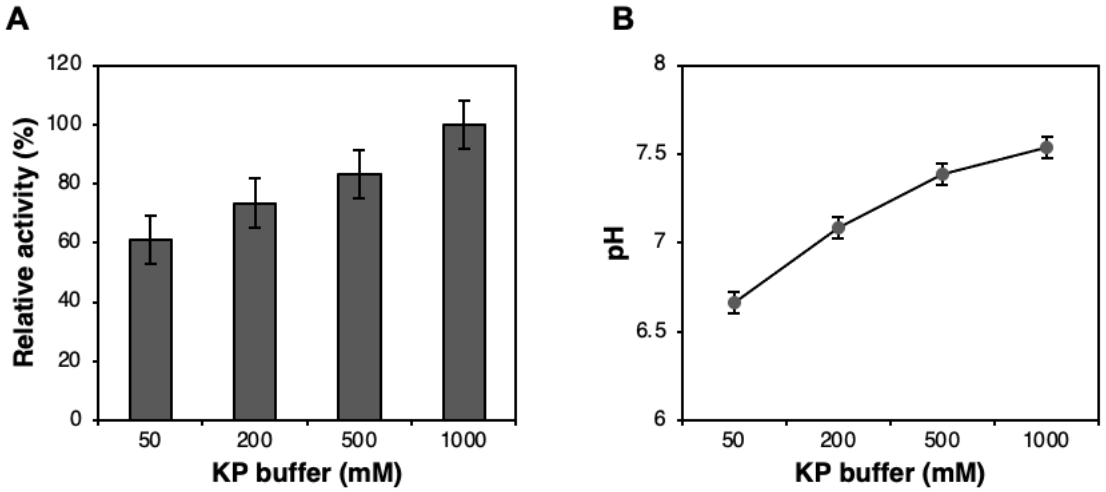

Fig. 5. (A) Formic production under different buffer concentrations at pH 8.0. (B) pH change after 24h of reaction in different pH concentrations.

As the increase in the concentration of KP buffer is in accordance with the decrease in ΔpH value from 8.0 (**Fig. 5B**), the highest yield of formate was observed under the high concentration buffer condition (1000 mM, ΔpH = 0.5). The results suggested that the rate of

formate production decreased as the pH changed during the reaction period (**Fig. 5A, B**). The catalytic activity was also dependent on the protein concentration of S-77 (**Fig. 6**).

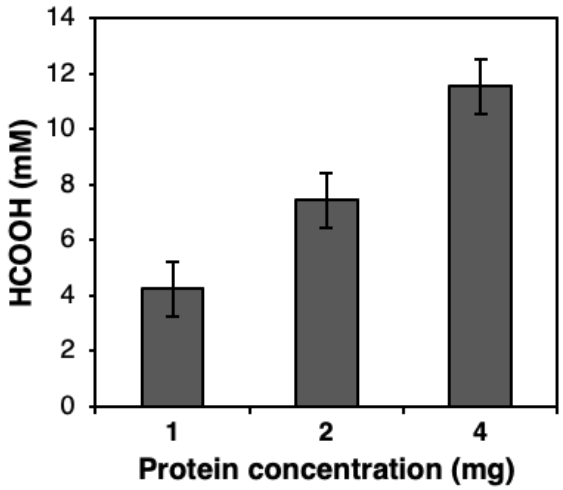

Fig. 6. Formate production rate depended on the protein concentration of S-77 cells.

2.3.4. HPLC and NMR analyses of reaction production

To characterize reaction products after H_2-driven CO_2 reduction using whole-cell S-77, HPLC and NMR spectral analysis of the reaction solution in 200 mM KP buffer (pH 7.0) were conducted. HPLC analysis of the reaction solution showed that only one peak assignable to formic acid was observed as a reaction product (**Fig. 7**).

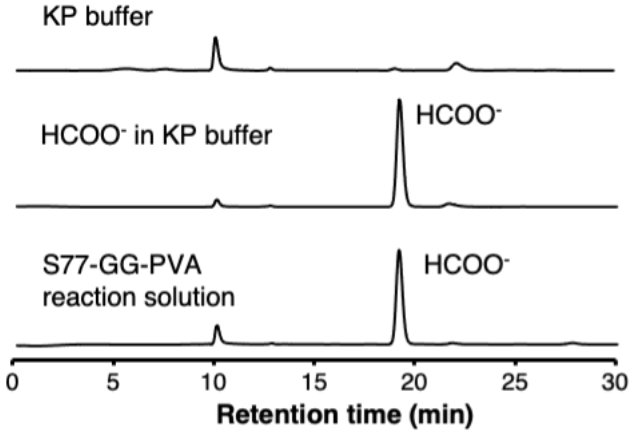

Fig. 7. HPLC analysis of the reaction solution after 24 h.

The ^{1}H NMR spectrum prepared with deuterium oxide revealed one single peak at 8.35 ppm, which was assigned to the α-hydrogen of the carboxyl group of $HCOO^-$ (**Fig. 8**). The ^{13}C

NMR spectrum showed three signals at 170.9, 160.2, and 124.6 ppm assignable to the carbon atoms of $HCOO^-$, HCO_3^-, and CO_2, respectively (**Fig. 9**), where the triplet signal of formate was due to the exchange reaction of H and D [28].

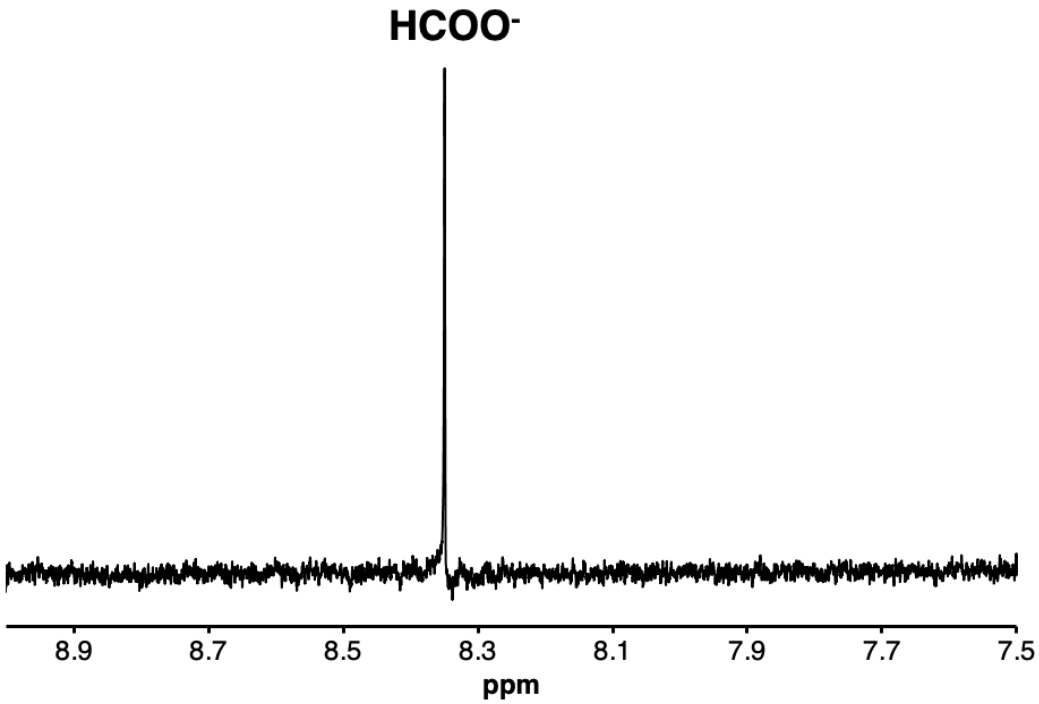

Fig. 8. ^{1}H NMR spectra of the reaction solution after 24 h

These results clearly illustrated that S-77 could catalyze the hydrogenation of CO_2 to yield only formate, while other biocatalytic systems have been reported to form succinate, lactate, and acetate together with formate [8,19,29]. To confirm the carbon source of formic acid formation, 200 mM $NaH^{13}CO_3$ was added to the reaction solution as a carbon source after bubbling with Ar (>200 mL·min^{-1}) and H_2 (>140 mL·min^{-1}). Isotopic labeling experiments were performed with ^{13}C-labeled $NaH^{13}CO_3$ as a sole carbon source. As a result, an apparent peak of ^{13}C-formate was detected at 170.9 ppm, corresponding to the splitting of the ^{13}C-formate signal (**Fig. 10**). This result showed that the carbon source of formate production is carbon dioxide.

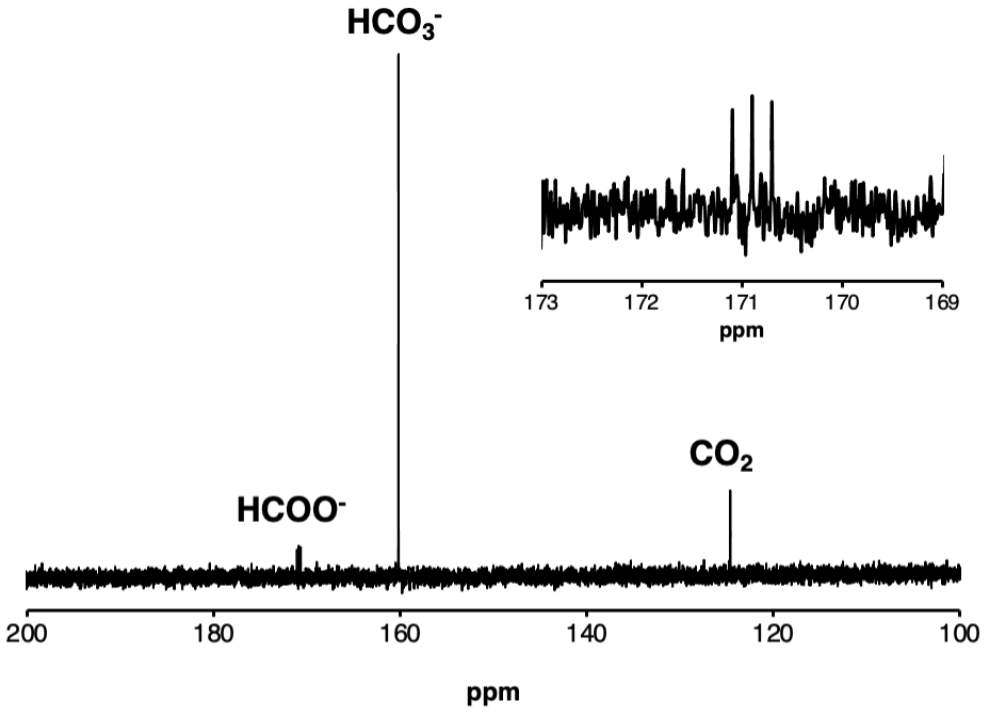

Fig. 9. ^{13}C NMR spectra of the reaction solution after 24 h. Inset: enlarged spectrum of the formate signal.

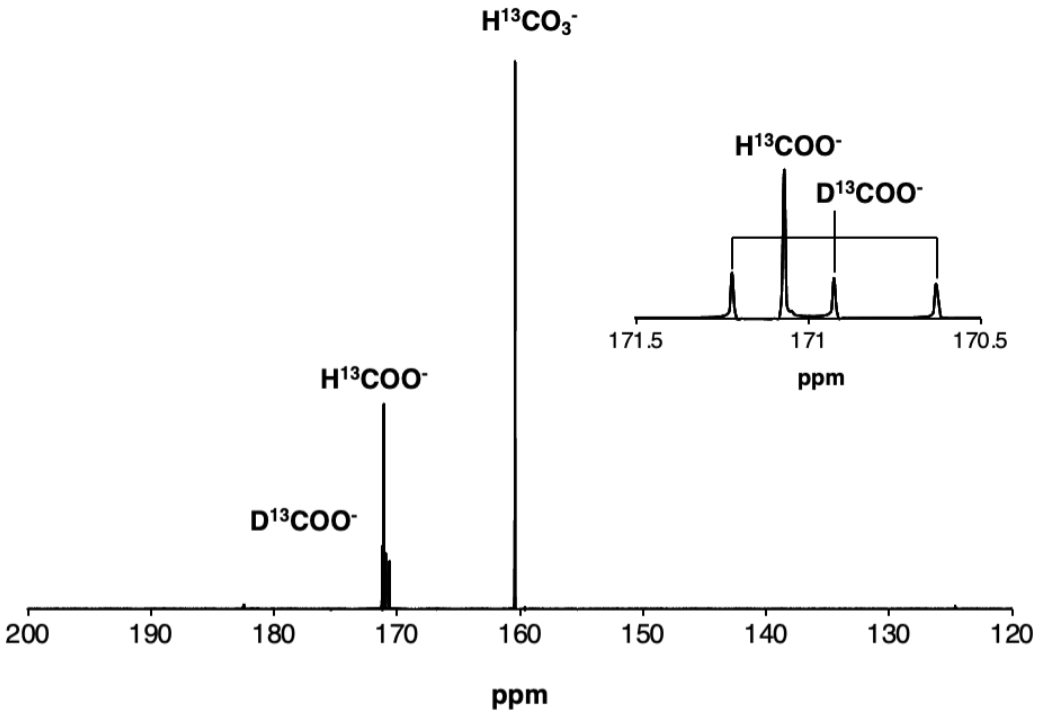

Fig. 10. ^{13}C NMR spectrum of the ^{13}C-formate production from the H_2-driven CO_2 reduction with $NaH^{13}CO_3$ as a sole carbon source after 24 h reaction. Inset: enlarged spectrum of the ^{13}C-formate signal.

Notably, the reaction using S-77 reached the formate concentration of 2.62 $mol \cdot L^{-1} \cdot g_{protein}^{-1}$ for 24 h at 30°C, pH 7.0, and 0.1 MPa with the reaction rate of 110 $mmol \cdot L^{-1} \cdot g_{protein}^{-1} \cdot h^{-1}$, which is comparable to that of whole-cell biocatalyst of *Desulfovibrio desalfuricans* [8]. In addition, the correlation between enzyme activity and H_2/CO_2 concentration was determined (**Fig. 11**); the concentrations of H_2 and CO_2 were calculated based on the solubility of the gases at 30°C [30]. The K_m values of H_2 and CO_2 for formate production were estimated as 0.235 mM and 1.94 mM, respectively. The K_m value for H_2 was reported to be higher than that of hydrogen-dependent CO_2 reductase (HDCR) [31]. The result indicated that the production of formic acid from H_2 and CO_2 efficiently proceeded under the mild reaction condition.

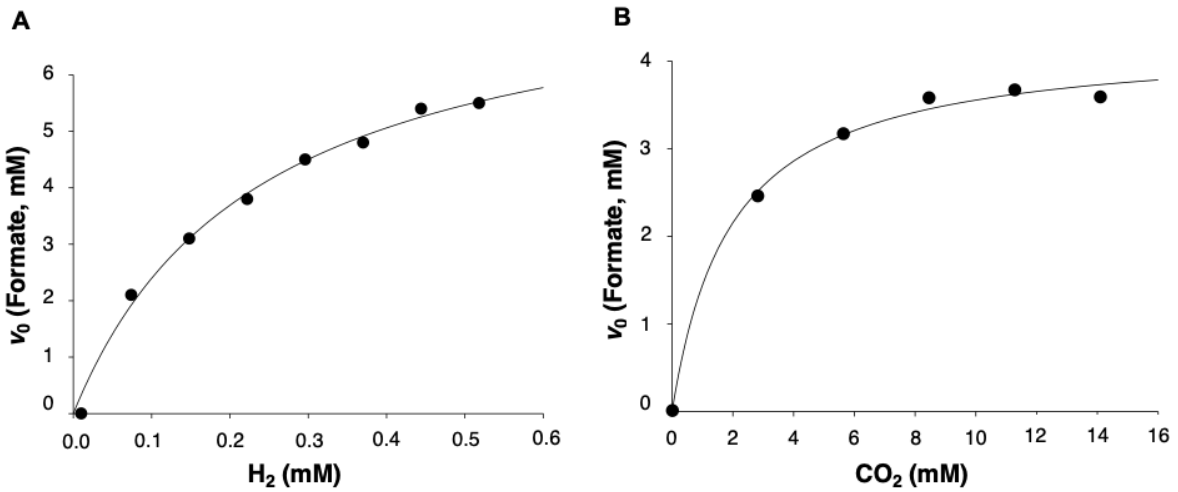

Fig. 11. Determination of K_m values for (A) H_2 and (B) CO_2 in the GG/PVA/S-77 catalyst system. Steady-state kinetic parameters were determined at 30 °C, pH 7.0 in the assay buffer. The detailed assay conditions were described in the Materials and methods. The obtained data were fitted to the Michaelis-Menten equation using nonlinear regression. The kinetic parameters of the enzyme were obtained as five different experimental data.

In addition, S-77 was removed by centrifugation during the catalytic reaction to verify whether the observed catalysis was intrinsically heterogeneous. As expected, the reaction was completely stopped after removing S-77 (**Fig. 12A**), and the ^1H and ^{13}C NMR spectra of the reaction solution showed no signals assignable to organic components of the cell including proteins. These results indicated that observed catalysis was truly heterogeneous.

Furthermore, the catalytic ability of S-77 in the presence of O_2 was investigated. When adding 1.1 μM of O_2 in the reaction solution, formate production was observed after 2 h with an induction period at the initial stage of the reaction (0–1 h), presumably because Hyds firstly catalyzed the reduction of O_2 to H_2O (**Fig. 12B**) [14]. This result was in good agreement with the previous study which showed the isolated Hyd and FDH from S-77 required some preincubation time to recover the original specific activities when these enzymes were exposed to O_2 [10,11]. Because of the O_2 stabilities of these enzymes, the catalytic hydrogenation of CO_2 successfully started even in the presence of O_2 after 1 h induction period (**Fig. 12B**). This result showed that the production of formate was initiated after the presence of O_2 in the reaction solution was consumed.

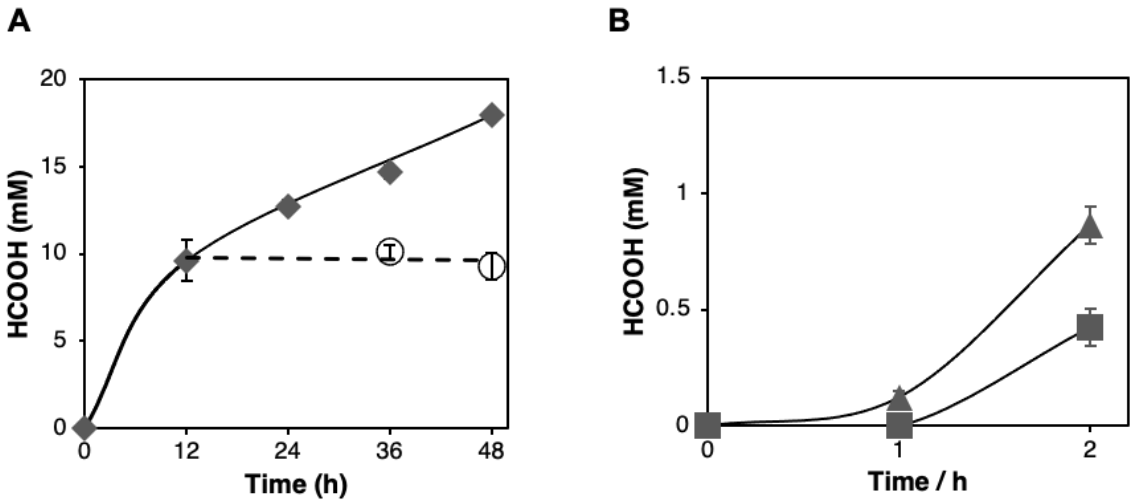

Fig. 12. (A) Biocatalytic hydrogenation of CO_2 using S-77 (blue rhombus). White circles represent formate concentrations when removing S-77 from the reaction solution. (B) The initial stage of the reaction is in the absence of O_2 (blue triangles) and in the presence of O_2 (blue squares).

The bacterial cells of *E. coli* also selectively produce formate by using FHL and FocA [19]. However, the living cell system of *E. coli* requires a constant flow of H_2 and CO_2 at high pressure (10 bars) for the cells to grow and continuously produce formate. On the other hand, in the GG/PVA/S-77 catalytic system, the hydrogenation of CO_2 efficiently proceeded under

very mild reaction conditions at 30°C, pH 7.0, and 0.1 MPa. The cultural system using whole-cell catalyst has a multi-step reaction to regenerate coenzymes of electron carriers and isolate purpose materials from products. More importantly, the continuous reusability of the living cell system has been an issue as living cells are easy to be damaged when collecting and washing. Additionally, traditional living-cell-based catalytic reactions are either liquid-phase homogeneous systems or liquid-solid-phase heterogeneous systems, making it challenging to build long-lasting stable catalytic reaction systems. For example, although the engineered *E. coli* has a high formate production rate of 1 $g \cdot L^{-1} \cdot h^{-1}$, this system can be reused only 3 times [32].

2.3.5. Encapsulation of whole-cells in hydrogel beads

To develop a robust and reusable system of microbial CO_2 hydrogenation for formate production, we designed an encapsulated resting-state bacterial cell by utilizing natural and synthetic polymers of GG and PVA. Because of the high hydrophilicity and biocompatibility of GG and PVA, hydropolymers are widely recognized as materials for pharmaceutical and biotechnology applications [33,34]. In this study, hydrogel beads (GG/PVA), which are cross-linked and polymerized from GG and PVA with calcium ions (Ca^{2+}), were used to encapsulate the whole-cells S-77 for catalytic CO_2 hydrogenation. The synthetic polymer of PVA is a physically or chemically cross-linked three-dimensional network polymer with high hydrophilicity, elasticity, and microporous structure [34]. The microcapsules by the chemical cross-linking of PVA and GG with Ca^{2+} allow the bacterial cells to be trapped in the network and protect cells from leakage and physical damage. In the resting state, the encapsulated cells were not observed to grow by the anionic polysaccharide GG. More significantly, the encapsulated cells don't require bacterial culture and extraction steps to isolate the produced formate under the anaerobic gas phase of H_2 and CO_2 conditions. In this system, FocA can also

efficiently function as a formate exporter via a cytoplasmic membrane to obtain pure formate. The preparation of GG/PVA/S-77 was carried out in two sequential steps. The harvested cells were mixed with PVA, and then, the resulting mixture was entrapped by gellan gum. To observe the morphology of GG/PVA/S-77 and the distribution of cells in hydrogels, the hydrogels of GG beads, GG/PVA beads, and GG/PVA/S-77 beads were characterized by SEM. The SEM images of GG/PVA beads showed an irregular gully shape consisting of open pores with diameters ranging from 1 to 2 μm, while these open pores were not observed in the GG beads (**Fig. 13A, 13B**). As the cell size of typical gram-negative rod bacteria of *Citrobacter* species is approximately 1-1.5 μm long and radius of 0.5 μm [35], it is thought that open pores in GG/PVA beads can act as suitable pockets to fit S-77 cells. The SEM image of GG/PVA/S-77 showed that S-77 cells were encapsulated into the GG/PVA beads with high density (**Fig. 13C, 13D**). This immobilization method has advantages in the aspect of practical application because materials used in the study are inexpensive, abundant, and environmentally benign, and the reaction proceeds under very mild reaction conditions. Therefore, the whole-cell microsphere using PVA and GG hydrophilic polymers appears to be a simple and promising method for developing effective heterogeneous biocatalysts.

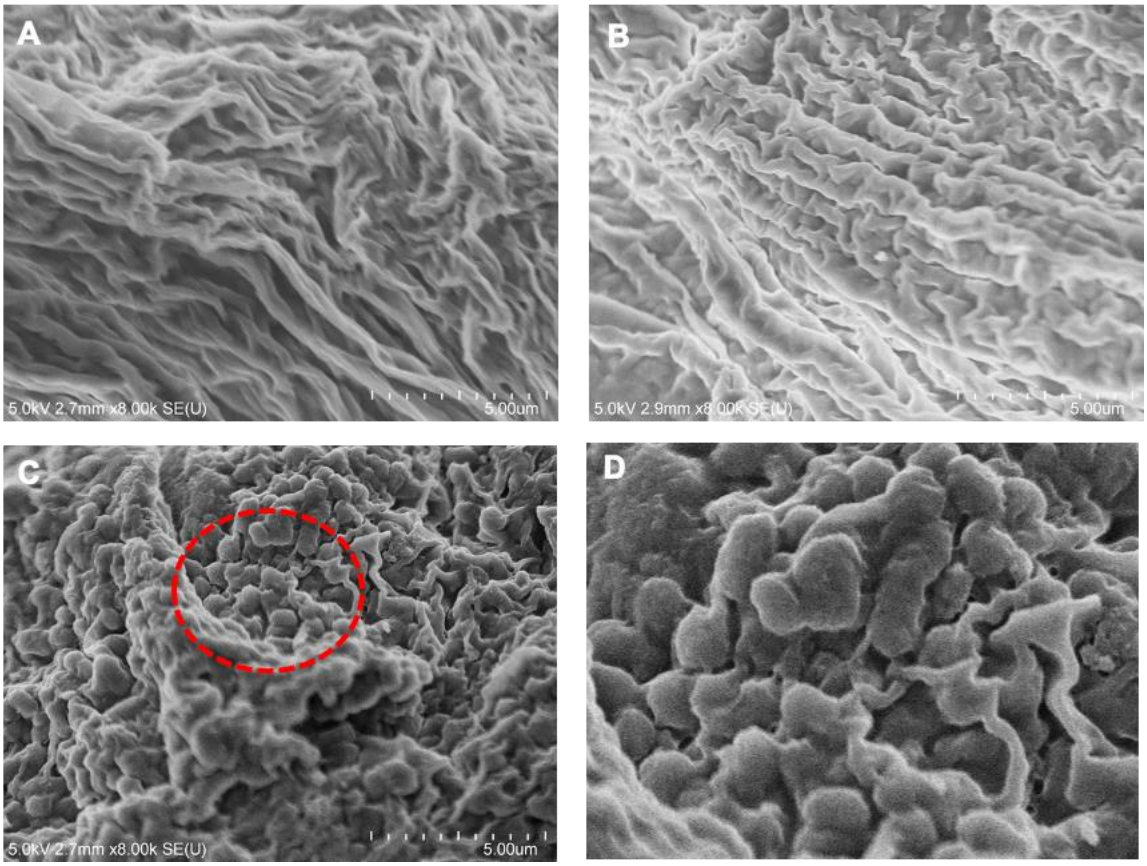

Fig. 13. SEM images of hydrogel beads (A) GG only, (B) GG/PVA, (C) GG/PVA/S-77 cells after drying with ethanol, (D) Enlargement of red circle Fig. 7C.

2.3.6. Reusability of the encapsulated whole-cell biocatalyst

Next, the catalytic reaction using encapsulated cells as whole-cell biocatalysts was performed in the presence of H_2 and CO_2 under mild reaction conditions at 30°C, pH 7.0, and 0.1 MPa. The reaction proceeded efficiently just after flowing the gas mixture when using S-77, whereas the induction period was observed when using GG/PVA/S-77 due to the impediment of H_2 and CO_2 gas accessibility and solubility in the hydrogel beads. The reaction rate of formate production after 2 h using GG/PVA/S-77 (0.40 $mmol \cdot L^{-1} \cdot h^{-1}$) was almost the same as that using nonencapsulated S-77 (0.43 $mmol \cdot L^{-1} \cdot h^{-1}$) (**Fig. 14A**). In addition, catalytic

activities of GG/PVA/S-77 after 24 h did not change by the encapsulation of S-77 (**Fig. 14B**) and remained active after 96 h of incubation (**Fig. 14C**).

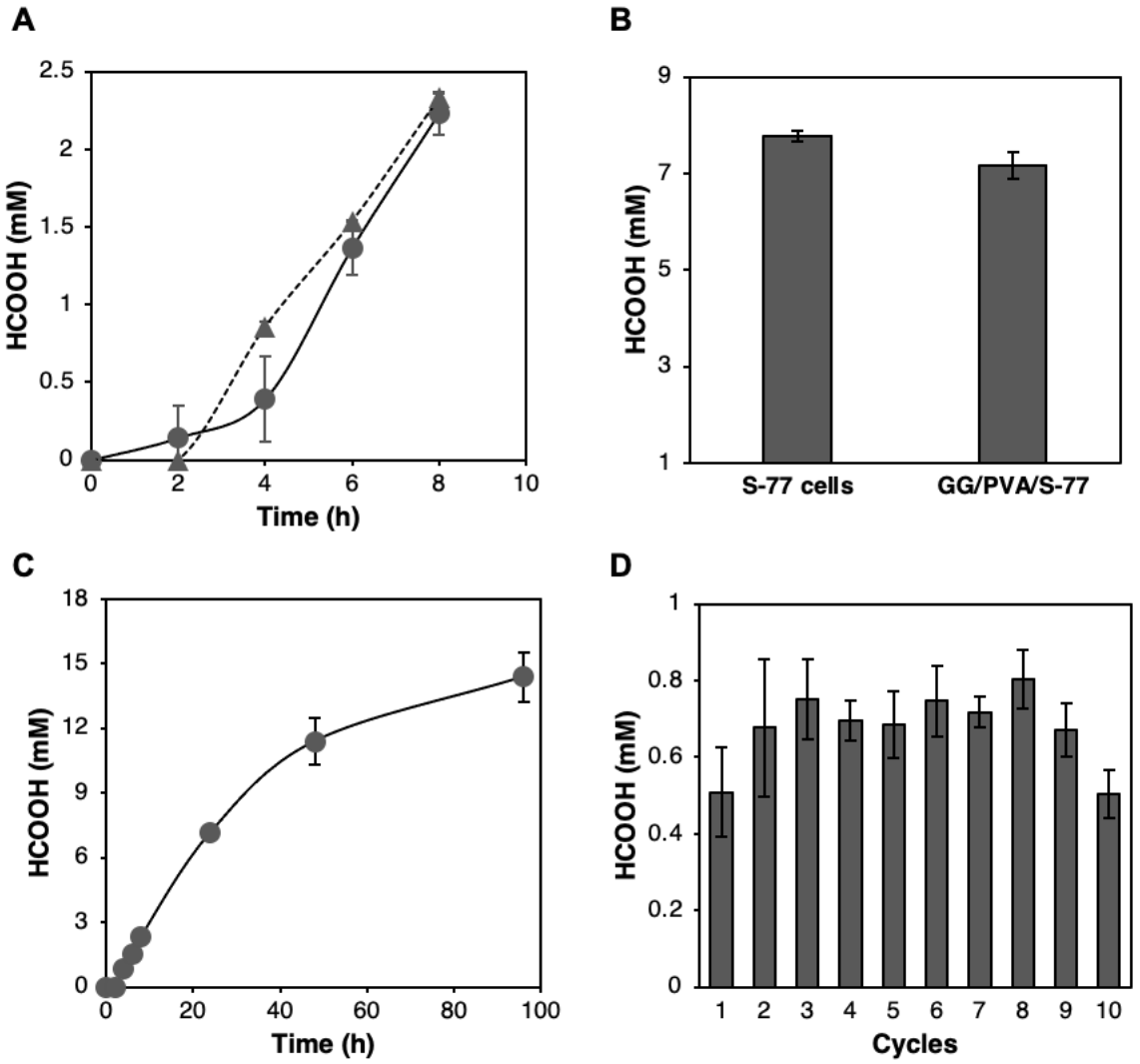

Fig. 8. (A) Time-dependent production of formate in nonencapsulated S-77 (black circles, black line) and GG/PVA/S-77 (black triangles, dashed line). (B) Comparable formate production rate of nonencapsulated S-77 cells and encapsulated GG/PVA/S-77 after the reaction of 24 h. (C) Formate production of GG/PVA/S-77 after 96 h of incubation. (D) Reusability of GG/PVA/S-77.

Since S-77 acts as heterogeneous catalysts, a reuse experiment was then examined. Each reaction was evaluated for 3 h, and GG/PVA/S-77 was utilized repeatedly after washing with 200 mM KP buffer. As a result, the encapsulated whole-cell catalysts could be reused at least 8 times while keeping their high catalytic activities in formate production (**Fig. 14D**). The

encapsulated hydrogel was gradually decomposed after 9th reuse, resulting in a decrease in formate production (**Fig. 15**). Based on these results, the encapsulated biocatalysts with GG/PVA hydrogels have a high capability for heterogeneous catalytic and highly selective formate production with excellent reusability. This aligns with the fact that the immobilization of living cells is effective in enhancing stability by providing a protective environment for the prolonged survival and metabolic activity of encapsulated cells [36]. To our knowledge, this is the first example of encapsulated whole-cell catalysts for the use of CO_2 reduction into formate under the resting state condition that can selectively produce formate with high reusability.

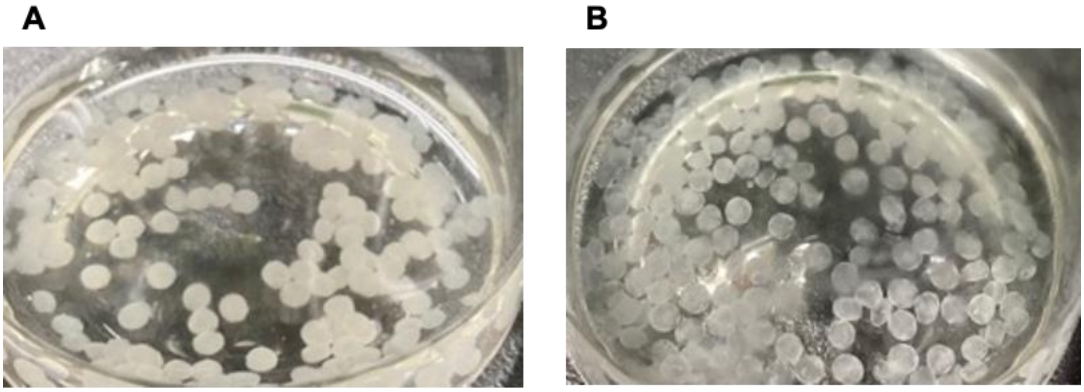

Fig. 15. (A) Image of hydrogel beads after the first reaction of GG/PVA/S-77 and (B) Image of hydrogel beads after the 10th reuse.

2.4. Conclusion

In conclusion, this study highlights the first investigation of formate production using the encapsulated whole-cell S-77 in hydrogels by cross-linked polymer networks of GG, PVA, and Ca^{2+}. Based on the experimental results, GG/PVA/S-77 as a heterogeneous catalyst efficiently catalyzed the hydrogenation of CO_2 to yield formate. This system has great advantages, such as the encapsulated resting cells producing only formate from H_2 and CO_2 without any byproducts under very mild conditions, and the encapsulated cells in hydrogels as a spatially heterogeneous catalyst practically prove to be robust to reuse several times without

losing catalytic activity. The study described here provides new insight into the encapsulation of bacterial cells in the hydrogel with high structural stability, which is expected to allow clean bioenergy generation as practical industrial biocatalysts.

2.5. References

[1] J. Eppinger, K. W. Huang, *ACS Energy Lett* **2017**, *2*, DOI 10.1021/acsenergylett.6b00574.

[2] A. Álvarez, A. Bansode, A. Urakawa, A. V. Bavykina, T. A. Wezendonk, M. Makkee, J. Gascon, F. Kapteijn, *Chem Rev* **2017**, *117*, DOI 10.1021/acs.chemrev.6b00816.

[3] G. H. Gunasekar, K. Park, K. D. Jung, S. Yoon, *Inorg Chem Front* **2016**, *3*, DOI 10.1039/c5qi00231a.

[4] N. Onishi, G. Laurenczy, M. Beller, Y. Himeda, *Coord Chem Rev* **2018**, *373*, DOI 10.1016/j.ccr.2017.11.021.

[5] R. Sun, Y. Liao, S. T. Bai, M. Zheng, C. Zhou, T. Zhang, B. F. Sels, *Energy Environ Sci* **2021**, *14*, DOI 10.1039/d0ee03575k.

[6] Y. S. Anteneh, C. M. M. Franco, *Front Microbiol* **2019**, *10*, DOI 10.3389/fmicb.2019.00077.

[7] K. Schuchmann, V. Müller, *Science (1979)* **2013**, *342*, DOI 10.1126/science.1244758.

[8] F. M. Schwarz, V. Müller, *Biotechnol Biofuels* **2020**, *13*, DOI 10.1186/s13068-020-1670-x.

[9] M. Roger, T. C. P. Reed, F. Sargent, *Appl Environ Microbiol* **2021**, *87*, DOI 10.1128/AEM.00299-21.

[10] S. Eguchi, K. S. Yoon, S. Ogo, *J Biosci Bioeng* **2012**, *114*, DOI 10.1016/j.jbiosc.2012.05.018.

[11] N. T. Nguyen, T. Yatabe, K. S. Yoon, S. Ogo, *J Biosci Bioeng* **2014**, *118*, DOI 10.1016/j.jbiosc.2014.03.011.

[12] A. B. Waight, J. Love, D. N. Wang, *Nat Struct Mol Biol* **2010**, *17*, DOI 10.1038/nsmb.1740.

[13] M. Kammel, R. Gary Sawers, *Microbiology (United Kingdom)* **2022**, *168*, DOI 10.1099/mic.0.001168.

[14] N. D. M. Noor, H. Matsuura, K. Nishikawa, H. Tai, S. Hirota, J. Kim, J. Kang, M. Tateno, K. S. Yoon, S. Ogo, S. Kubota, Y. Shomura, Y. Higuchi, *Chemical Communications* **2018**, *54*, DOI 10.1039/c8cc06261g.

[15] P. M. Vignais, B. Billoud, *Chem Rev* **2007**, *107*, DOI 10.1021/cr050196r.

[16] W. Lubitz, H. Ogata, O. Rüdiger, E. Reijerse, *Chem Rev* **2014**, *114*, DOI 10.1021/cr4005814.

[17] F. Sargent, in *Adv Microb Physiol*, **2016**.

[18] A. J. Finney, F. Sargent, *Adv Microb Physiol* **2019**, *74*, DOI 10.1016/bs.ampbs.2019.02.004.

[19] M. Roger, F. Brown, W. Gabrielli, F. Sargent, *Current Biology* **2018**, *28*, DOI 10.1016/j.cub.2017.11.050.

[20] Y. Wang, Y. Huang, J. Wang, C. Cheng, W. Huang, P. Lu, Y. N. Xu, P. Wang, N. Yan, Y. Shi, *Nature* **2009**, *462*, DOI 10.1038/nature08610.

[21] W. Lü, J. Du, N. J. Schwarzer, T. Wacker, S. L. A. Andrade, O. Einsle, *Biol Chem* **2013**, *394*, DOI 10.1515/hsz-2012-0339.

[22] M. Mukherjee, A. Gupta, R. Sankararamakrishnan, *Biophys J* **2020**, *118*, DOI 10.1016/j.bpj.2019.12.024.

[23] K. Peters, F. Sargent, *Biochim Biophys Acta Bioenerg* **2023**, *1864*, DOI 10.1016/j.bbabio.2022.148919.

[24] M. Masi, M. Winterhalter, J. M. Pagès, in *Subcell Biochem*, **2019**.

[25] C. Pinske, F. Sargent, *Microbiologyopen* **2016**, *5*, DOI 10.1002/mbo3.365.

[26] R. Steinhilper, G. Höff, J. Heider, B. J. Murphy, *Nat Commun* **2022**, *13*, DOI 10.1038/s41467-022-32831-x.

[27] P. G. Jessop, F. Joó, C. C. Tai, *Coord Chem Rev* **2004**, *248*, DOI 10.1016/j.ccr.2004.05.019.

[28] S. Moret, P. J. Dyson, G. Laurenczy, *Nat Commun* **2014**, *5*, DOI 10.1038/ncomms5017.

[29] A. Alissandratos, C. J. Easton, *Beilstein Journal of Organic Chemistry* **2015**, *11*, DOI 10.3762/bjoc.11.259.

[30] G. W. C. Kaye, T. H. Laby, *Zeitschrift fur Kristallographie - New Crystal Structures* **1997**, *212*, DOI 10.1524/zkri.1997.212.5.400.

[31] F. M. Schwarz, K. Schuchmann, V. Müller, *Biotechnol Biofuels* **2018**, *11*, DOI 10.1186/s13068-018-1236-3.

[32] A. Alissandratos, H. K. Kim, C. J. Easton, *Bioresour Technol* **2014**, *164*, DOI 10.1016/j.biortech.2014.04.064.

[33] A. Baawad, C. Rice, T. Hamil, K. Murphy, J. Park, D. S. Kim, *J Food Sci* **2021**, *86*, DOI 10.1111/1750-3841.15887.

[34] L. Shao, Y. Li, Z. Ma, Y. Bai, J. Wang, P. Zeng, P. Gong, F. Shi, Z. Ji, Y. Qiao, R. Xu, J. Xu, G. Zhang, C. Wang, J. Ma, *ACS Appl Mater Interfaces* **2020**, *12*, DOI 10.1021/acsami.0c07717.

[35] R. Qiu, B. Zhao, J. Liu, X. Huang, Q. Li, E. Brewer, S. Wang, N. Shi, *J Hazard Mater* **2009**, *164*, DOI 10.1016/j.jhazmat.2008.09.039.

[36] J. M. Guisan, *Immobilization of Enzymes and Cells* **2013**, *1051*.

Chapter 3

H_2-driven reduction of CO_2 to formate using bacterial plasma membranes.

(*Bioresour. Technol.*, **2023**, 390, 129921)

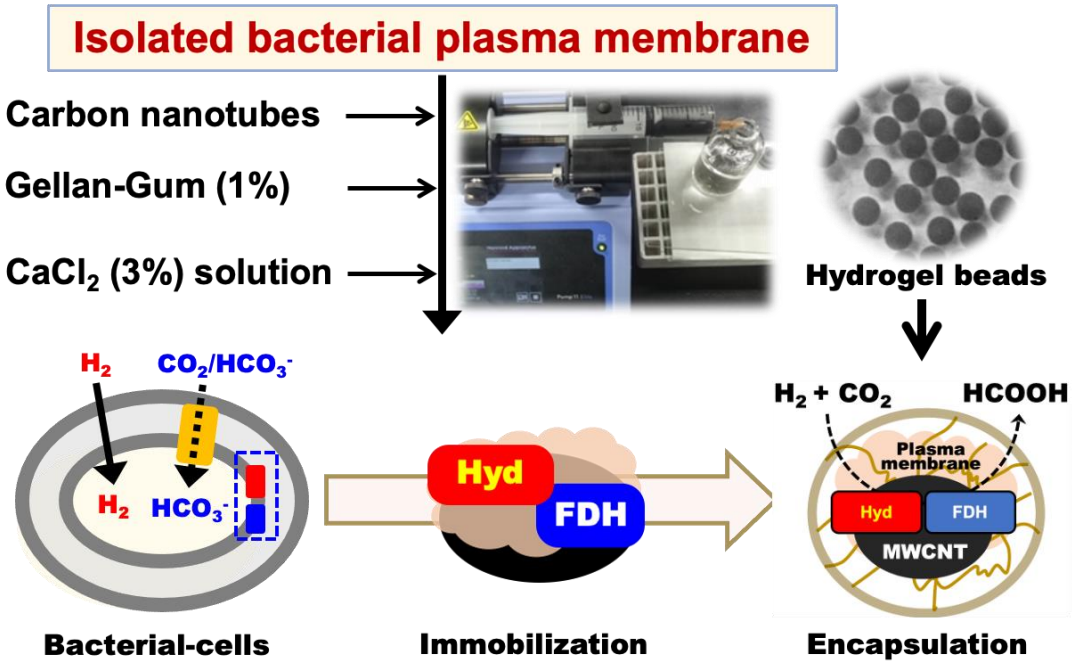

ABSTRACT

Bacterial membranes shield the intracellular compartment by selectively allowing unwanted substances to enter, which in turn reduces overall catalytic efficiency. This report presents a model system using the isolated plasma membranes of *Citrobacter* sp. S-77 harbors oxygen-stable [NiFe] hydrogenase and [Mo] formate dehydrogenase, which is integrated into a natural catalytic nanodevice through an electron transfer relay. This naturally occurring nanodevice exhibited selectivity and efficiency in catalyzing the H_2-driven conversion of CO_2 to formate with the rate of 816.7 $mmol \cdot L^{-1} \cdot g_{protein}^{-1} \cdot h^{-1}$ under mild conditions of 30°C, pH 7.0, and 0.1 MPa. When the isolated plasma membranes of *Citrobacter* sp. S-77 was immobilized with multi-walled carbon nanotubes and encapsulated in hydrogel beads of gellan-gum cross-linked with calcium ions, the catalyst for formate production remained stable over at least ten repeated uses, representing the first case of efficient and selective formate production from H_2 and CO_2 using bacterial plasma membranes.

3.1 Introduction

The development of efficient systems to reduce CO_2 into useful fuels is considered one of the most important catalytic reactions. Among them, the conversion of CO_2 into formate has received increased attention because of the growing importance of carbon abatement technologies, efficient hydrogen energy carriers, and carbon-neutral chemical feedstocks [1]. Many synthetic catalyst-based technologies that achieve high reaction efficiency through electrochemistry or photochemistry rely on precious metals and volatile organic solvents, meaning that high costs, environmental vulnerability, and low product selectivity are challenges for these technologies [2–4]. Biocatalysts are attracting significant attention as they overcome these issues due to their exceptional catalytic efficiency, substrate or product selectivity, and environmental viability, and numerous investigations on the biocatalytic hydrogenation of CO_2 into formate utilizing living bacteria are underway [5–10]. The outer membrane of whole-cells prevents the entry of toxic compounds and maintains structural integrity; however, it also imposes a significant barrier to substrate entry, meaning that the catalytic performance of a whole-cell can be 10–100 times slower than that of free enzymes [11,12]. Additionally, although non-charged molecules such as H_2 and N_2 can freely pass through the cell membrane, HCO_3^- ions, which form readily from CO_2 in water, cannot permeate the outer membrane. This is because stagnant water layers, known as unstirred layers, develop directly outside of the outer membrane of whole-cell bacteria [13,14]. Thus, enhancing the biocatalytic systems of whole-cells is challenging, even with the application of artificial engineering [11,12]. In contrast, the isolated plasma membrane can be manipulated by the oriented immobilization of membrane-bound enzymes for maintained functionality and catalytic activity. It was hypothesized that the enzyme-bound plasma membrane could directly catalyze reactions of the substrates H_2 and CO_2, thus enabling the construction of an efficient and selective system for formate production. By removing unwanted proteins and cellular

debris bound to the outer membrane, the active sites of the membrane-bound [NiFe] hydrogenase and [Mo] formate dehydrogenase enzymes will be more accessible to substrates, improving the specificity of the catalytic reaction and the efficiency of selective formate production. This innovative approach provides exciting new possibilities for the development of an enzyme-based system for CO_2 hydrogenation- using isolated plasma membrane.

Chapter 2 has demonstrated the H_2-driven reduction of CO_2 into formate using immobilized resting-cells of *Citrobacter* sp. S-77 showed highly efficient and selective catalytic production of formate under ambient conditions [15]. The encapsulated resting cells with water-soluble polymers of gellan gum (GG) and polyvinyl alcohol can selectively and efficiently produce formate from CO_2 and H_2 under ambient conditions. However, it has been challenging to engineer a bacterial system for the H_2-driven reduction of CO_2 using encapsulated living cells while maintaining catalytic activity. Therefore, chapter 3 describes the development of a novel system involving isolated plasma membranes of *Citrobacter* sp. S-77 (S77PM) for efficient and selective formate production by H_2-dependent direct reduction of CO_2. The S77PM can efficiently and selectively produce formate under ambient conditions without any external mediator. This bacterial membrane system serves as a model for the hydrogenation of CO_2 to produce formate and offers a promising alternative to the conventional approaches of whole-cell biocatalysts, artificial membrane photocatalysts, or electrochemical catalysts.

3.2. Materials and Methods

3.2.1. Chemicals

Yeast extract powder and hipolypepton were purchased from Funakoshi Co., Ltd. (Japan). Magnesium sulfate heptahydrate ($MgSO_4 \cdot 7H_2O$) and nickel(II) chloride hexahydrate ($NiCl_2 \cdot 6H_2O$) were purchased from Sigma-Aldrich (Japan). Dipotassium hydrogen phosphate

(K_2HPO_4), potassium hydrogen phosphate (KH_2PO_4), sodium chloride (NaCl), ammonium sulfate $(NH_4)_2SO_4$), sodium formate (HCOONa), D(+)-glucose, ammonium iron(III) citrate, brown, calcium chloride ($CaCl_2$), sodium hydroxide (NaOH), sodium tungstate(VI) dihydrate ($Na_2WO_4 \cdot 2H_2O$), disodium molybdate(VI) dihydrate ($Na_2MoO_4 \cdot 2H_2O$), sodium selenite ($Na_2S_2O_3$), gellan gum (GG), (±)-dithiothreitol (DTT), 2-amino-2-hydroxymethyl-1,3-propanediol hydrochloride (Tris·HCl), sodium bicarbonate ($NaHCO_3$), and multi-walled carbon nanotubes (MWCNTs, 20 ~ 30 nm) were purchased from FUJIFILM Wako Pure Chemical Corporation (Japan). Deuterium oxide (D_2O) and ^{13}C-sodium bicarbonate ($NaH^{13}CO_3$) were purchased from Cambridge Isotope Laboratories (USA). All chemical reagents were used as received unless otherwise specified.

3.2.2. Cell culture

Citrobacter sp. S-77 cells were grown in 20-L plastic bottles at 30°C for 5 days with the supplements of the following reagents (g/L): 3.0 g yeast extract, 3.0 g hipolypeptone, 0.5 g $MgSO_4 \cdot 7H_2O$, 2.0 g K_2HPO_4, 1.0 g KH_2PO_4, 3.0 g $(NH_4)_2SO_4$, 1.0 g (±)-D-glucose, 2.0 g HCOONa, 0.2 g ammonium iron(III) citrate, and 0.1 g of $CaCl_2$ and the minor mineral components of 0.1 μM $NiCl_2$, 0.1 μM Na_2WO_4, 0.1 μM Na_2MoO_4, and 0.2 μM $Na_2Se_2O_3$ (as of the final concentration of the medium at pH 7.0). Collected cells (wet weight, 42.0 g) were suspended in 20 mM potassium phosphate (KP) buffer (pH 7.0) containing 1.0 mM DTT and 0.1 mM NaCl, used as a standard buffer in this study.

3.2.3. Preparation of plasma membrane

The collected cells were disrupted by sonication three times for 6 min with an interval of 3 minutes in an ice bath at 60 W with an Ultrasonic Disruptor UD-200 (Tomy Seiko Inc., Tokyo, Japan). The broken cells were centrifuged at 2000 *g* for 20 min to remove cell debris

and unbroken cells. The resulting supernatant was further subjected to ultracentrifugation (Optima L-90K, Beckman Coulter Inc., Brea, CA, USA) at 100,000 *g* for 1 h, at 4°C to give the membrane and soluble cell extracts. The harvested membrane was suspended in the standard buffer (pH 7.0) at 10 mg/mL and then ultracentrifuged at the same condition. The washed membrane was suspended in 20 mM KP buffer (pH 7.0) containing 1.0 mM DTT. The protein content of the isolated S77PM was quantified by the Lowry method using the DC protein assay (Bio-Rad, Hercules, CA, USA). Bovine serum albumin was used as the standard protein to establish the calibration curve.

3.2.4. Enzyme assays

Enzyme activities of hydrogenase and formate dehydrogenase were measured spectrophotometrically using a V-670 spectrophotometer (JASCO, Tokyo, Japan) following the reduction of methyl viologen (MV) at 30°C in glass cuvettes sealed with a rubber stopper and an aluminum cap. The reaction solutions containing the membrane suspension in 50 mM KP buffer (pH 7.0) were prepared in a Coy anaerobic chamber (Coy Laboratory Products, Grass Lake, MI, USA) under an atmosphere of 98% N_2 and 2% H_2. To perform H_2 oxidation, H_2 was flashed for 5 min in hydrogenase assay mixture, whereas formate oxidation was performed by addition of sodium formate to the final concentration of 10 mM, followed by flushing with argon (Ar) gas for 5 min in assay mixture. Enzymatic assays of hydrogenase and formate dehydrogenase were carried out under anaerobic conditions at 30°C with the addition of MV solution at the final 10 mM concentrations. Enzymatic activities were calculated by increasing the absorbance of MV (ε= 8.25 $mM^{-1} \cdot cm^{-1}$) at 600 nm (Yu et al., 1969) using a UV-vis spectrophotometer. Note that the specific activities of H_2 and formate oxidation were calculated by 2-electron reactions of MV. Steady-state kinetic parameters, K_m and V_{max} values of H_2 and CO_2 were determined by fitting the data to the Michaelis-Menten equation using nonlinear

regression. The data were analyzed using Enzyme Kinetics Module 1.1 of SigmaPlot 8.0 software (Jandel Scientific, Corte Madera, CA, USA). At least three independent experiments were performed to plot the data analysis.

3.2.5. Formate production of the isolated S77PM

Biocatalytic CO_2 conversion into formate was performed by using glass bottles (ca. 177 mL) sealed with a rubber stopper and an aluminum cap. The procedure for the reaction using S77PM was as follows: S77PM suspension was suspended in 400 mM phosphate buffer (pH 7.0) in bottles, and the reaction solution was bubbled with Ar for 10 min (>200 mL/min). Then the reaction solution was subsequently bubbled with the gas mixture of H_2 (140 mL/min) and CO_2 (60 mL/min) for 10 min and incubated at 0.1 MPa and 30°C for a certain period of time. The format produced was quantified by high-performance liquid chromatography (HPLC) system (Agilent, Santa Clara, CA, USA) coupled with an ion-exclusion chromatography column (Shodex RSpak KC-811, Shodex, Tokyo, Japan) and confirmed by ^{1}H and ^{13}C nuclear magnetic resonance (NMR) measurements using an AVANCE III HD 600 NMR spectrometer (Bruker, Billerica, MA, USA) with 5-mm tubes (^{1}H, 600.13 MHz; ^{13}C, 150.92 MHz).

3.2.6. Encapsulation of S77PM with MWCNTs and GG

S77PM was encapsulated using GG and MWCNTs through the following steps: First, a 1.0% (w/v) ultrasonicated MWCNTs solution was added to a suspension of S77PM and mixed well in a glove box. Then, the MWCNTs/S77PM mixture was added to a 1.4% (w/v) GG solution to obtain a final concentration of 0.2% (w/v) MWCNTs and 1.0% (w/v) GG. This resulting solution was slowly dropped to a 3.0% (w/v) calcium chloride solution to create S77PM-encapsulated GG/MWCNTs/S77PM beads. The beads were washed with a standard buffer to remove excess calcium ions. The morphology of freeze-dried GG/MWCNTs/S77PM

beads were characterized by a scanning electron microscope (SEM, SU8000, Hitachi Co., Tokyo, Japan). The encapsulated S77PM were then used for formate production under mild conditions of 30°C, pH 7.0 at 0.1 MPa in the gas mixture of H_2 and CO_2 (60:40, v/v %).

3.2.7 Reusability of the encapsulated S77PM in hydrogel beads

The procedure for the reuse experiment using hydrogel beads (GG/MWCNTs/S77PM) was as follows: The hydrogel beads were added to the reaction solution of 400 mM KP buffer (pH 7.0) and then flushed by Ar gas (>200 $mL \cdot min^{-1}$) for 10 min. The reaction solution was subsequently flowed by the gas mixture of H_2 (140 $mL \cdot min^{-1}$) and CO_2 (60 $mL \cdot min^{-1}$) for 10 min. After the reaction for 5 h at 30°C, the hydrogel beads GG/PVA/S-77 were washed with 400 mM KP buffer and used for the next reuse experiment. All of the reactions were performed at 30°C under atmospheric pressure. At least three independent experiments were performed to plot the data analysis.

3.2.8. Analytical Method

Formate was quantitatively analyzed by using HPLC and HPLC-UV Detection (Agilent) at 210 nm. A 3.0 mM $HClO_4$ aqueous solution was used as the eluent (flow rate, 0.7 $mL \cdot min^{-1}$). The column oven temperature was maintained at 40°C. Qualitative analysis of formate was performed by using an AVANCE III HD 600 NMR spectrometer with 5-mm tubes. Chemical shifts (δ) were reported in parts per million (ppm) downfield from solvent (D_2O) for ^{1}H and ^{13}C NMR spectra. The identity of the formate was confirmed by HPLC and ^{1}H NMR profiles with those of the standard formate. To confirm the H_2-driven CO_2 reduction to ^{13}C-formate production, a series of experiments was conducted with 200 mM $NaH^{13}CO_3$ as the sole carbon source. Formate production was confirmed by ^{13}C NMR (100.6 MHz, number of scans: 10,000).

3.3. Results and Discussion

3.3.1. H_2-driven CO_2 reduction of S77PM

The comprehensive whole-genome analysis (www.ncbi.nlm.nih.gov) and previous studies revealed *Citrobacter* sp. S-77 to contain membrane-associated metalloenzymes for H_2 and formate metabolism; namely, [NiFe]hydrogenases (Hyd-1 and Hyd-2), [Mo]formate dehydrogenases (FDH-N and FDH-O), and a formate hydrogenase (FHL) complex [16–19]. All these enzymes contain metal complexes in their catalytic sites, which play an important role in the membrane-associated proton-coupled electron transfer in living cells. In the previous studies, the highly active and O_2-stable Hyd-2 and FDH-N from the plasma membrane of *Citrobacter* sp. S-77 were purified and characterized [16,18]. To assess the role of the membrane-bound enzymes, the catalytic specificity was determined at different ratios of H_2 and CO_2 in the reaction. The optimal CO_2 conversion into formate was observed under a mixed gas condition of H_2:CO_2 (60:40, v/v, %) (**Fig. 1A**). Notably, there were no detectable HPLC peaks indicating formate in conditions of either 100% CO_2 or 100% H_2, which suggests formate production was dependent on the substrate ratio. The amount of formate production was correlated with the amount of S77PM, with high levels of formate production at a rate of 816.7 $mmol \cdot L^{-1} \cdot g_{protein}^{-1} \cdot h^{-1}$, achieved (**Fig. 1B**).

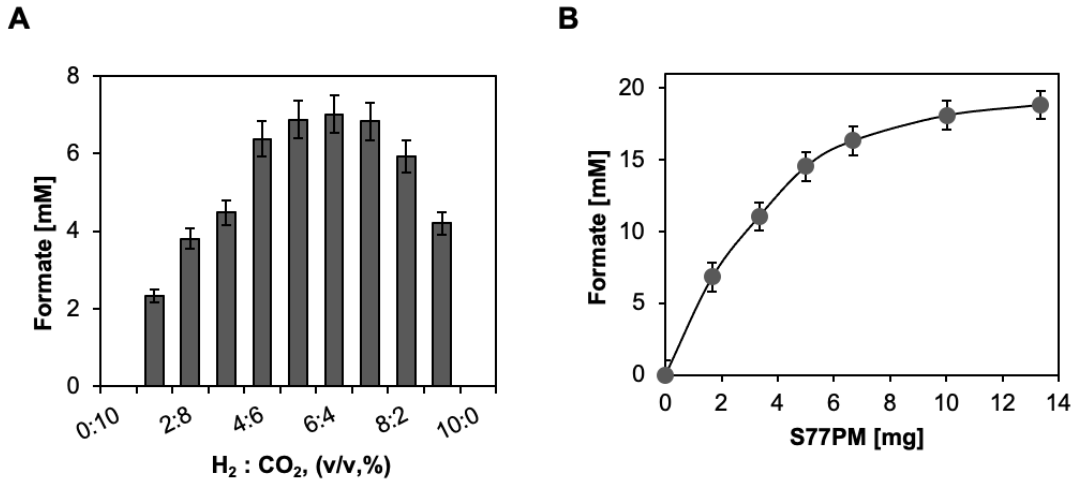

Fig. 1. (A) Gas ratio-dependent from H_2 and CO_2 in different gas ratios.
and (B) S77PM loading formate production

Kinetic analysis of H_2 and CO_2 dependence using cell membranes under conditions of pH 7.0 and 30°C revealed the K_m values of H_2 and CO_2 for formate production to be 0.1 and 3.5 mM, respectively (**Fig. 2**). The V_{max} value was about 14.5 μmol/min/mg, corresponding to 870 $mmol \cdot L^{-1} \cdot g_{protein}^{-1} \cdot h^{-1}$. The specificity constant (V_{max}/K_m) of H_2 was 26 times higher than that of CO_2, which indicates that H_2 donates electrons via H_2 oxidation of hydrogenase and is a favorable electron donor for CO_2 reduction. Thus, H_2 may play an important role in supplying electrons that mediate membrane-linked electron transfer between hydrogenase and formate dehydrogenase [20,21]. Given the catalytic specificity of this reaction, our observations offer insight into the mechanism underlying formate production in the gas mixture of H_2/CO_2 with the isolated plasma membrane. Removing the outer membrane of bacterial cells increases CO_2 diffusion [22] and facilitates the direct formation of formate from dissolved bicarbonate ions and H_2 with high catalytic efficiency [23]. This result provides an important platform for the biological reduction of CO_2 to formate, which can help to support enzymatic reactions, regulate molecular transport, and support electron transfer processes essential for efficient CO_2 conversion and assimilation into organic compounds within cells.

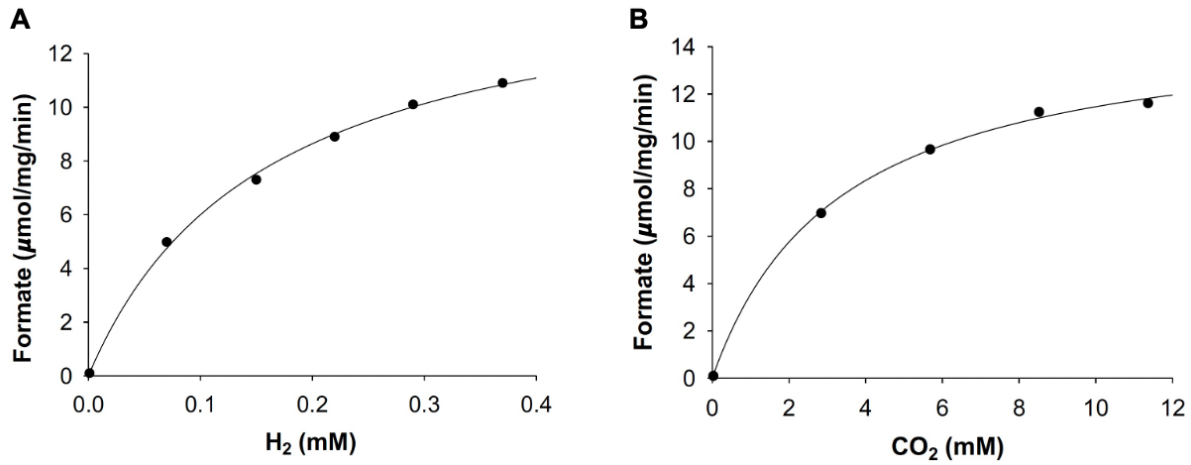

Fig. 2. Determination of K_m values for (A) H_2 and (B) CO_2 of the non-encapsulated S77PM. Steady-state kinetic parameters were determined at 30°C in 400 mM KP buffer (pH 7.0). The detailed assay conditions were described in materials and methods. The obtained data were fitted to the Michaelis-Menten equation using nonlinear regression.

3.3.2. Effect of pH and temperature

The optimal level for catalytic efficiency of S77PM was observed at pH 8.0 (**Fig. 3A**), which is consistent with a recent report evaluating the formation of formate via H_2-driven CO_2 reduction in living cells [9]. The rate of formate production decreased sharply above this point, in line with the results of a previous study on whole-cell hydrogenation of CO_2 [9]. Furthermore, it is noteworthy that S77PM can exhibit substantial catalytic activity of approximately 50.8% at pH 6.5. Our examination of the temperature dependence of formate production revealed that the [NiFe] hydrogenase and [Mo] formate dehydrogenase purified from the plasma membrane of *Citrobacter* sp. S-77 had high thermal stability at the optimal reaction temperatures of 65°C and 80°C [16,18], respectively.

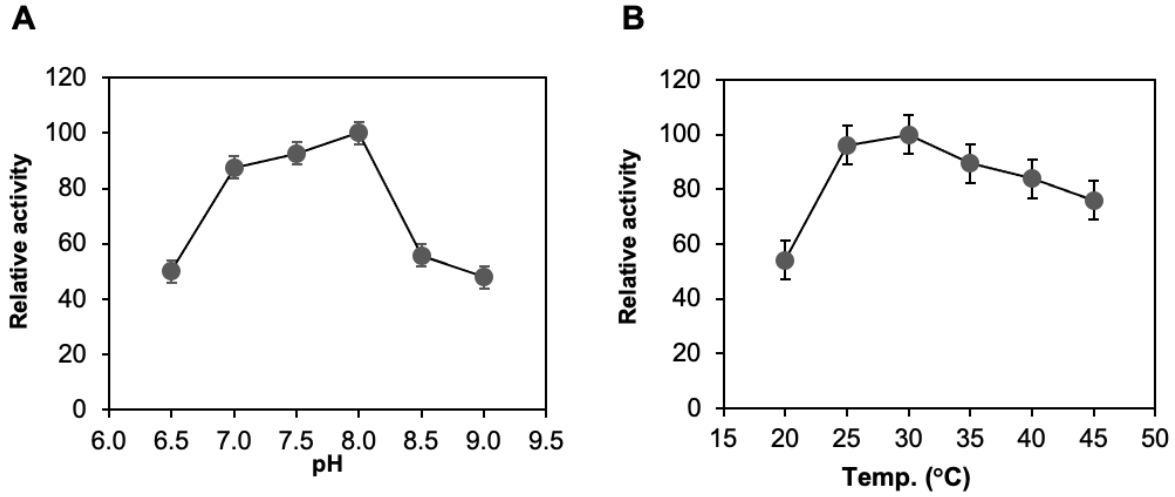

Fig. 3. (A) Effect of pH in 0.4 M KP buffer (pH 6.5–8.0) and 0.4 M Tris buffer (pH 7.5–9.0) and (B) Effect of temperature on formate production.

The optimal formate production of S77PM was achieved as 816.7 $mmol \cdot L^{-1} \cdot g_{protein}^{-1} \cdot h^{-1}$ at a reaction temperature of 30°C (**Fig. 3B**). However, when the temperature was increased to 60°C, the rate of formate production gradually decreased from 816.7 to 443.1 $mmol \cdot L^{-1} \cdot g_{protein}^{-1} \cdot h^{-1}$. This may be attributable to disorder in the isolated plasma membranes, which seem to be sensitive to temperature due to local distortion of the lipid bilayer membrane structure. The time dependence of formate production in the presence of various H_2 and CO_2

concentrations in the isolated plasma membrane was also examined. In the initial reaction conditions, the specific formate production rate of 816.7 $mmol \cdot L^{-1} \cdot g_{protein}^{-1} \cdot h^{-1}$ was obtained after 5 h, but the production rate decreased after 10 h as the pH of reaction solution dropped by formate production (**Fig. 4A**). Under the reaction conditions of 1.0 M KP buffer at 30°C, the production of formate proceeded at a rate of 1.22 $mol \cdot L^{-1} \cdot g_{protein}^{-1} \cdot h^{-1}$ after 4 h, after which the rate decreased gradually (**Fig. 4B**). These findings demonstrate the high potential of isolated plasma membranes for the hydrogenation of CO_2 into formate under mild reaction conditions.

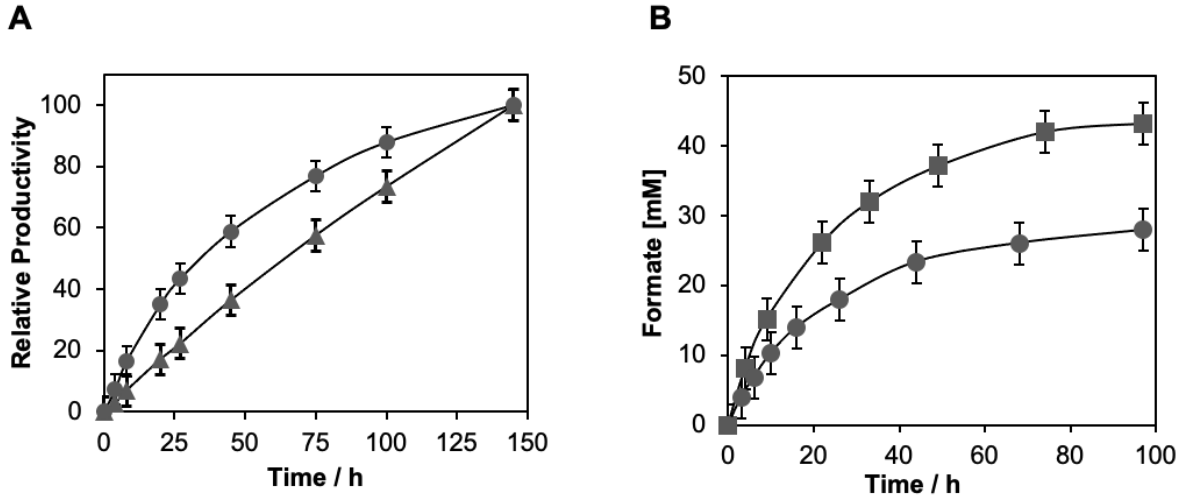

Fig. 4. (A) Comparative study of formate production of non-encapsulated S77PM (round shape) and encapsulated with GG/MCNTs/S77PM (triangle shape). (B) Time-dependent formate production of S77PM in 0.4 M KP buffer (pH 7.0) (round shape) and 1.0 M KP buffer (pH 8.0) (square shape).

3.3.3. Chromatography and NMR analysis of reaction products

The HPLC analysis revealed only one peak assigned to formate as a reaction product. The ^{1}H NMR spectrum exhibited a single signal at 8.35 ppm (**Fig. 5**), assigned to the hydrogen atom of $HCOO^-$ ions [24,25], while the ^{13}C NMR spectrum displayed four distinct signals at chemical shifts of 171.0, 170.9, 160.2, and 124.6 ppm (**Fig. 6**). These signals were assigned to the carbon atoms of $HCOO^-$, $DCOO^-$, HCO_3^-, and CO_2, respectively (**Fig. 6**). The triplet signals observed at 171.2, 170.9, and 170.6 ppm were attributed to the deuterium-carbon

coupling in $DCOO^-$ [24,25], as the proton in formate readily exchanges with deuterium from the solvent. Catalysis with S77PM under the same reaction conditions with isotopically enriched $NaH^{13}CO_3$ as the $^{13}CO_2$ source in the presence of H_2 gas gave an expected doublet with peaks at 8.50 and 8.18 ppm in ^1H NMR with a coupling constant of J = 195 Hz (**Fig. 7**), and a stronger triplet with peaks at 171.1, 170.9, and 170.7 ppm with a coupling constant of J = 29.85 Hz in the ^{13}C spectrum (**Fig. 8**). This was due to deuterium formate ($DCOO^-$). A small peak at 171.1 ppm was observed due to the proton-containing formate, $HCOO^-$ [24,25]. Additionally, the reaction did not proceed in the absence of either CO_2 or H_2 (**Fig. 1A**). As expected, without S77PM, no signals assignable to any byproducts were detected from analysis of the reaction solution, suggesting that only formate was predominantly produced by the hydrogenation reaction. These results demonstrate the very high efficiency and specificity of S77PM as a biocatalytic system, which produces only formate from CO_2 and H_2 under ambient reaction conditions. In nature, HCO_3^- is the predominant form of inorganic carbon in seawater, comprising approximately 90% of the total inorganic carbon [26]. Increasing atmospheric CO_2 concentrations have led to increased concentrations of HCO_3^- in seawater and consequent ocean acidification, which poses significant challenges to marine ecosystems. Although several techniques have been developed to remove oceanic CO_2, no effective system has been developed to date [27]. The results of the present work will contribute to the development of sustainable CO_2-hydrogenation processes and provide a promising approach to addressing environmental problems such as ocean acidification.

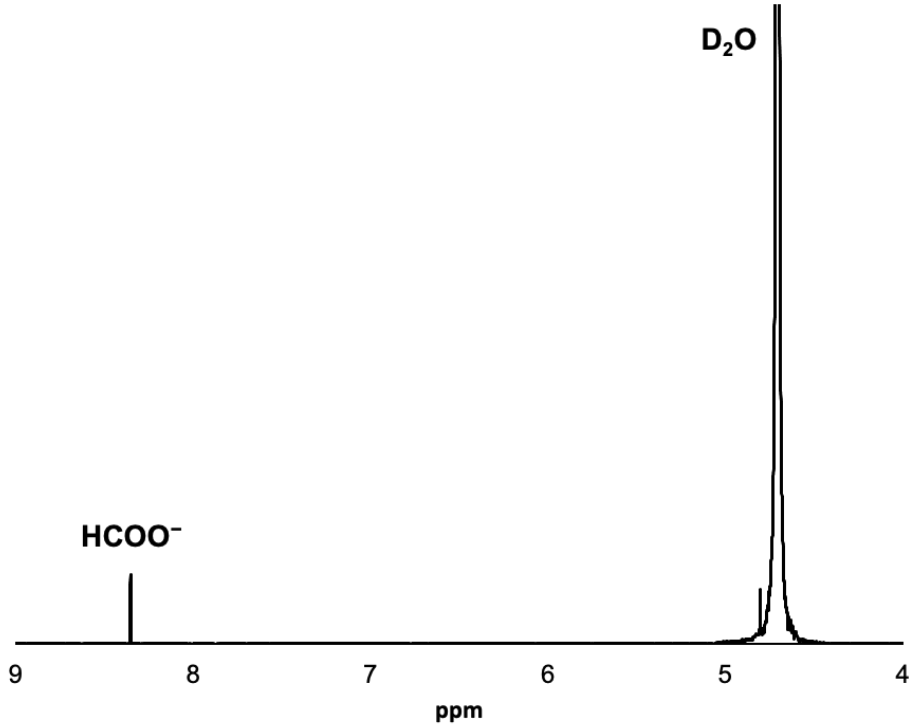

Fig. 5. ^{1}H NMR of formate produced from CO_2 and H_2 gas at 0.1 MPa by S77PM suspended in 0.4 M KP buffer (pH 7.0) prepared with D_2O.

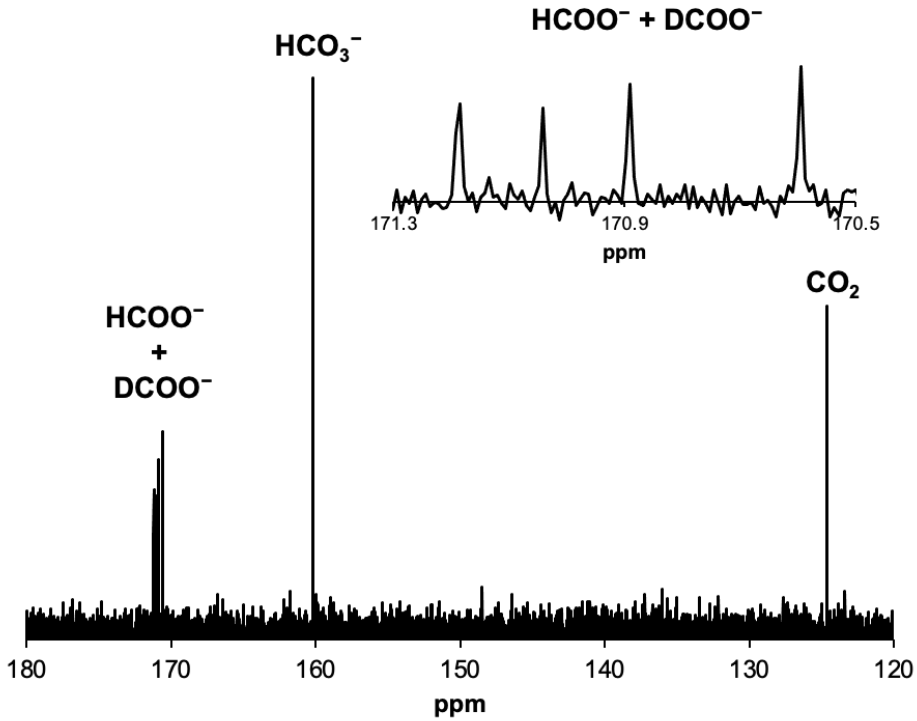

Fig. 6. ^{13}C NMR of formate produced from CO_2 and H_2 gas at 0.1 MPa by S77PM suspended in 0.4 M KP buffer (pH 7.0) prepared with D_2O.

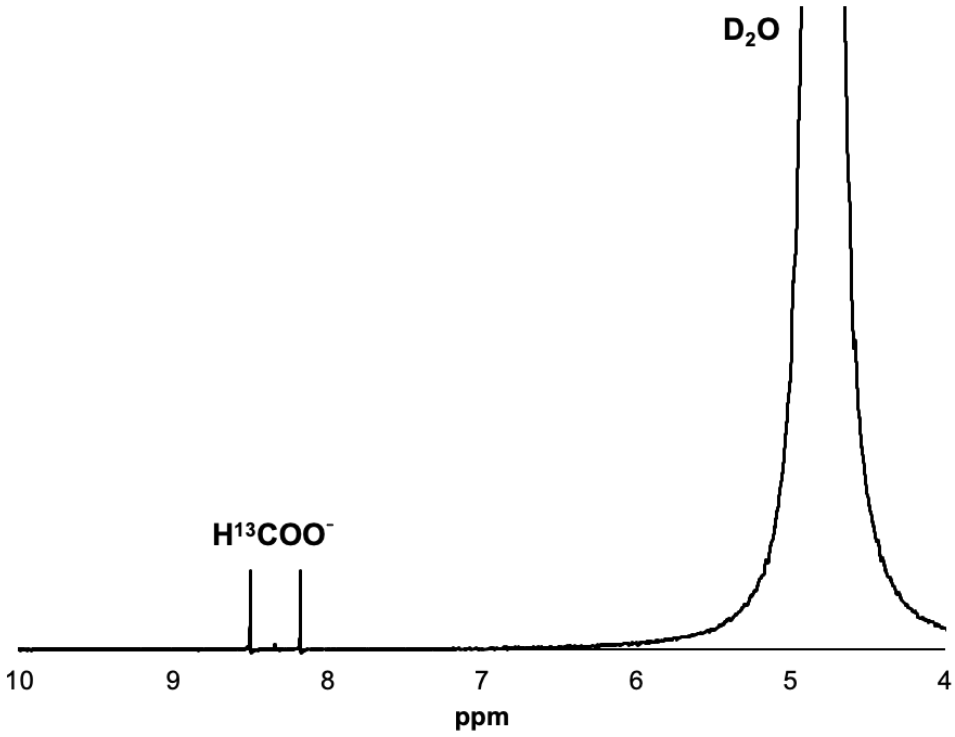

Fig. 7. ^{1}H NMR of formate produced from 250 mM $NaH^{13}CO_3$ as the source of $^{13}CO_2$

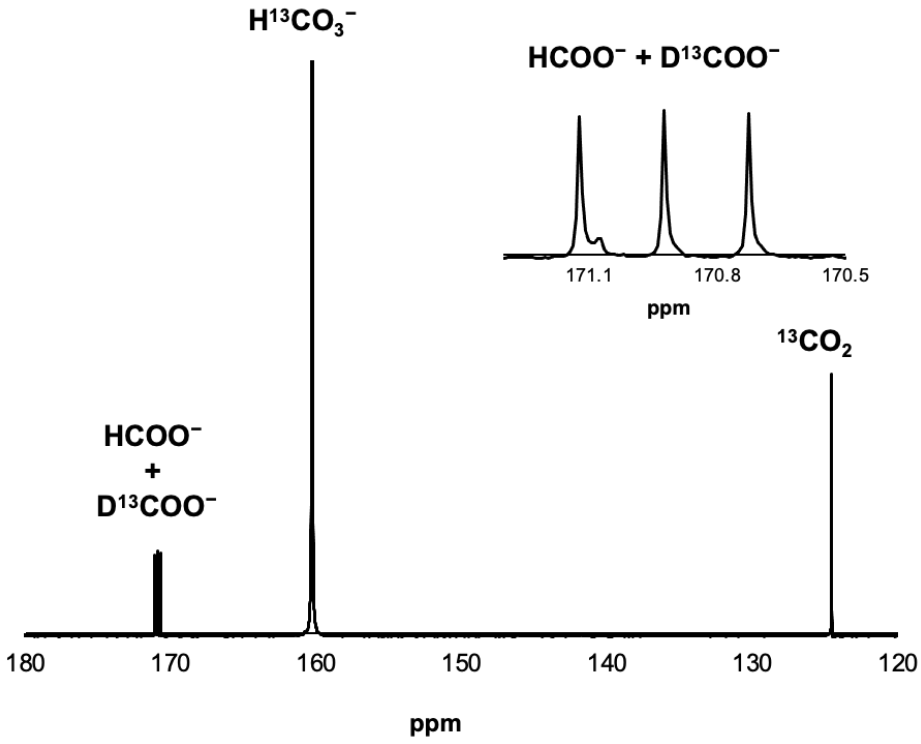

Fig. 8. ^{13}C NMR of formate produced from 250 mM $NaH^{13}CO_3$ as the source of $^{13}CO_2$

3.3.4. Formate production by encapsulated S77PM

Next, an environmentally friendly heterogeneous catalytic platform for hydrogenation of CO_2 to formate production was developed by using the isolated plasma membrane adhered to MWCNTs with a combination of biodegradable GG. In such stride, MWCNTs serve as a good platform for immobilizing S77PM due to their high surface area and excellent conductivity [28–30], which enable the attachment of substantial quantities of S77PM while maintaining efficient electron transfer properties. The encapsulated plasma membrane in hydrogel beads was constructed by mixing S77PM with MWCNTs and entrapping the resulting mixture in GG in the presence of calcium ions (Ca^{2+}). To observe the morphology of encapsulated S77PM and the distribution of the plasma membranes in hydrogels, characterization of GG, GG/MWCNTs, and GG/MWCNTs/S77PM beads was conducted by scanning electron microscopy (**Fig. 9**). The images show that MWCNTs can be physically adsorbed onto the GG matrix through van der Waals forces or electrostatic interactions [31–33], and the attachment of MWCNTs to the GG matrix resulted in a GG/MWCNTs-bead matrix with a homogeneous, rough surface with micropores of approximately 0.1 μm. The hydrophobic interaction between the GG/MWCNTs matrix and plasma membranes is attributed due to hydrophobic nature of MWCNTs, which may interact with greater affinity with the hydrophobic phospholipids constituting the primary components of the plasma membrane; thus the interactions may be responsible for the high mechanical strength of the GG/MWCNTs/S77PM beads [28–30]. These were considered to be ideal physical entrapment sites for the S77PM. The SEM analysis of GG/MWCNTs/S77PM revealed high-density entrapment of S77PM within the GG/MWCNTs beads. This method of immobilization offers practical advantages as the materials used are inexpensive, readily available, and environmentally friendly.

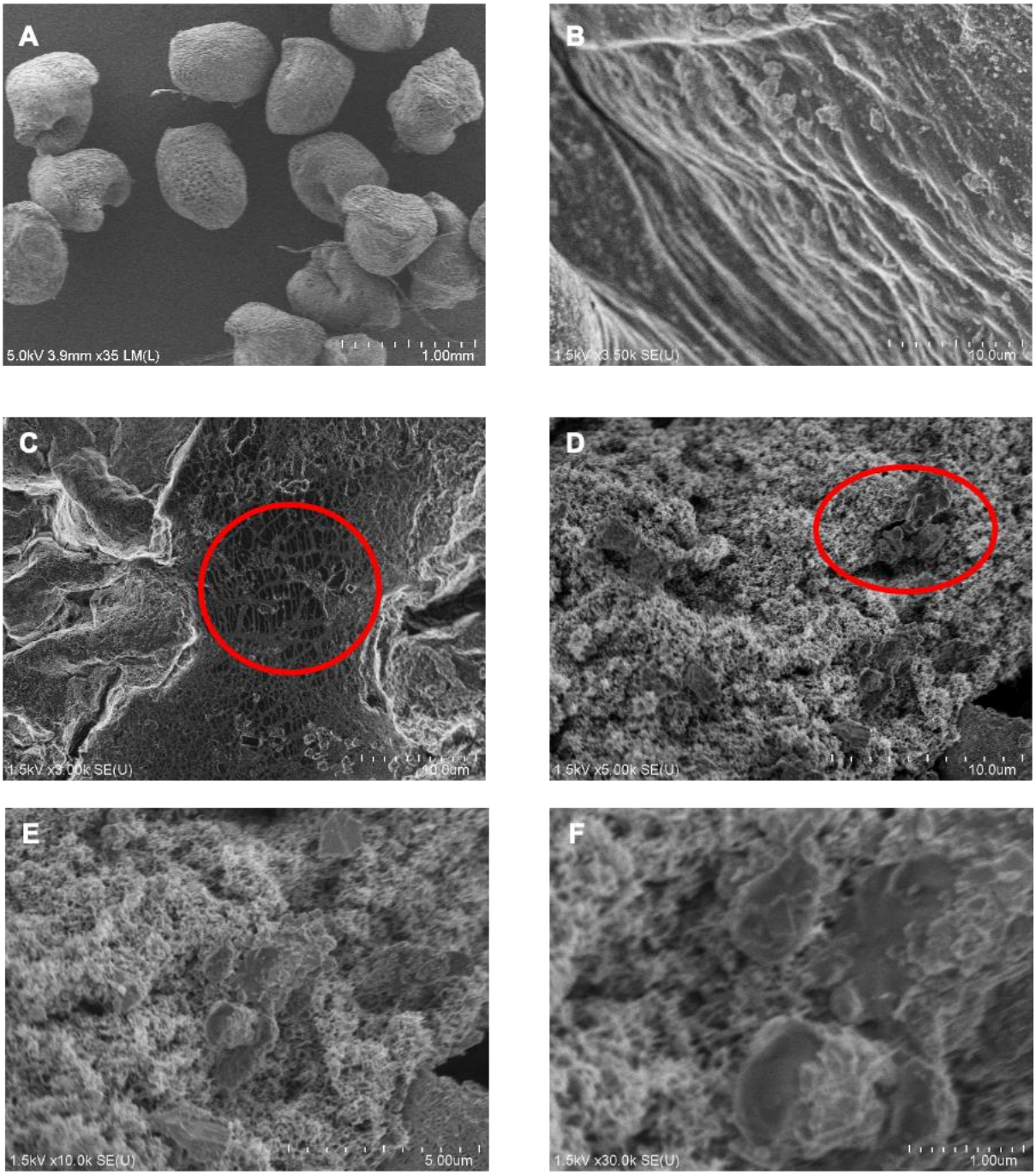

Fig. 9. SEM images of (A) freeze-dried hydrogel beads surface (GG/MWCNTs/S77PM). SEM images of (B) GG (1.0%, w/v), (C) GG (1.0%, w/v) with MWCNTs (0.2%, w/v), (D) hydrogel beads prepared with GG and MWCNTs and S77PM named as GG/MWCNTs/S77PM, (E) GG/MWCNTs/S77PM at scale bar 5.0 µm and (F) GG/MWCNTs/S77PM at scale bar 1.0 µm.

Furthermore, this method increases the reusability of the biocatalyst. The rate of formate production using GG/MWCNTs/S77PM in the presence of H_2 and CO_2 under mild reaction conditions was slightly lower than that achieved using non-immobilized S77PM (**Fig. 10A**). However, the formate production using the GG/MWCNTs/S77PM system consistently exceeded those in the GG/S77PM system over the 74 h. This outcome serves as a strong indicator of the inherent electrical conductivity associated with MWCNTs. Additionally, the catalytic activity of GG/MWCNTs/S77PM remained unchanged even after 145 h of reaction, which confirms the high reactivity and longevity of encapsulated S77PM in hydrogel beads (**Fig. 4A**). When the GG/MWCNTs/S77PM beads were tested for their reusability as heterogeneous catalysts, the immobilized plasma membrane catalysts were able to be reused at least 10 times without significant decrease in catalytic activity (**Fig. 10B**).

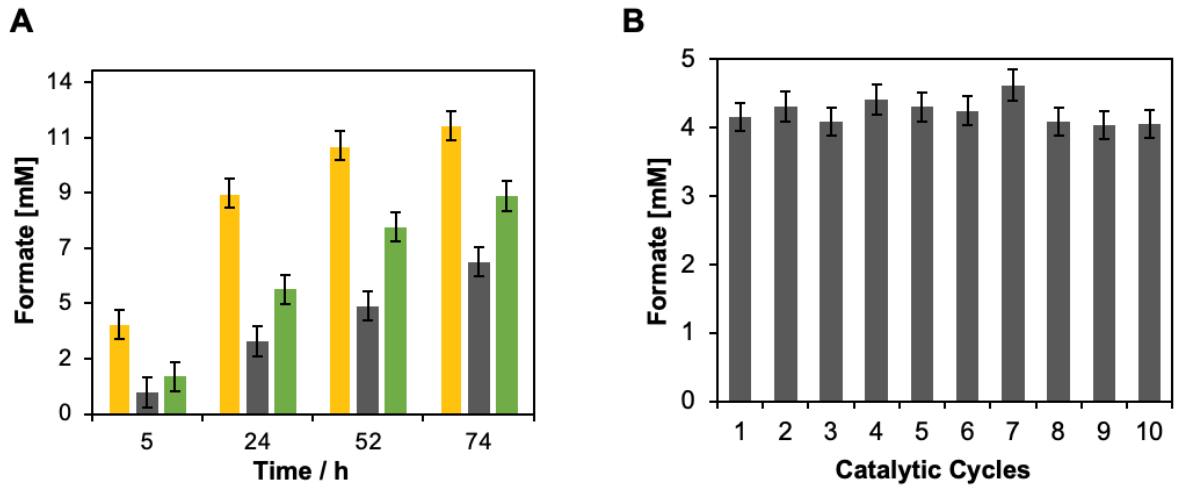

Fig. 10. (A) Time-dependent formate production from H_2 and CO_2 by S77PM (yellow), GG/S77PM (gray), and GG/MWCNTs/S77PM (green) at 30 °C and 0.1 MPa in 400 mM Tris-HCl buffer (pH 7.0). (B) Reusability of GG/MWCNTs/S77PM hydrogel beads as a heterogeneous catalyst.

These findings highlight the exceptional reusability and high capability of biocatalysts encapsulated in GG/MWCNTs hydrogels for heterogeneous catalytic reactions; specifically, for the selective production of formate. Encapsulation of the plasma membranes enhances the

stability by providing a protective environment, allowing for prolonged survival. This study presents, to the best of our knowledge, the first example of encapsulation of bacterial plasma membranes as effective catalysts for the reduction of CO_2 into formate under mild conditions, providing a robust heterogeneous catalyst.

Very recently, synthetic systems using liposomes incorporating semiconductor materials, chemical photosensitizers, and cocatalysts have been developed to mimic natural thylakoid membranes for the photocatalytic reduction of CO_2 [34,35]. In addition, isolated bacterial plasma membranes have been manipulated with the inorganic semiconductor TiO_2 and the metal cocatalyst Pd for CO_2 reduction [36]. However, many of these are poor replicas of naturally occurring thylakoid membranes and exhibit low reactivity and selectivity, high catalyst loading, and low electron transport due to the lack of appropriately designed lipids, semiconductor materials, photosensitizers, and active catalysts [34–37]. In addition, external sacrificial electron donors and/or electron mediators are inevitably required as sources of electrons or to transport electrons to the active sites of the catalysts [34–36]. The living cell system has limited capacity to maintain catalytic activity for long periods under reaction conditions, and the complexity of the system makes it difficult to control and optimize reaction conditions. Bacterial plasma membranes provide precisely synchronized catalytic environments, which effectively achieve electron and proton transfer to the reactant with low energy barriers. Under the optimal experimental conditions, the H_2-driven reduction of CO_2 to formate production using plasma membranes was obtained as 1218.5 $\mu mol \cdot g_{protien}^{-1} \cdot h^{-1}$, which is almost 22 times higher than 56.4 $\mu mol \cdot g_{catalyst}^{-1} \cdot h^{-1}$ of the artificially created membrane catalysts [36]. Our encapsulated system involving S77PM offers high reusability without significant loss of catalytic activity, which has great potential for the development of systems or the biocatalytic CO_2 hydrogenation to formate from CO_2 and H_2 under mild reaction conditions.

3.4. Conclusions

In summary, a feasible method for the H_2-driven reduction of CO_2 into formate using encapsulated bacterial plasma membranes in hydrogel beads was presented. HPLC and NMR analysis revealed that formate was produced with a high and selective reaction rate of 816.7 $mmol \cdot L^{-1}$ $g_{protein}^{-1} \cdot h^{-1}$ at ambient conditions. The immobilization of S77PM onto MWCNTs and subsequent encapsulation in GG demonstrated a sustainable heterogeneous biocatalyst platform that enhanced the overall catalytic stability and paved the way for practical applications. This study enhances our knowledge of bacterial plasma membranes and demonstrates their potential for catalyzing CO_2 reduction to create valuable organic compounds.

3.5 References

[1] A. M. Appel, J. E. Bercaw, A. B. Bocarsly, H. Dobbek, D. L. Dubois, M. Dupuis, J. G. Ferry, E. Fujita, R. Hille, P. J. A. Kenis, C. A. Kerfeld, R. H. Morris, C. H. F. Peden, A. R. Portis, S. W. Ragsdale, T. B. Rauchfuss, J. N. H. Reek, L. C. Seefeldt, R. K. Thauer, G. L. Waldrop, *Chem Rev* **2013**, *113*, DOI 10.1021/cr300463y.

[2] A. Alok, R. Shrestha, S. Ban, S. Devkota, B. Uprety, R. Joshi, *J Environ Chem Eng* **2022**, *10*, DOI 10.1016/j.jece.2021.106922.

[3] W. H. Wang, Y. Himeda, J. T. Muckerman, G. F. Manbeck, E. Fujita, *Chem Rev* **2015**, *115*, DOI 10.1021/acs.chemrev.5b00197.

[4] J. Wu, Y. Huang, W. Ye, Y. Li, *Advanced Science* **2017**, *4*, DOI 10.1002/advs.201700194.

[5] A. Alissandratos, H. K. Kim, C. J. Easton, *Bioresour Technol* **2014**, *164*, DOI 10.1016/j.biortech.2014.04.064.

[6] F. Leo, F. M. Schwarz, K. Schuchmann, V. Müller, *Appl Microbiol Biotechnol* **2021**, *105*, DOI 10.1007/s00253-021-11463-z.

[7] T. B. Madavi, S. Chauhan, A. Keshri, H. Alavilli, K. Y. Choi, S. D. V. N. Pamidimarri, *Biofuels, Bioproducts and Biorefining* **2022**, *16*, DOI 10.1002/bbb.2331.

[8] C. Mourato, M. Martins, S. M. da Silva, I. A. C. Pereira, *Bioresour Technol* **2017**, *235*, DOI 10.1016/j.biortech.2017.03.091.

[9] M. Roger, F. Brown, W. Gabrielli, F. Sargent, *Current Biology* **2018**, *28*, DOI 10.1016/j.cub.2017.11.050.

[10] F. M. Schwarz, V. Müller, *Biotechnol Biofuels* **2020**, *13*, DOI 10.1186/s13068-020-1670-x.

[11] R. R. Chen, *Appl Microbiol Biotechnol* **2007**, *74*, DOI 10.1007/s00253-006-0811-x.

[12] Y. Ni, R. R. Chen, *Biotechnol Bioeng* **2004**, *87*, DOI 10.1002/bit.20202.

[13] C. Hannesschlaeger, A. Horner, P. Pohl, *Chem Rev* **2019**, *119*, DOI 10.1021/acs.chemrev.8b00560.

[14] V. Endeward, S. Al-Samir, F. Itel, G. Gros, *Front Physiol* **2014**, *4 JAN*, DOI 10.3389/fphys.2013.00382.

[15] H. K. Nguyen, T. Minato, M. Moniruzzaman, Y. Kiyasu, S. Ogo, K. S. Yoon, *J Biosci Bioeng* **2023**, *136*, 182.

[16] S. Eguchi, K. S. Yoon, S. Ogo, *J Biosci Bioeng* **2012**, *114*, DOI 10.1016/j.jbiosc.2012.05.018.

[17] T. Matsumoto, S. Eguchi, H. Nakai, T. Hibino, K. S. Yoon, S. Ogo, *Angewandte Chemie - International Edition* **2014**, *53*, DOI 10.1002/anie.201404701.

[18] N. T. Nguyen, T. Yatabe, K. S. Yoon, S. Ogo, *J Biosci Bioeng* **2014**, *118*, DOI 10.1016/j.jbiosc.2014.03.011.

[19] N. D. M. Noor, H. Matsuura, K. Nishikawa, H. Tai, S. Hirota, J. Kim, J. Kang, M. Tateno, K. S. Yoon, S. Ogo, S. Kubota, Y. Shomura, Y. Higuchi, *Chemical Communications* **2018**, *54*, DOI 10.1039/c8cc06261g.

[20] A. Bassegoda, C. Madden, D. W. Wakerley, E. Reisner, J. Hirst, *J Am Chem Soc* **2014**, *136*, DOI 10.1021/ja508647u.

[21] K. Schuchmann, V. Müller, *Science (1979)* **2013**, *342*, DOI 10.1126/science.1244758.

[22] M. Michenkova, S. Taki, M. C. Blosser, H. J. Hwang, T. Kowatz, F. J. Moss, R. Occhipinti, X. Qin, S. Sen, E. Shinn, D. Wang, B. S. Zeise, P. Zhao, N. Malmstadt, A. Vahedi-Faridi, E. Tajkhorshid, W. F. Boron, *Interface Focus* **2021**, *11*, DOI 10.1098/rsfs.2020.0090.

[23] K. P. Sokol, W. E. Robinson, A. R. Oliveira, S. Zacarias, C. Y. Lee, C. Madden, A. Bassegoda, J. Hirst, I. A. C. Pereira, E. Reisner, *J Am Chem Soc* **2019**, *141*, DOI 10.1021/jacs.9b09575.

[24] S. Moret, P. J. Dyson, G. Laurenczy, *Dalton Transactions* **2013**, *42*, DOI 10.1039/c3dt00081h.

[25] T. Chatterjee, E. Boutin, M. Robert, *Dalton Transactions* **2020**, *49*, DOI 10.1039/c9dt04749b.

[26] C. Poschenrieder, J. A. Fernández, L. Rubio, L. Pérez, J. Terés, J. Barceló, *Int J Mol Sci* **2018**, *19*, DOI 10.3390/ijms19051352.

[27] J. Hartmann, A. J. West, P. Renforth, P. Köhler, C. L. De La Rocha, D. A. Wolf-Gladrow, H. H. Dürr, J. Scheffran, *Reviews of Geophysics* **2013**, *51*, DOI 10.1002/rog.20004.

[28] J. Geng, K. Kim, J. Zhang, A. Escalada, R. Tunuguntla, L. R. Comolli, F. I. Allen, A. V. Shnyrova, K. R. Cho, D. Munoz, Y. M. Wang, C. P. Grigoropoulos, C. M. Ajo-Franklin, V. A. Frolov, A. Noy, *Nature* **2014**, *514*, DOI 10.1038/nature13817.

[29] V. Pérez-Luna, C. Moreno-Aguilar, J. L. Arauz-Lara, S. Aranda-Espinoza, M. Quintana, *Sci Rep* **2018**, *8*, DOI 10.1038/s41598-018-36531-9.

[30] G. Panda, S. Dash, S. K. Sahu, *Membranes (Basel)* **2022**, *12*, DOI 10.3390/membranes12100914.

[31] A. A. Abalymov, C. A. B. Santos, L. Van der Meeren, D. Van de Walle, K. Dewettinck, B. V. Parakhonskiy, A. G. Skirtach, *Adv Mater Interfaces* **2021**, *8*, DOI 10.1002/admi.202002202.

[32] X. W. Liu, Y. X. Huang, X. F. Sun, G. P. Sheng, F. Zhao, S. G. Wang, H. Q. Yu, *ACS Appl Mater Interfaces* **2014**, *6*, DOI 10.1021/am500624k.

[33] A. Vashist, A. Kaushik, A. Vashist, V. Sagar, A. Ghosal, Y. K. Gupta, S. Ahmad, M. Nair, *Adv Healthc Mater* **2018**, *7*, DOI 10.1002/adhm.201701213.

[34] N. Ikuta, S. Y. Takizawa, S. Murata, *Photochemical and Photobiological Sciences* **2014**, *13*, DOI 10.1039/c3pp50429h.

[35] D. M. Klein, S. Rodríguez-Jiménez, M. E. Hoefnagel, A. Pannwitz, A. Prabhakaran, M. A. Siegler, T. E. Keyes, E. Reisner, A. M. Brouwer, S. Bonnet, *Chemistry - A European Journal* **2021**, *27*, DOI 10.1002/chem.202102989.

[36] Z. Chen, H. Zhang, P. Guo, J. Zhang, G. Tira, Y. J. Kim, Y. A. Wu, Y. Liu, J. Wen, T. Rajh, J. Niklas, O. G. Poluektov, P. D. Laible, E. A. Rozhkova, *J Am Chem Soc* **2019**, *141*, DOI 10.1021/jacs.9b05564.

[37] N. Kornienko, J. Z. Zhang, K. K. Sakimoto, P. Yang, E. Reisner, *Nat Nanotechnol* **2018**, *13*, DOI 10.1038/s41565-018-0251-7.

Chapter 4

Disassembly and reassembly of the non-conventional thermophilic C-phycocyanin

(*J. Biosci. Bioeng.*, **2023**, *accepted*)

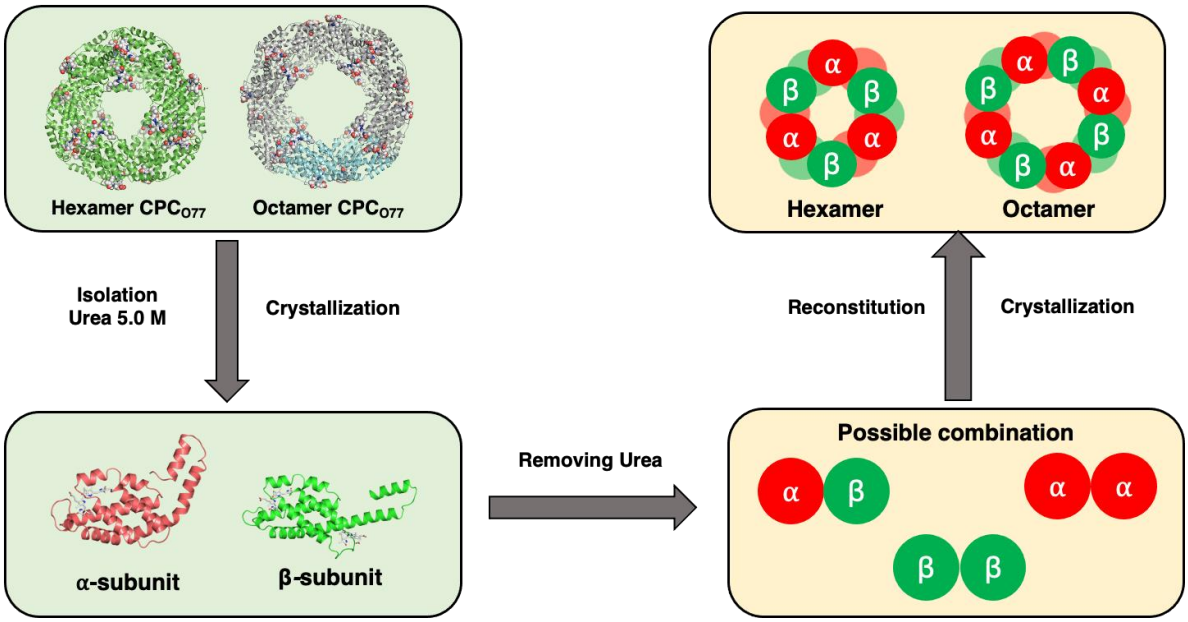

ABSTRACT

C-phycocyanin (CPC), which contains open-chain tetrapyrroles, is a major light-harvesting red-fluorescent protein with an important role in aquatic photosynthesis. Recently, we reported a non-conventional CPC from *Thermoleptolyngbya* sp. O-77 (CPC_{O77}) that contains two different structures—a hexameric structure and a non-conventional octameric structure. However, the assembly and disassembly mechanisms of the non-conventional octameric form of CPC remain unclear. To understand this assembly mechanism, an *in vitro* experiment was performed to study the disassembly and reassembly behaviors of CPC using isolated CPC subunits. The dissociation of the CPC_{O77} subunit was performed using a Phenyl-Sepharose column in 20 mM KP buffer (pH 6.0) containing 7.0 M urea. For the first time, crystals of isolated CPC subunits were obtained and analyzed after separation. After the removal of urea from the purified α and β subunits, CPC was reassembled *in vitro* and the reconstructed CPC was analyzed using spectrophotometric and X-ray crystal structure analyses. The crystal structure of the reassembled CPC was nearly identical to that of the original CPC_{O77}. The findings of this study indicate that the octameric CPC_{O77} is a naturally occurring form in the thermophilic cyanobacterium *Thermoleptolyngbya* sp. O-77.

4.1 Introduction

Phycobilisome (PBS), which attaches to the thylakoid membrane of cyanobacteria and algae, is a water-soluble light-harvesting protein complex that is unlike the light-harvesting protein complex that binds to the thylakoid membrane of higher plants [1,2]. PBS plays an important role in the photosynthetic system through light energy absorption and facilitating the high-efficiency transfer to photosystem I and II in water [3–6]. PBS, which has a molecular weight from 7 to 15 MDa, is composed of a core and peripheral rod protein complex with acidic chromophore polypeptides (phycobiliproteins, PBPs) and hydrophobic polypeptides called linker proteins[7]. The giant protein complex of PBS typically consists of three pigment proteins: phycoerythrin, phycocyanin, and allophycocyanin [8,9]. Among these three proteins, C-phycocyanin (CPC) is the most abundant component. It consists of two different polypeptides (the α and β subunits) that form αβ structures of monomers, trimers, or hexamers [10]. Owing to its abundance, water-solubility, and non-toxicity, CPC has garnered interest from researchers in various fields, including biotechnological and pharmaceutical applications [11,12]. The open-chain tetrapyrroles of phycocyanobilin (PCB) are the major light receptors in CPC [6]. PCB is covalently bound to the conserved cysteine residues via thioether linkages by attaching one PCB to the α subunit of CPC and two PCBs to the β subunit [13,14]. *In vitro*, depending on the concentration of buffers and proteins, CPC can exist as three forms of monomer, trimer, and hexamer [15–17]. Therefore, it is thought that the biosynthesis pathway of CPC is based on the assembly of monomer (αβ) into trimers $(\alpha\beta)_3$ and hexamers $(\alpha\beta)_6$, followed by the insertion of linker proteins *in vivo* [18,19].

During the studies of oxygenic photosynthesis, Ogo laboratory isolated a thermophilic and non-heterocystous cyanobacterium *Leptolyngbya* sp. O-77 from a hot spring [20]. The O-77 strain grows well at temperatures of 50°C–60°C, with an optimal growth temperature of 55°C. Owing to its thermophilic characteristics, the O-77 strain was re-classified into the new genus

of *Leptolyngbya*-like thermophilic cyanobacterium, named *Thermoleptolyngbya* sp. O-77 [21]. Following studies of photosystem II and water-soluble light-harvesting complexes [20,22], the first report on the non-conventional octameric CPC from the O-77 strain (CPC_{O77}) was presented [23]. CPC_{O77} can be assembled spontaneously *in vitro* from an equilibrium between the hexamer and octamer structures. Furthermore, the analytical ultracentrifugation result showed evidence that suggests the existence of a dimeric state as an intermediate. This opened other possibilities for self-assembly mechanisms of CPC *in vitro* and *in vivo* [23]. *In vitro*, the analytical ultracentrifugation and PISA program calculation demonstrated that monomer–dimer–octamer assembly is kinetically favorable and can be the process to form octamer CPC. However, the *in vivo* assembly mechanism of CPC_{O77} has not been clearly elucidated. To study this self-assembly mechanism *in vivo*, investigation of protein subunits and their assembly mechanism is necessary because subunits are the fundamental building blocks that constitute the monomers and other oligomers of proteins, and any change in the subunit structure and sequence might affect the overall structure and the overall assembly process [24,25]. Therefore, in this study, an *in vitro* reassembly experiment was performed using isolated α and β subunits from CPC_{O77}. The investigation of the reassembly of the isolated α and β subunits in this study may reveal new biosynthesis pathways from the α and β monomers to the hexamer and octamer. To demonstrate the disassembly and assembly of native CPC_{O77}, homogeneously purified CPC_{O77} was dissociated into the α and β subunits by reacting at pH 6.0 and 30°C in 7.0 M urea buffer. The isolated α and β subunits from CPC_{O77} were used to perform the *in vitro* reassembly experiment. The disassembled subunits could be identically reassembled to be hexameric and octameric CPC_{O77}, suggesting that octameric CPC_{O77} appears to occur during the natural assembly process of CPC in a thermophilic non-heterocystous cyanobacterium of the new genus of *Thermoleptolyngbya* sp. O-77.

4.2 Materials and Methods

4.2.1 Bacterium and growth conditions

Cell culture was carried out with a 10-L bioreactor (Model MBF-1000ME, EYELA, Tokyo Rikakikai Co., Ltd) in a modified DH+Fe medium containing the following components (per litter): 0.1 g nitrilotriacetic acid, 1.7 g $NaNO_3$, 0.3 g K_2HPO_4, 0.1 g $MgSO_4 \cdot 7H_2O$, 0.1 g $CaSO_4 \cdot 2H_2O$, 0.03 g $FeCl_3 \cdot 6H_2O$, 3.0 mg H_3BO_3, 2.0 mg $MnSO_4 \cdot H_2O$, 0.1 mg $ZnSO_4 \cdot 7H_2O$, 75 μg $CoCl_2 \cdot 6H_2O$, 75 μg $NiCl_2 \cdot 6H_2O$, 80 μg $CuSO_4 \cdot 5H_2O$, and 80 μg $Na_2MoO_4 \cdot 2H_2O$. The medium was adjusted to pH 7.5 by 0.1M NaOH. Cells were grown in an 8-L culture medium under agitation at 150 rpm. The cell culture was carried out at 55°C under a constant flow (200 $mL \cdot min^{-1}$) of an aerobic gas mixture (dried air/CO_2 = 99/1, v/v %) at a constant illumination by using four 60 W incandescent lamps.

4.2.2 Purification of CPC_{O77}

The harvested cells were washed twice with 20 mM potassium phosphate (KP) buffer (pH 7.0) containing 50 mM NaCl. The cells were then suspended in the same buffer, after that the cell suspension was disrupted by sonication five times for 2 minutes in an ice bath at 30 W with an Ultrasonic Disruptor UD-200 (Tomy Seiko Inc. Japan). Cell debris and unbroken cells were removed by centrifugation (10,000g, 10 min, 4°C) and the supernatant was then centrifuged at 150,000g for 1 hour by using Optima L-90K (Beckman Coulter Inc. USA). The supernatant of soluble cell extract was loaded onto a DEAE Sepharose fast flow column (2.6x15 cm, GE Healthcare, UK), pre-equilibrated with 20 mM KP buffer (pH 7.0). The column was washed with 150 mL of the same buffer at a flow rate of 7 $mL \cdot min^{-1}$. A stepwise gradient method was used, which consisted of 400 mL of buffer containing a gradient of 0 M to 0.25 M NaCl, 100 mL of isocratic elution of buffer containing 0.25 M NaCl, 200 mL of 0.25 M to 0.5 M NaCl, and 150 mL of 0.5 M to 1.0 M NaCl. The two major blue-colored proteins

corresponding to CPC and allophycocyanin were eluted at 0.1–0.2 M and 0.2–0.25 M NaCl, respectively, at ionic conductivities between 12.7 and 23.5 $mS \cdot cm^{-1}$. The fraction containing CPC was combined and then diluted 3-fold with non-salt buffer and then applied onto a Q Sepharose high-performance column (1.6 x 12 cm, GE Healthcare, UK) pre-equilibrated with 20 mM phosphate buffer (pH 7.0). The column was then washed with 60 mL of the same buffer containing 0.1 M NaCl and then followed by stepwise gradients of 100 mL of buffer containing a gradient of 0.1 M to 0.3 M NaCl, 40 mL of isocratic elution of buffer containing 0.3 M NaCl, and 60 mL of 0.3 M to 1.0 M NaCl at a flow rate of 4 $mL \cdot min^{-1}$. A major blue soluble protein was eluted by approximately 0.15 M NaCl. The purity of CPC was measured by the absorption ratio of A_{615}/A_{280}. The concentrations of CPC and allophycocyanin were estimated by using the following equation [26]:

$$\text{C-phycocyanin (mg/mL)} = [A_{615} - 0.474(A_{652})]/5.34$$

$$\text{Allophycocyanin (mg/mL)} = [A_{652} - 0.208(A_{615})]/5.09$$

4.2.3 Dissociation conditions of α/β subunit in urea

In order to obtain the homogeneously α and β subunit, the optimal conditions for pH and urea concentration were investigated. The homogeneously purified CPC (1.7 $mg \cdot mL^{-1}$) was suspended in different concentrations of 1.0 M to 8.0 M urea containing 20 mM KP buffer (pH 6.0). The CPC solutions were incubated for 1 h at room temperature and then centrifugated at 10,000*g* for 10 min. UV-visible absorption and circular dichroism (CD) spectra of the CPC solutions depended on pH changes and urea concentrations were recorded to detect the change in protein structure. UV-visible absorption spectra of each sample were recorded at 25°C with a JASCO V-670 spectrophotometer (JASCO, Tokyo, Japan) by using 1 cm-path length cuvettes. The UV-visible absorption spectrum was measured between 250 and 750 nm. CD spectra of

CPC_{O77} were measured at 25 °C on a Chirascan qCD spectrophotometer (Applied Photophysics Ltd., UK). The spectra of each sample were recorded in near-UV-visible (250-700 nm) regions.

4.2.4 Purification of α and β subunits from CPC_{O77}

Phenyl-Sepharose high performance (2.6 x 10 cm, GE Health Care, UK) was used to purify each subunit of CPC_{O77} disassembled under 7.0 M urea. The column was pre-equilibrated with 20 mM K-P buffer (pH 5.0) containing 1.0 mM dithiothreitol (DTT), 7.0 M urea, 1.0 M ammonium sulfate (AS), and 10% w/v glycerol. The homogeneously purified CPC (10 $mg \cdot mL^{-1}$) was incubated in 7.0 M urea, 1.0 M AS, and 10% glycerol for 1 h under room temperature. The sample was loaded onto the column and eluted at a flow rate of 3.5 $mL \cdot min^{-1}$. A stepwise gradient method was used, which consisted of 40 mL of buffer containing a gradient of 1.0 M to 0.55 M AS, 60 mL of isocratic elution of buffer containing 0.55 M AS, a gradient of 40 mL of 0.55 M to 0.3 M AS, 40 mL of isocratic elution of buffer containing 0.3 M AS, a gradient of 40 mL of 0.3 M to 0 M AS, and 60 mL of isocratic elution under no salt in 20 mM KP buffer. All fractions were collected and examined by SDS-PAGE. The results showed that two peaks corresponding to α and β subunits were detected at 0.1 M and 0.3 M AS gradient respectively, with conductivity of 15.6 and 38.9 $mS \cdot cm^{-1}$ respectively. All the fractions of these two peaks were collected and loaded onto the desalting column pre-equilibrated with 50 mM KP buffer (pH 7.0) at a flow rate of 10 $mL \cdot min^{-}1$ to remove urea from the solution. The homogeneously isolated α/β subunit was analyzed by SDS-PAGE, UV-visible, and CD spectrophotometers.

4.2.5 Characterization of isolated α and β subunit of CPC_{O77}

The UV-visible absorption spectra of isolated α and β subunits were measured between 250 and 750 nm. The CD spectra of α and β subunits were recorded in near-UV-visible (250-

700 nm) regions and far-UV (180-250 nm) regions. The far-UV CD spectra were deconvoluted by the CDNN 2.1 program for the percentage of secondary structure. The thermostability of CPC_{O77} and isolated subunits was determined by CD spectra analysis. The desired wavelength was set at 222 nm and the temperature range was from 25°C to 90°C. The rate of heating was set to $1°C \cdot min^{-1}$ with the desired temperature interval of 0.5°C. MALDI-TOF mass spectra of isolated α and β subunits were obtained by the double-layer method. The saturated sinapinic acid solution in ethanol was deposited onto a ground steel MALDI target plate to form a matrix layer. A mixture of α/β subunits and sinapinic acid in a solvent of acetonitrile and 0.1% trifluoroacetic acid (3/7, v/v) was then dropped on the matrix layer and dried at room temperature. The MALDI-TOF spectrum was measured by BRUKER microflex LT (Bruker Daltonics, Inc., Billerica, MA, USA). The molecular weight of isolated α and β subunits were determined by gel filtration using a Superdex 200 column calibrated with the molecular marker of bovine thyroglobulin (M_r = 670,000), bovine γ-globulin (M_r = 158,000), chicken ovalbumin (M_r = 44,000), horse myoglobin (M_r = 17,000), and vitamin B_{12} (M_r = 1350).

4.2.6 Protein crystalization

Crystals of subunits were prepared by the hanging-drop vapor-diffusion method using HR3-170 crystallization plate (Hampton Research, USA). A 1 μL drop of subunits (20 $mg \cdot mL^{-1}$) was mixed with 1 μL drop of precipitant [15% (w/v) PEG 3,350, 10 mM $MgCl_2 \cdot 6H_2O$, 5 mM $NiCl_2 \cdot 6H_2O$, 100 mM HEPES, pH 7.0 for α subunit and 20% (w/v) PEG 3,350, 0.2 M $Mg(CH_3COO)_2 \cdot 4H_2O$ for β subunit] and equilibrated against a 500 μL reservoir consisting of precipitant solution. Crystals of α and β subunit CPC appeared after 2–3 days at 283 K.

4.2.7 Reassembly of α and β subunits

The isolated α and β subunits in urea solutions (0.5 $mg \cdot mL^{-1}$, KP buffer pH 7.0) were mixed at a ratio of 1:1 at room temperature. The mixture was then loaded onto the desalting column and pre-equilibrated with 50 mM KP buffer (pH 7.0) to remove urea and facilitate the reassembly process. The reassembly process was observed by UV-visible, CD, and MALDI-TOF spectral analysis. The UV-visible absorption spectra were measured between 250 and 750 nm for 1 h intervals over reaction periods at room temperature. The CD spectra of the mixture before the desalting column and after 1 h incubation were recorded in a near-UV-visible (250-700 nm) region. The MALDI-TOF spectra of the mixture after 1 h and 48 h were obtained by double-layer method.

4.2.8 Crystallization of reassembled CPC

Crystals of reassembled CPC were prepared by the hanging-drop vapor-diffusion method using HR3-170 crystallization plate (Hampton Research, USA). A 1 μL drop of subunits (20 $mg \cdot mL^{-1}$) was mixed with 1 μL drop of precipitant [15% (w/v) PEG 3,350, 10 mM $MgCl_2 \cdot 6H_2O$, 5 mM $NiCl_2 \cdot 6H_2O$, 100 mM HEPES, pH 7.0 for α subunit and 20% (w/v) PEG 3,350, 0.2 M $Mg(CH_3COO)_2 \cdot 4H_2O$ for β subunit] and equilibrated against a 500 μL reservoir consisting of precipitant solution. Crystals of α and β subunit CPC appeared after 2-3 days at 283 K.

4.3 Results and Discussions

4.3.1 Purification of the dissociated α and β subunits of CPC_{O77}

The thermophilic CPC from *Thermoleptolyngbya* sp. O-77 was purified by following methods of previous studies [23]. The purity of CPC_{O77} was estimated to be 5.1, as calculated from the A_{615}/A_{280} ratio. This is a relatively high purity compared with other C-phycocyanins purified from various cyanobacteria [11,27,28]. The molar extinction coefficient of CPC_{O77} at 615

nm was determined to be 2.16×10^5 $M^{-1} \cdot cm^{-1}$ based on the monomer molecular mass of 37.1 kDa. The molecular mass of CPC_{O77} was calculated from the deduced amino acid sequence of the α-subunit (17,414 $g \cdot moL^{-1}$) and the β-subunit (17,935 $g \cdot moL^{-1}$), which included the molecular mass of three phycocyanobilins (588.69 $g \cdot moL^{-1}$). To dissociate each subunit from homogenously purified CPC_{O77}, we determined the optimal conditions for the dissociation of CPC_{O77} by examining different concentrations of urea and reaction pH conditions. Urea is a well-known denaturing agent that can reversibly disassociate proteins into their subunits [29]. After urea is removed from the reaction solution, the dissociated protein components can be reassembled to the original structure. In this experiment, to dissociate CPC_{O77}, we incubated the protein at room temperature for 1 h in urea at concentrations from 0 M to 8.0 M. The spectral features of the supernatant after centrifugation at 10,000 *g* for 10 min indicated that the absorption decreased gradually at high urea concentrations. The maximum absorption peak at 615 nm of CPC_{O77} was significantly decreased above urea concentrations of 5.0 M (**Fig. 1**). This result suggests that CPC_{O77} starts to disassociate into each subunit above urea concentrations of 5.0 M.

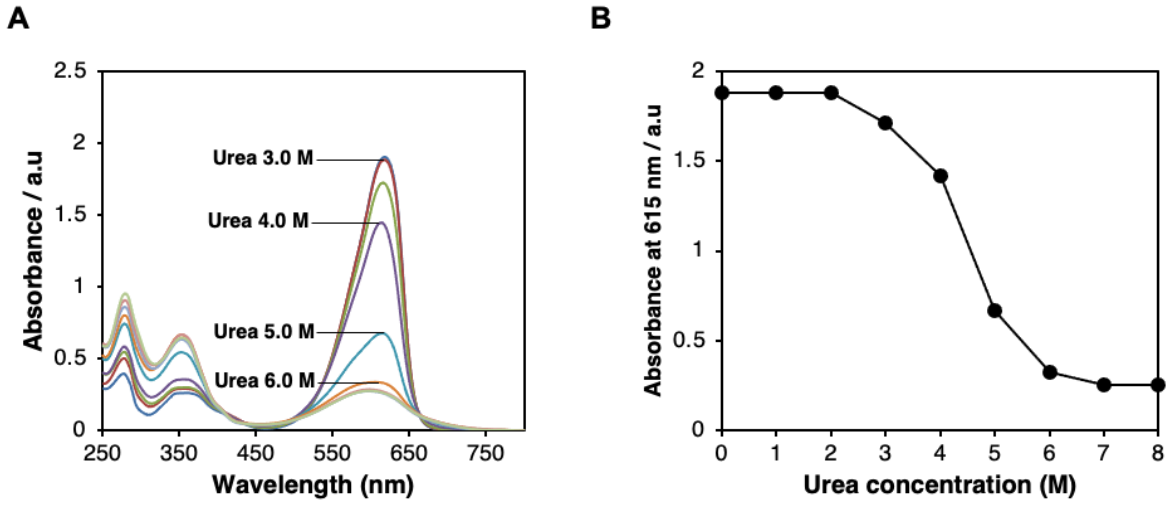

Fig. 1. (A) The UV absorption spectral profiles of the purified CPC_{O77} after adding different urea concentrations (between 1.0 M and 8.0 M). (B) The absorption spectral profiles at 615 nm of the purified CPC_{O77} after adding different urea concentrations between 0 and 8.0 M.

In addition, to stabilize CPC_{O77} and its subunits in high concentrations of urea, we determined the effect of reaction pH on the effective and stable disassembly of CPC_{O77} subunit. The CD spectra of CPC_{O77} contained a strong positive band at 605 nm and a negative band at 332 nm between pH 5.0 and 6.0 range, but in other pH conditions (i.e., below pH 5.0 and above pH 6.0), no significant peak was observed (**Fig. 2A**). The optical emission from 550 to 650 nm arises from the optically active charge-transfer transitions of the open-chain tetrapyrrole, which are presumed to be sensitive to changes in conformation. Therefore, the disappearance of the absorption peak suggests that CPC_{O77} was denatured in low and high pH conditions. The protein stability was also examined using a 15% SDS-PAGE (**Fig. 2B**). In solutions with a pH of 5.0 and 6.0, SDS-PAGE analysis of CPC_{O77} exhibited two bands with molecular masses determined to be approximately 17.5 and 22.5 kDa. However, the protein bands of CPC_{O77} were not observed when the pH ranged from 6.0 to 11.0 and were scattered when the pH ranged from 2.0 to 5.0.

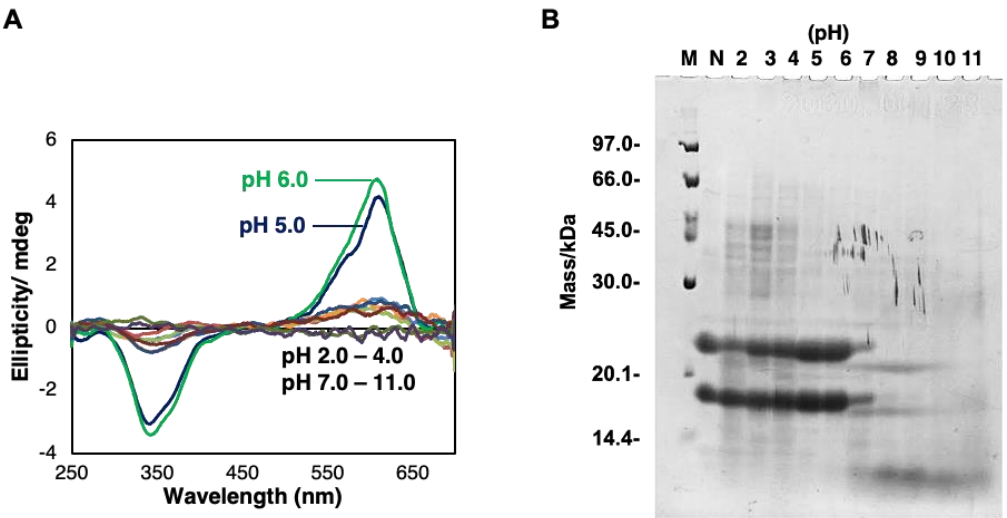

Fig. 2. (A) CD spectral changes of CPC dissolved of 5.0 M urea after incubation for 1 h in the different pH condition between pH 2.0 and pH 11.0 (B) SDS-PAGE analysis of the purified CPC_{O77} after incubation for 1 h containing 5.0 M urea in different pHs between pH 2.0 and pH 11.0.

This indicates that the dissociated α and β subunits of CPC_{O77} were stabilized in the pH range between 5.0 and 6.0, although CPC_{O77} was unstable in highly acidic and alkaline conditions.

Notably, CPC_{O77} was highly unstable and readily decomposed in an alkaline buffer containing a high concentration of urea.

Previously, research has reported a subunit separation method for CPC that involves cation exchange chromatography [30]. Based on these studies, the α and β subunits of phycocyanin were dissociated by a stepwise urea gradient between 5.0 and 10 M at pH 2.2 of acidic buffer. However, the dissociation of each subunit in CPC_{O77} appears to be unstable at an acidic pH, as shown by the presence of contaminating bands of the β and α subunits in the SDS-PAGE analysis. Native CPC_{O77} might be denatured by hydrolyzation of proteins under highly acidic conditions. Furthermore, high pH from 8.0 to 9.0 in urea solution also denatures CPC, as shown by the SDS-PAGE analysis. Therefore, to stabilize the subunits, we performed the isolation under neutral pH using a hydrophobic column. Using this separation process, the isolated α and β subunits both showed high stability and could be used for further analysis (**Fig. 3**). In the chromatographic analysis, the β subunit eluted first at a concentration of 0.3 M AS (**Fig. 3**).

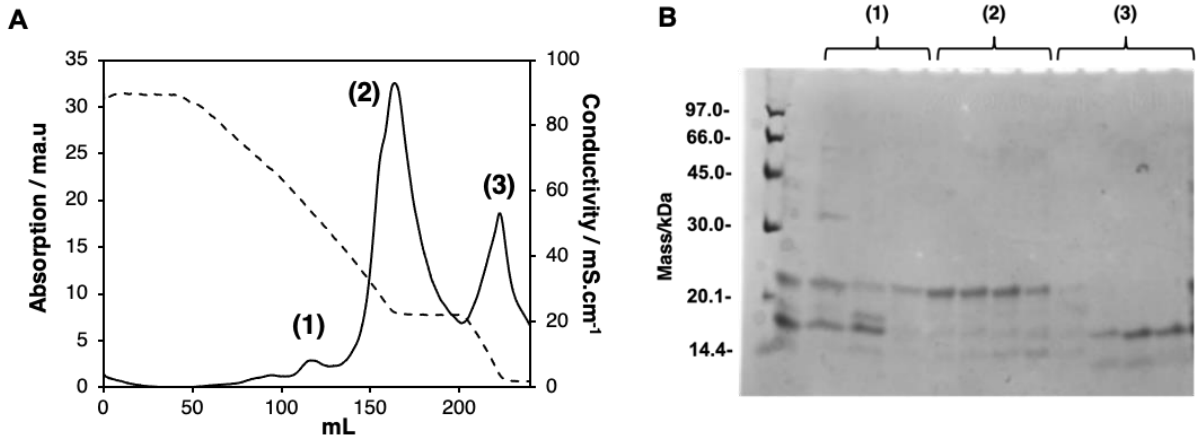

Fig. 3. (A) Chromatographic separation of CPC subunit by hydrophobic column of Phenyl-Sepharose high performance, (B) SDS-PAGE analysis after fractionation from 1 to 3, corresponding to non-dissociated CPC, the isolated β and α subunit, respectively.

This suggested that the β subunit is less hydrophobic than the α subunit. This result agrees well with previous observations of the β subunit. The amino acid sequence analysis showed that the β subunit contained high amounts of basic amino acids; for example, the β subunit comprised

4.1% lysine and 5.8% arginine. At pH 6.0, which is below the isoelectric point of CPC (pI = 7.4), these basic amino acids are protonated and reduce the hydrophobicity of the β subunit. Therefore, the β subunit is less salted out by AS and elutes first. More interestingly, the high percentage of basic amino acids in the β subunit might explain the unusual shift in the SDS-PAGE analysis of the β subunit.

4.3.2 Spectral analysis of dissociated α and β subunits from CPCo77

The α and β subunits were successfully purified using the Phenyl-Sepharose High Performance hydrophobic column with KP buffer (pH 6.0) containing 7.0 M urea at room temperature. The purification of the α and β subunits from the protein was confirmed by SDS-PAGE, with two bands observed: 17.5 kDa for the α subunit and 22.5 kDa for the β subunit (**Fig. 4A**).

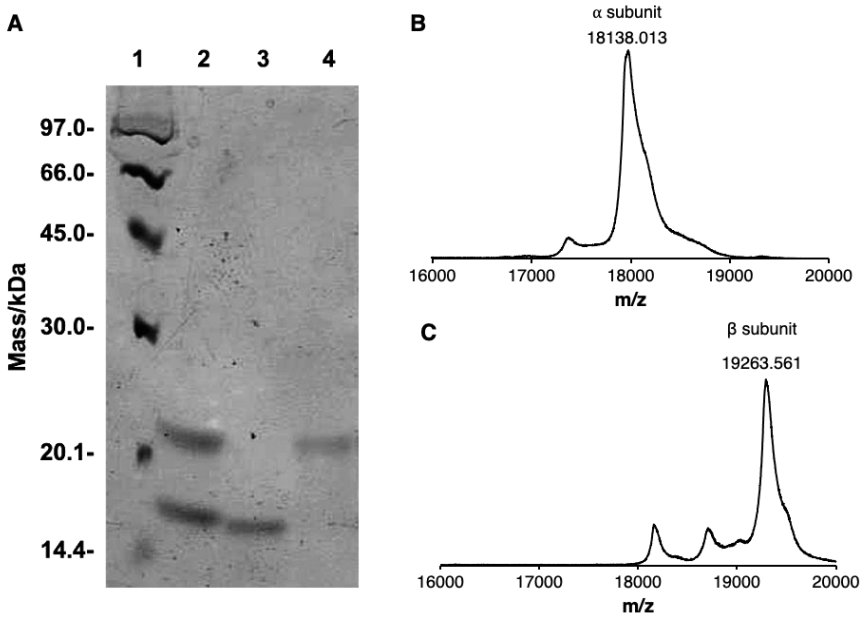

Fig. 4. (A) SDS-PAGE of α and β subunit. Lane 1: Standard marker proteins, Lane 2: homogeneously purified CPC before disassembly experiment, Lane 3 and 4: the isolalated α subunit and β subunit after column chromatography of PSHP, respectively. (B) MALDI-TOF spectra of the dissociated α subunit. (C) MALDI-TOF spectra of the dissociated β subunit

The molecular weights of the isolated α and β subunits were estimated to be 34 ± 2 kDa and 36 ± 2 kDa, respectively, by gel filtration column chromatography, indicating that both the isolated α and β subunits exist in a dimeric state after isolation. The signal in the MALDI-TOF mass spectra at *m/z* 18138 (**Fig. 4B**) was assignable to the α subunit with a PCB (calcd. 18130.29), and the signal at *m/z* 19263 was assignable to the β subunit with two PCBs and one methylated βAsn72 (calcd. 19249.87) (**Fig. 4C**).

The UV–visible spectral features of the α and β subunits were found at 617 nm and 610 nm, respectively (**Fig. 5A**). The spectral observations were consistent with those of previous studies from cryptomonads and marine cyanobacteria [30,31]. This result presumably suggests that the α subunit contains a chromophore that absorbs longer wavelengths (the f type of chromophore). In contrast, the β subunits contain a chromophore that absorbs shorter wavelengths (the s type of chromophore) [32].

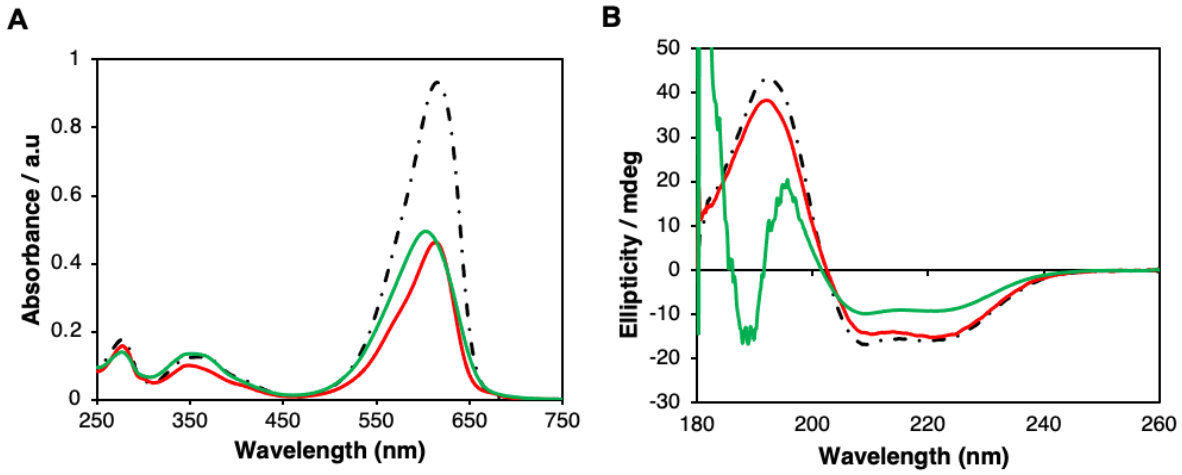

Fig. 5. (A) UV and (B) far-UV CD spectral analysis of α-subunit (solid line), β-subunit (dashed line), and original CPC (dashed and dotted line).

The analysis of the far-UV–CD spectra indicates the contrast in the components of the α-helix and β-sheet in each subunit compared with the original CPC (**Fig. 5B**). Conversely, the far-UV CD spectra of CPC indicated a composition of 29.9% α-helix, 23.6% β-turn, 16.6% β-sheet, and 29.9% random coil; although the α-helix still comprises the majority of the CPC structure,

we observed a lower percentage of the α-helix structure in CPC compared with the α subunit. As previous studies showed that a higher percentage of α-helix leads to a more stable protein structure [33,34], these results suggest that the isolated α subunit is more stable than the isolated β subunit.

4.3.3 X-ray crystallographic analysis of dissociated α and β subunits from CPCo77

As the stable isolation of α and β subunits was successfully performed, crystals of those subunits were then obtained after examining a variety of crystallization conditions. The initial screening of crystals showed that isolated α subunit crystal belonged to the space group of *P*62 and β subunit crystal belonged to the space group of $C222_1$ (**Table 1**). The X-ray structural analysis at a resolution of 2.45Å for the isolated α subunit and 1.94Å for the isolated β subunit (**Table 1**) revealed that the α and β subunits were crystallized as homodimers (**Fig. 6A, B**).

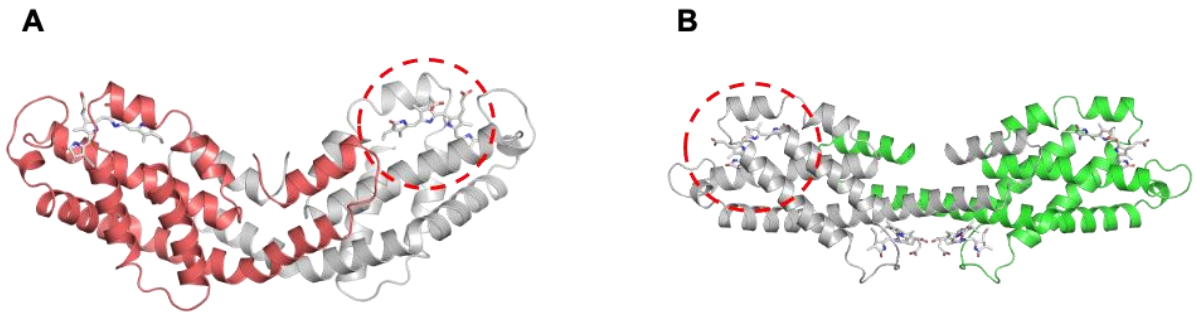

Fig. 6. Crystal structures of (A) isolated α homodimer and (B) isolated β homodimer. Main and side chains of α subunit and β subunit are represented by red and green ribbon models, respectively. PCBs are circled and represented by gray lines.

The crystal structure of the isolated α and β subunits revealed identical amino acid sequences to the α and β subunits of CPC. This proved that both the α and β subunits were successfully isolated without any modification to the C or N termini of the amino acid sequence. To the best of our knowledge, this is the first example of the crystal structure and crystal analysis of isolated α and β subunits from CPC. The isolated α subunit was essentially isostructural to the crystal structures of the α subunit within the hexamer (PDB ID: 7EFW, RMSD value of 0.99

Å over 157 Cα atoms) and the octamer (PDB ID: 7EFV, RMSD value of 0.85 Å over 161 Cα atoms). However, the angle between helices B and C (βSer21 – βAsp33 – βAsn47) in the isolated β subunit was drastically increased (199°) compared with the β subunits within the hexamer (149°) and the octamer (149°), resulting in slightly large RMSD values, mainly because of the interfacial interaction between βLys32 and PCB (Cys183) in the β homodimer, which was not observed in the (αβ) monomer or the octamer and hexamer. The basic side chain of βLys32 allows it to interact with PCB in Cys183 in the β homodimer, which results in the change in the isolated β subunit compared with the β subunit within the octamer and hexamer CPC (**Fig. 8**). Interestingly, the βLys32 is not conserved and is rarely observed in previously reported CPC sequences, suggesting that the phenomenon in the isolated β subunit might be unique to CPC_{O77} (**Fig. 7**).

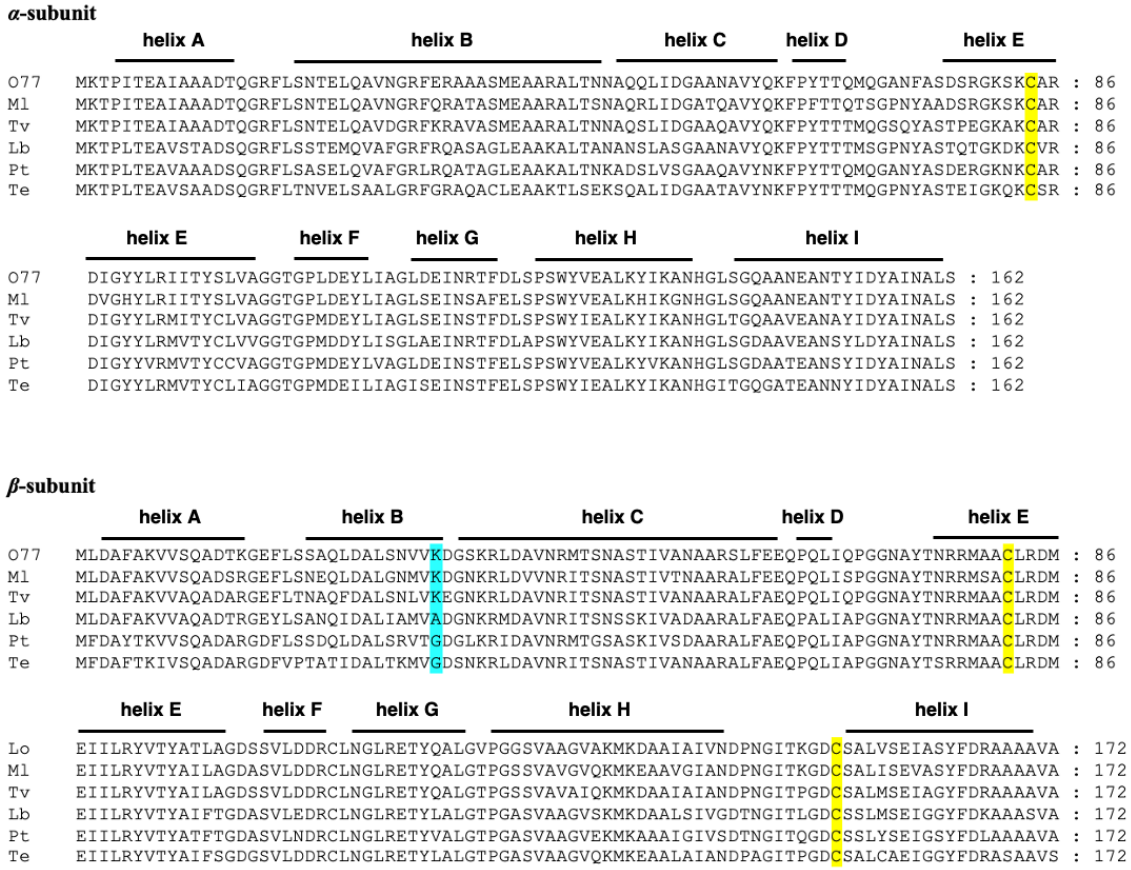

Fig. 7. CPC sequences from *Thermoleptolyngbya* sp. O-77 (O77), *Thermosynechococcus vulcanus* (Tv), *Mastigocladus laminosus* (Ml), *Leptolyngbya boryana* (Lb), *Phormidium tenue* (Pt), and *Trichodesmium erythraeum* (Te). β32 are highlighted in blue.

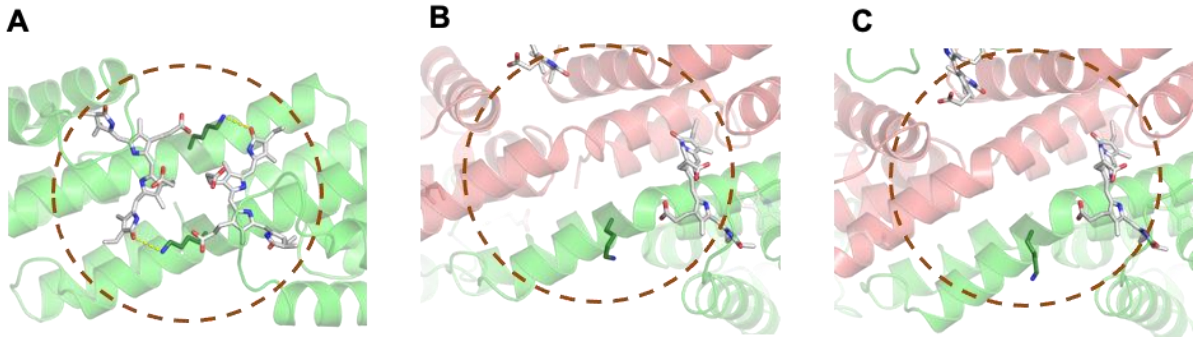

Fig. 8. Hydrogen bond network of the βLys32 in the interface interaction of (A) isolated β homodimer, (B) hexamer (αβ) monomer, and (C) octamer (αβ) monomer (E). Main and side chains of α subunit and β subunit are represented by red and green ribbon models, respectively. PCBs and βLys32 are represented by gray and green lines, respectively, and hydrogen bond networks are represented by yellow dashed lines.

Table 1 Crystallographic data collection and refinement statistics.

(PDB ID)	**Isolated PCα** (####)	**Isolated PCβ** (####)	**Reassembled CPC-6** (####)	**Reassembled CPC-8** (####)
Data collection				
Space group	*P*62	$C222_1$	$P22_12_1$	*I*432
Cell dimensions				
a, *b*, *c* (Å)	170.0, 170.0, 126.0	38.5, 145.1, 66.1	107.7, 115.1, 187.0	230.5, 230.5, 230.5
α, β, γ (°)	90.0, 90.0, 120.0	90.0, 90.0, 90.0	90.0, 90.0, 90.0	90.0, 90.0, 90.0
Resolution (Å)	50.0–2.45 (2.59–2.45)	50.0–1.94 (2.05–1.94)	50.0–1.98 (2.09–1.98)*	50.0–2.63 (2.78–2.63)*
R_{means}	17.8 (135.0)	15.8 (221.7)	29.9 (190.6)	70.2 (415.6)
$CC_{1/2}$	99.7 (45.5)	99.8 (55.0)	99.1 (43.5)	99.6 (49.0)
$I / \sigma I$	6.31 (1.13)	10.0 (0.68)	7.1 (1.04)	12.7 (1.06)
Completeness (%)	99.8 (45.5)	99.9 (99.5)	99.9 (99.5)	99.9 (99.8)
Redundancy	5.3 (5.2)	6.9 (6.8)	7.0 (7.1)	42.1 (40.5)
Refinement				
Resolution (Å)	47.86–2.45	48.87–1.94	49.00–1.98	47.11–2.50
No. reflections	75898	14192	162251	36274
R_{work} / R_{free} (%)	24.8 / 29.3	20.3 / 23.2	18.2 / 22.0	20.5 / 23.5
No. atoms				
Protein	14811	1268	15190	5009
Other	522	86	774	258
Water	152	95	1993	19
B-factors				
Protein	57.5	41.1	26.6	60.6
Other	48.8	43.4	26.6	64.5

Water	56.5	46.5	36.0	54.2
R.m.s. deviations				
Bond lengths (Å)	0.002	0.002	0.004	0.003
Bond angles (°)	0.954	0.592	0.821	0.663
Ramachandran plot				
Favored (%)	97.5	98.8	98.5	97.9
Allowed (%)	2.5	1.2	1.5	2.1
Disallowed (%)			0	0

*Values in parentheses are for highest-resolution shell.

4.3.4 Characterization of reassembled CPC_{O77}

To investigate the self-assembly mechanism of the novel octameric CPC, I performed an *in vitro* reassembly experiment using the isolated α and β subunits. In the UV–vis spectra, the absorption peak of CPC_{O77} at 615 nm was significantly increased after 1 h of incubation **(Fig. 9A)**. We continued to observe the reassembly process for 24 h and there was no significant increase in the absorption peak after a 24-hour incubation period as compared to a 1-hour incubation period (**Fig. 9A**). Furthermore, the absorption peaks of reassembled CPC_{O77} were observed at 280 and 355 nm, with a maximum peak at 615 nm, which is identical to those of the original $CPC_{O77.}$ These results suggest that the reassembly occurred spontaneously after 1 hour of incubation at room temperature. The far-UV CD spectra confirmed the reassembly process, revealing a significant change in the protein secondary structure, which became identical to the native CPC_{O77} after incubation a 1-hour incubation period (**Fig. 9B**). In addition, the far-UV CD spectra indicated that the environment surrounding the β subunit had returned to the environment within the original CPC_{O77}. The spectra were identical to those of previous studies of original CPC_{O77}, with the molecular peaks at *m/z* 18138 for the α subunit and *m/z* 19263 for the β subunit, as shown the by MALDI-TOF mass spectra after measurement after 1 h and 48 h (**Fig. 9C, D**). The reassembled CPC_{O77} was characterized as identical to the natural CPC_{O77} reported in previous studies, suggesting that CPC_{O77} was successfully reassembled into native CPC from the isolated α and β subunits.

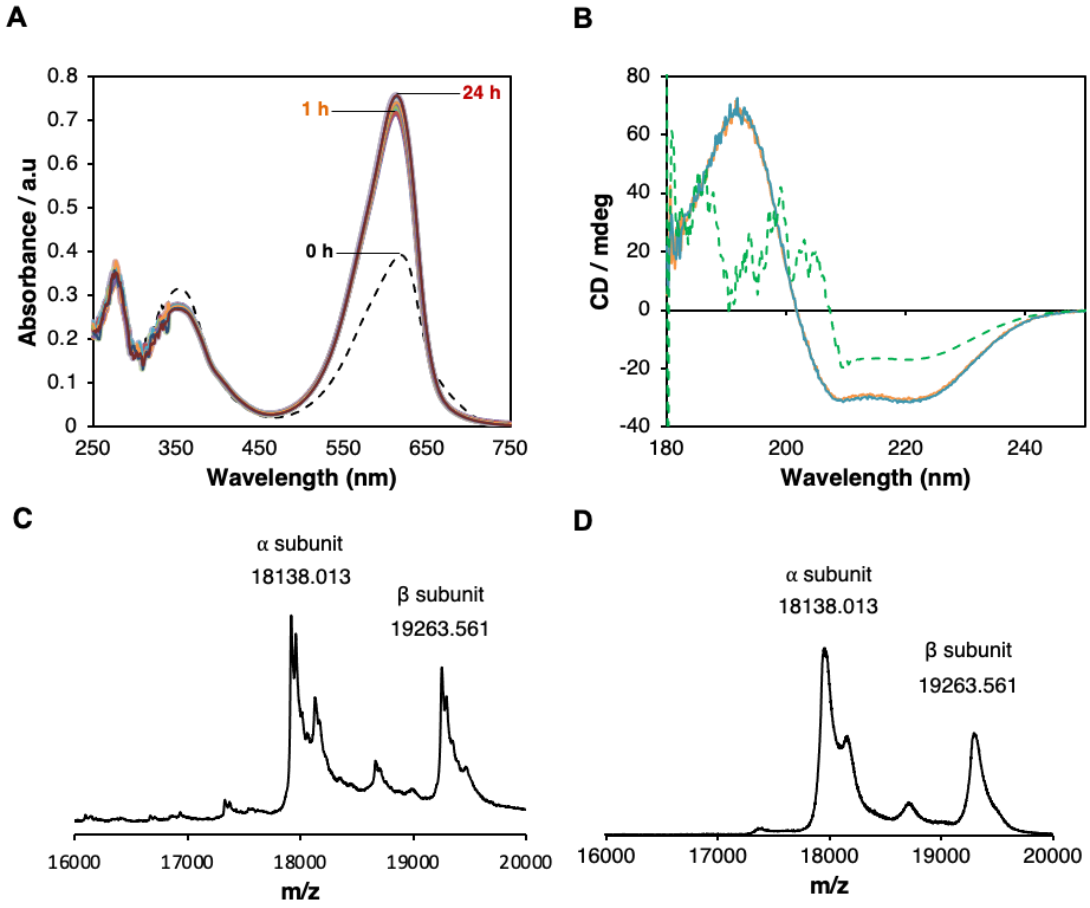

Fig. 9. (A) UV spectra of the reassembly process of CPC after mixing of the isolated α and β-subunit, (B) CD spectra profiles of the reassembled CPC, green dashed line represented a mixture of α and β-subunit before reassemble, the blue line represented reassembled CPC and orange line represented the original CPC. MALDI-TOF mass spectra of reassembled CPC after incubation for (C) 1h and (D) 48 h at room temperature.

4.3.5 X-ray crystallographic analysis of reassembled CPC

To elucidate the oligomeric state of the reassembled CPC_{O77}, the crystallization of reassembled CPC_{O77} was examined under various conditions. The X-ray crystallographic analysis of reconstituted CPC_{O77} from the α and β subunits confirmed the reassembly process was successful. The initial screening of crystals revealed that the reassembled CPC_{O77} crystal belonged to the space group of $P22_12_1$, representing the hexamer $(\alpha\beta)_6$ state and $I432$, representing the octamer state $(\alpha\beta)_8$ (**Table 1**). Crystals of reassembled CPC_{O77} were

determined at a resolution of 1.98Å for the hexamer state and 2.63Å for the octamer state. The X-ray structural analysis of the reassembled CPC indicates that the octameric CPC clearly originated from the dissociated α and β subunits. This *in vitro* reassembly experiment is the first experimental evidence for the construction of both hexameric and octameric CPC_{O77} (**Fig. 10**). The crystal structures of the reassembled hexamer or octamer were essentially isostructural to the previous crystal structures of the hexamer or octamer, respectively (PDB ID: 7 EFW, RMSD value of 0.50 Å over 2004 Cα atoms; PDB ID: 7 EFV, RMSD value of 0.35 Å over 668 Cα atoms). These results provide a strong indication that the α and β subunits of CPC can be assembled into both hexamers and octamers *in vitro* without linker proteins.

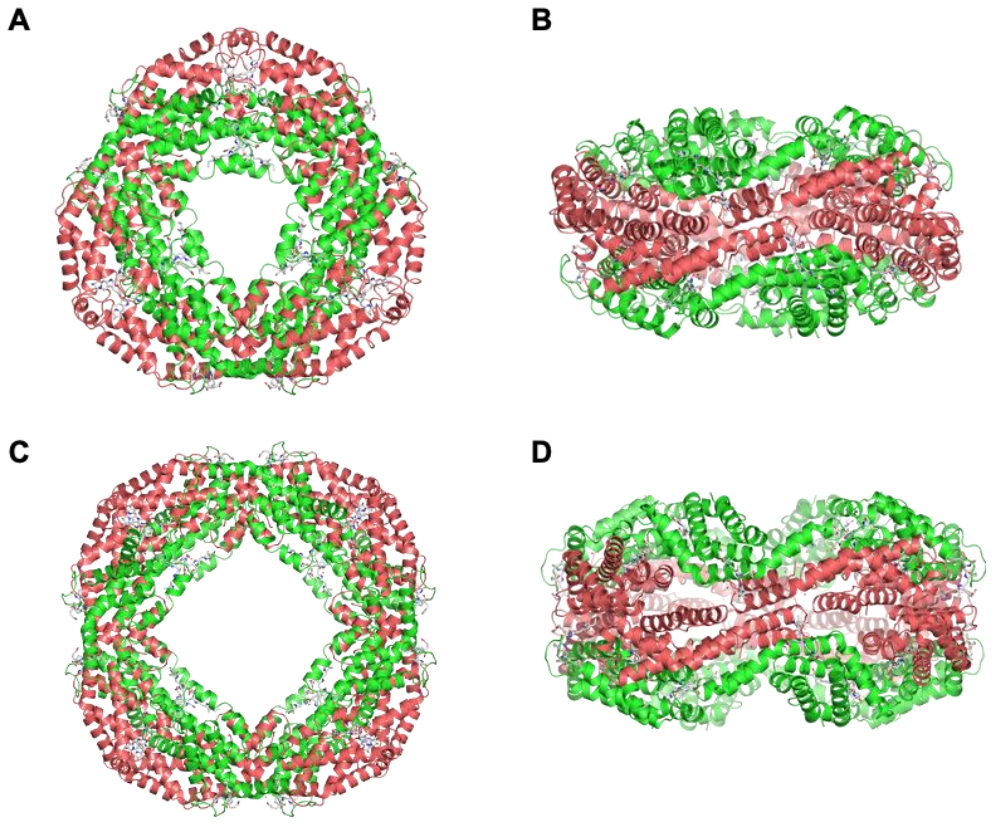

Fig. 10. (A) Top view and (C) side view of the crystal structure of reassembled hexamer CPC, (B) Top view and (C) side view of the crystal structure of reassembled octamer CPC. Main and side chains of α subunit and β subunit are represented by red and green ribbon models, respectively. PCBs are represented by gray lines.

In this study, the reassembled CPC_{O77} from the isolated subunits resulted in both the hexameric and octameric structures, which may open new biosynthetic pathways for studying the diversity of the thermophilic light-harvesting protein complex of CPC. Furthermore, this finding expands the application of CPC in protein assembly design, which has attracted attention as an effective way to build highly functional macromolecular biosystems [35]. Since the isolated α and β subunits from CPC_{O77} show high versatility, which can form both hexamer and octamer structures, this study can provide new insights into the biomolecular design for protein assembly.

4.4 Conclusion

In conclusion, CPC_{O77} was disassembled into α and β subunits and then reassembled to its native structure. I characterized the isolated α and β subunits by UV–Vis, CD, and MALDI-TOF spectrometry and successfully obtained crystals of these isolated subunits for the first time. The results showed that the α and β subunits formed homodimers after isolation and the detailed comparison of isolated subunits with the subunits within the native octameric and hexameric CPC_{O77} was conducted. Although the α subunit had an identical structure in both isolated conditions and within the octamer/hexamer, the structure of the isolated β subunit significantly changed after isolation owing to the formation of a new interface interaction. Notably, I found that CPC_{O77} could be reconstituted spontaneously from the isolated subunits and the X-ray crystal structural analysis of the reassembled CPC_{O77} showed the existence of both the hexameric and octameric structures. Understanding the subunit structure and assembly mechanism of non-conventional octameric CPC is essential for the development of designed protein assembly; thus, this research contributes to the fundamental knowledge needed for further application of CPC for this purpose.

4.5 References

[1] R. Croce, H. Van Amerongen, *Nat Chem Biol* **2014**, *10*, DOI 10.1038/nchembio.1555.

[2] M. Watanabe, M. Ikeuchi, *Photosynth Res* **2013**, *116*, DOI 10.1007/s11120-013-9905-3.

[3] N. Adir, S. Bar-Zvi, D. Harris, *Biochim Biophys Acta Bioenerg* **2020**, *1861*, DOI 10.1016/j.bbabio.2019.07.002.

[4] G. Ferraro, P. Imbimbo, A. Marseglia, R. Lucignano, D. M. Monti, A. Merlino, *Biochim Biophys Acta Bioenerg* **2020**, *1861*, DOI 10.1016/j.bbabio.2020.148236.

[5] B. R. Green, W. W. Parson, *Advances in photosynthesis and respiration ;* **2003**, *13*.

[6] R. MacColl, *J Struct Biol* **1998**, *124*, DOI 10.1006/jsbi.1998.4062.

[7] R. R. Sonani, S. Patel, B. Bhastana, K. Jakharia, M. G. Chaubey, N. K. Singh, D. Madamwar, *Bioresour Technol* **2017**, *245*, DOI 10.1016/j.biortech.2017.08.129.

[8] A. R. Grossman, M. R. Schaefer, G. G. Chiang, J. L. Collier, *Microbiol Rev* **1993**, *57*, DOI 10.1128/mr.57.3.725-749.1993.

[9] L. N. Liu, X. L. Chen, Y. Z. Zhang, B. C. Zhou, *Biochim Biophys Acta Bioenerg* **2005**, *1708*, DOI 10.1016/j.bbabio.2005.04.001.

[10] P. M. Gault, H. J. Marler, *Handbook on Cyanobacteria: Biochemistry, Biotechnology and Applications*, **2009**.

[11] N. T. Eriksen, *Appl Microbiol Biotechnol* **2008**, *80*, DOI 10.1007/s00253-008-1542-y.

[12] Y. C. Seo, W. S. Choi, J. H. Park, J. O. Park, K. H. Jung, H. Y. Lee, *Int J Mol Sci* **2013**, *14*, DOI 10.3390/ijms14011778.

[13] M. Kupka, H. Scheer, *Biochim Biophys Acta Bioenerg* **2008**, *1777*, DOI 10.1016/j.bbabio.2007.10.009.

[14] T. J. Ashaolu, K. Samborska, C. C. Lee, M. Tomas, E. Capanoglu, Ö. Tarhan, B. Taze, S. M. Jafari, *Int J Biol Macromol* **2021**, *193*, DOI 10.1016/j.ijbiomac.2021.11.064.

[15] I. Eisenberg, D. Harris, Y. Levi-Kalisman, S. Yochelis, A. Shemesh, G. Ben-Nissan, M. Sharon, U. Raviv, N. Adir, N. Keren, Y. Paltiel, *Photosynth Res* **2017**, *134*, DOI 10.1007/s11120-017-0406-7.

[16] A. Marx, N. Adir, *Biochim Biophys Acta Bioenerg* **2013**, *1827*, DOI 10.1016/j.bbabio.2012.11.006.

[17] K. L. Thoren, K. B. Connell, T. E. Robinson, D. D. Shellhamer, M. S. Tammaro, Y. M. Gindt, *Biochemistry* **2006**, *45*, DOI 10.1021/bi061140+.

[18] W. M. Schluchter, G. Shen, R. M. Alvey, A. Biswas, N. A. Saunée, S. R. Williams, C. A. Mille, D. A. Bryant, *Adv Exp Med Biol* **2010**, *675*, DOI 10.1007/978-1-4419-1528-3_12.

[19] L. David, A. Marx, N. Adir, *J Mol Biol* **2011**, *405*, DOI 10.1016/j.jmb.2010.10.036.

[20] H. Nakamori, T. Yatabe, K. S. Yoon, S. Ogo, *J Biosci Bioeng* **2014**, *118*, DOI 10.1016/j.jbiosc.2014.01.009.

[21] K. Sciuto, I. Moro, *Mol Phylogenet Evol* **2016**, *105*, DOI 10.1016/j.ympev.2016.08.010.

[22] K. Yamada, T. Yatabe, K. S. Yoon, S. Ogo, *J Organomet Chem* **2022**, *964*, DOI 10.1016/j.jorganchem.2022.122302.

[23] T. Minato, T. Teramoto, N. Adachi, N. K. Hung, K. Yamada, M. Kawasaki, M. Akutsu, T. Moriya, T. Senda, S. Ogo, Y. Kakuta, K. S. Yoon, *Commun Biol* **2021**, *4*, DOI 10.1038/s42003-021-02767-x.

[24] R. Inoue, Y. Sakamaki, T. Takata, K. Wood, K. Morishima, N. Sato, A. Okuda, M. Shimizu, R. Urade, N. Fujii, M. Sugiyama, *Sci Rep* **2021**, *11*, DOI 10.1038/s41598-021-82250-z.

[25] V. Eckey, H. Landmesser, E. Schneider, *Biochim Biophys Acta Biomembr* **2010**, *1798*, DOI 10.1016/j.bbamem.2010.03.001.

[26] A. Patel, S. Mishra, R. Pawar, P. K. Ghosh, *Protein Expr Purif* **2005**, *40*, DOI 10.1016/j.pep.2004.10.028.

[27] M. Gantar, D. Simović, S. Djilas, W. W. Gonzalez, J. Miksovska, *J Biotechnol* **2012**, *159*, DOI 10.1016/j.jbiotec.2012.02.004.

[28] B. Soni, U. Trivedi, D. Madamwar, *Bioresour Technol* **2008**, *99*, DOI 10.1016/j.biortech.2006.11.010.

[29] S. Raghunathan, T. Jaganade, U. D. Priyakumar, *Biophys Rev* **2020**, *12*, DOI 10.1007/s12551-020-00620-9.

[30] D. Guard-Friar, R. MacColl, *Photochem Photobiol* **1986**, *43*.

[31] A. N. Glazer, S. Fang, D. M. Brown, *Journal of Biological Chemistry* **1973**, *248*, DOI 10.1016/s0021-9258(19)43559-x.

[32] F. W. Teale, R. E. Dale, *Biochem J* **1970**, *116*, DOI 10.1042/bj1160161.

[33] J. Dzubiella, *J Am Chem Soc* **2008**, *130*, DOI 10.1021/ja805562g.

[34] M. Wolny, M. Batchelor, G. J. Bartlett, E. G. Baker, M. Kurzawa, P. J. Knight, L. Dougan, D. N. Woolfson, E. Paci, M. Peckham, *Sci Rep* **2017**, *7*, DOI 10.1038/srep44341.

[35] J. Zhu, N. Avakyan, A. Kakkis, A. M. Hoffnagle, K. Han, Y. Li, Z. Zhang, T. S. Choi, Y. Na, C. J. Yu, F. A. Tezcan, *Chem Rev* **2021**, *121*, DOI 10.1021/acs.chemrev.1c00308.

Chapter 5

Concluding remarks

In this dissertation, I reported on the development of the biocatalytic system for the conversion of atmospheric CO_2 into formate – a useful chemical feedstock and hydrogen carrier. As a result, two selective, highly efficient, and reusable biocatalytic systems were presented: the encapsulated whole-cell biocatalytic system (**Chapter 2**) and the plasma membrane biocatalytic system (**Chapter 3**). In addition, I also studied the disassembly and reassembly of the thermophilic C-phycocyanin (CPC) by isolating and analyzing its subunit to bring more insights to the assembly mechanism of non-conventional octameric CPC. For the first time, the structure of isolated subunits was analyzed, and octamer CPC was proven to be a natural assembly (**Chapter 4**).

Chapter 2

I developed a hydrogel system by encapsulating the whole-cell S-77 in the cross-linked polymer networks of GG, PVA, and Ca^{2+}. The results showed that GG/PVA/S-77 as a heterogeneous catalyst efficiently catalyzed the hydrogenation of CO_2 to yield formate. This strategy of immobilizing resting cells can selectively produce formate from H_2 and CO_2 without any byproducts under very mild conditions, and the encapsulated cells in hydrogels can act as a robust biocatalytic system that can be reused several times without losing its catalytic activity. The study provides new insight into the encapsulation of bacterial cells in the hydrogel with high structural stability, which is expected to allow clean bioenergy generation as practical industrial biocatalysts.

Chapter 3

I presented a feasible method for the H_2-driven reduction of CO_2 into formate using encapsulated bacterial plasma membranes in hydrogel beads. The results indicated that formate was produced with a high and selective reaction rate at ambient conditions. The immobilized

system of the plasma membrane, multiwalled carbon nanotube, and gellan gum demonstrated a sustainable heterogeneous biocatalyst platform that enhanced the overall catalytic stability and paved the way for practical applications. This study is the first study using plasma membranes for biocatalytic systems, which enhances our knowledge of bacterial plasma membranes and demonstrates their potential as a useful strategy for CO_2 hydrogenation to create valuable organic compounds.

Chapter 4

I isolated the α and β subunits from CPC_{O77} and then reassembled them back to its native structure. For the first time, the isolated α and β subunits was structurally characterized by X-ray crystallographic analysis. The results bring new insights about the difference between isolated and within-native-form subunits. For instance, the α and β subunits formed homodimers after isolation, and the structure of the isolated β subunit significantly changed after isolation owing to the formation of a new interface interaction. More significantly, I found that CPC_{O77} could be reconstituted spontaneously from the isolated subunits and the X-ray crystal structural analysis of the reassembled CPC_{O77} showed the existence of both the hexameric and octameric structures. Therefore, this research contributes to the fundamental knowledge needed for further application of CPC for this purpose.

List of publication

1. Selective formate production from H_2 and CO_2 using encapsulated whole-cells under mild reaction conditions.

Hung Khac Nguyen, Takuo Minato, Mohammad Moniruzzaman, Yu Kiyasu, Seiji Ogo, and Ki-Seok Yoon*

J. Biosci. Bioeng., **2023**, 136, 182–189. doi: 10.1016/j.jbiosc.2023.06.002.

2. H_2-driven reduction of CO_2 to formate using bacterial plasma membranes

Mohammad Moniruzzaman, **Hung Khac Nguyen**, Kiyasu Yu, Takumi Hirose, Handa Yuya, Taro Koide, Seiji Ogo, and Ki-Seok Yoon*

Bioresour. Technol., **2023**, 390, 129921. doi: 10.1016/j.biortech.2023.129921. (Press release)

3. Non-conventional octameric structure of C-phycocyanin

Takuo Minato, Takamasa Teramoto, Naruhiko Adachi, **Hung Khac Nguyen**, Kaho Yamada, Masato Kawasaki, Masato Akutsu, Toshio Moriya, Toshiya Senda, Seiji Ogo, Yoshimitsu Kakuta*, Ki-Seok Yoon*

Commun. Biol., **2021**, 4(1),1238. doi: 10.1038/s42003-021-02767-x. (Press release)

4. Disassembly and reassembly of the non-conventional thermophilic C-phycocyanin

Hung Khac Nguyen, Takuo Minato, Takamasa Teramoto, Seiji Ogo, Yoshimitsu Kakuta, Ki-Seok Yoon*

J. Biosci. Bioeng., **2023**, accepted.

Acknowledgment

First of all, I would like to state my deepest sincere appreciation to Professor **Seiji Ogo** for his continuous support, guidance, and motivation during the course of my study in Ogo laboratory.

I would like to express my greatest gratitude to Associate Professor **Ki-Seok Yoon** for his kind supervision, insightful discussions, and a lot of important suggestions and guidance throughout the research.

I wish to thank Associate Professor **Takahiro Matsumoto**, Associate Professor **Takahashi Yukina**, Assistant Professor **Yatabe Takeshi**, and Assistant Professor **Koide Taro** for their support and guidance.

I would like to thank Professor **Yoshimitsu Kakuta**, Assistant Professor **Takamasa Teramoto**, Assistant Professor **Takuo Minato** and Dr. **Mohammad Moniruzzaman** for their collaboration, kind support, and guidance.

I would like to send my acknowledgment to Ms. **Yukiko Shigematsu** for her kind assistance and support.

I would like to send my gratitude to all the members and technical staff at Ogo Laboratory for providing the warmest welcome and guidance.

Last but not least, I am deeply indebted to my family in Vietnam and my friends. Without the endless emotional support from them, there would not be a chance for me to be here and complete my doctoral course.

It is such an honor for me to be a part of Ogo Laboratory. Even though there were difficult times over these past years, even though people had to leave, everyone surely took place in this wonderful memory.

Hung Khac Nguyen